Abstract

In this thesis we investigate the use of adaptive optical devices in three different areas of vision science. These areas are defocus perception, retinal imaging and severe vision loss.

Birefringent material has been utilised to produce optical components that can control the angle of refraction of incident light. Using a ferroelectric liquid crystal (FLC) the orientation of linear polarised light can be controlled. This provides us with the ability to switch between the two refractive indices of birefringent materials at very high speeds.

A focus switchable lens (FSL) has been made from barium borate (BBO), and a ferroelectric liquid crystal to switch between equal and opposite defocus levels to determine the optimum focus correction by making use of the human eye's sensitivity to flicker. Flicker simulation result indicate that there is a high dependence of flicker sensitivity to the flicker frequency. High spatial frequencies also increased the ability to perceive small defocus shifts. Promising results have been obtained showing a person is able to find a point of equal defocus using flicker more accurately than they would be able to find perfect focus.

The same focus switching lens system has the ability to produce fast focus switching cameras. Its potential has been analysed for the use in retinal cameras to ease the process of obtaining good quality images of the optic nerve and providing such cameras with the ability to switch focus within the depth of the optic nerve head at high speeds. Simulation results showed that two FSLs positioned within the zoom system of the imaging arm are able to create focal point shifts of very small amounts.

Finally, collaborative research has been conducted in the use of a birefringent prism in conjunction with an FLC to create image jitter that can enhance visual performance in people with severe visual impairment. Image jitter created on-screen and via an optical system was tested. Patients were able to increase their reading speed and improve their ability to discriminate between happy and sad faces.

Adaptive Optical Devices in Vision Science

Fraser Charles Scobie

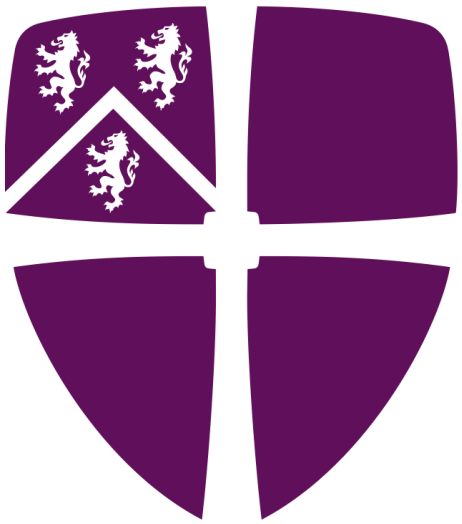

Thesis submitted in accordance with the requirements for the degree of Doctor of Philosophy

Department of Physics
University of Durham
September 2012

Contents

List of Figures

Glossary

CSLO - Confocal Scanning Laser Ophthalmoscopy

C/D - Cup-to-Disc Ratio

FFL - Front Focal Length

FLC - Ferroelectric Liquid Crystal

FSL - Focus Switchable Lens

LC - Liquid Crystal

logMAR - Logarithm of the Minimum Angle of Resolution

MTF - Modular Transfer Function

NRA - Neuroretinal Rim Area

OCT - Optical Coherence Tomography

ONH - Optic Nerve Head

POAG - Primary Open-Angle Glaucoma

PSF - Point Spread Function

RNFL - Retinal Nerve Fibre Layer

SEM - Standard Error of the Mean

SLP - Scanning Laser Polarimetry

SSFLC - Surface Stabilised Ferroelectric Liquid Crystal

Declaration

I hereby declare that this dissertation entitled *Adaptive Optical Devices for Vision Science* is not substantially the same as any that I have submitted for a degree or diploma or other qualification at any other University.

Chapter 2 is a review of optical devices that have been created and documented by previous authors.

Chapter 3 is a review of previous work by other authors in three different fields of Vision Science: Defocus Perception, Retinal Imaging and Involuntary Eye Movements.

Chapter 4 and 5 are documentations of my own work except where indicated in the text.

Chapter 6 is based on the paper *Image jitter enhances visual performance when spatial resolution is impaired*. The research was conducted in collaboration with Lynne Watson, Manahilov Velitchko and Niall Strang of the Glasgow Caledonian University. My work consisted of designing and implementing the optical system that was used to create image jitter.

Statement of Copyright

Acknowledgements

Many, many thanks go to my supervisor Gordon Love for providing invaluable guidance, without whose support I would have not been able to get through to the end of my PhD. I very much appreciate the effort you put in over the years and feel lucky to have had you as a supervisor.

A huge thanks goes out to the entire CfAI department at Durham University. So many of you have helped out in several ways throughout my four years as a postgrad from helping me get to grips with Python programming to giving me a hand with a host of electronic issues in the lab. Being able to work in such an environment helps inspire oneself to do good work.

My utmost gratitude goes to Lynne, Manahilov and Niall at the Glasgow Caledonian University. It was such a great pleasure to have had the opportunity to work among you and it provided with such a fantastic experience of working with another University to achieve a greater goal.

I'd like to thank all of my family members for showing such a keen interest in my work and progress and being so supportive throughout my long time at Durham.

Thank you to all the people I have met and all the friends I have made at Durham. While only a few of you have directly influenced my research as a PhD student you all helped me enjoy life, which can only have a positive effect on my work!

Thank you also to David and Sarah for their support, not least for always having

their farm available for regular recuperation weekends!

Last, but not least, I have to thank my girlfriend Flora for being so supportive of my work and staying with me in Durham even after she graduated.

Chapter 1

Introduction

1.1 Improve vision science, improve quality of life

Vision is our most important sensory perception and our eyes are therefore classed as our most valuable sensory organ. The vast majority of our environment is perceived using our eyes and their condition heavily impacts our quality of life.

The eye is an incredibly complex system and its performance can therefore vary considerably. There are many age related factors that affect the eye's performance as well. For these reasons it is very important to have regular check ups and produce techniques to help maintain and improve a person's vision.

The eye can be broken down into two major sections that are responsible for producing vision. These are the physiological optics and the retina. The physiological optics of the eye consist of the cornea, iris and lens. Figure 1.1 shows the major components that make up the eye. To view an object in perfect focus there are certain dimensional criteria the eye must have. The cornea has to be smoothly curved and have a particular radius of curvature. The lens must be the appropriate thickness for the depth of the eye as well. If the eye is the correct shape and the retina can process the information

correctly, then the optic nerve transmits an in-focus image to the brain [1].

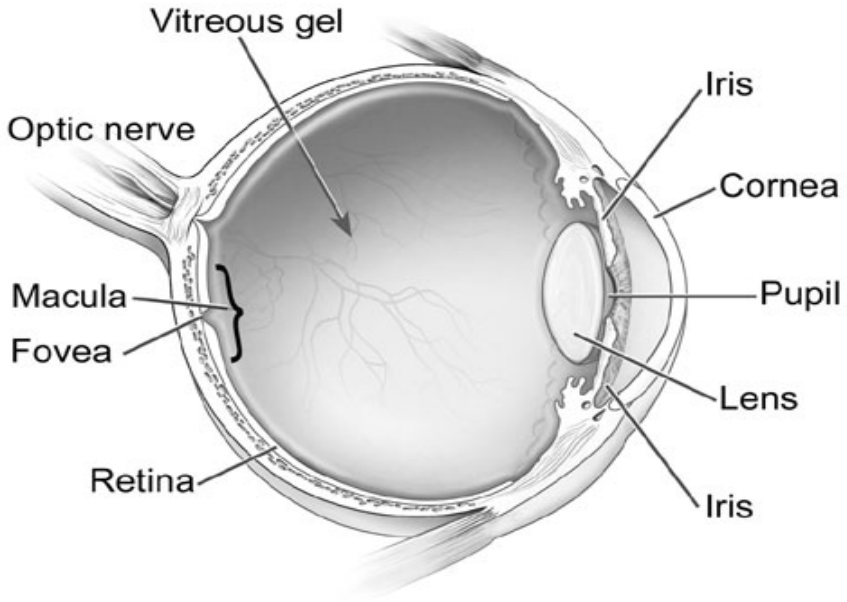

Figure 1.1: Diagram of the eye pointing out the location of the key features, from [2].

Not only does the cornea play a crucial part in focusing the light on the retina, it also is the protective membrane preventing anything from entering the eye. In order for it to remain transparent it has to maintain deturgescence, which is the relative dehydration of the cornea. This means there is a water deficit relative to the solutes present. If there are any abnormalities on the surface of the cornea vision can become blurred due to the change in refraction angle of the rays entering the eye.

The cornea and lens both contribute to the light being focused onto the retina. The power of the cornea is approximately $43D$ and the lens has a power of about $19D$. The lens is the eye's very own variable lens. The lens is held in place by zonular fibres, which are controlled by the ciliary muscle. If the ciliary muscle is in a relaxed state, the eye is able to bring distant objects into focus. As the ciliary muscle contracts the

tension in the zonular fibres is reduced allowing the lens to assume a more spherical shape. In this state closer objects are brought into focus.

The retina is very complex ocular tissue, whose structure is shown in figure 1.2. The layers of the retina are ordered as follows, starting the inner most layer: inner limiting membrane, ganglion cell layer, amacrine cells, bipolar cells, horixontal cells, photoreeptor layer consisting of rods and cones, and pigment epithelium. The retina must therefore be partially transparent to allow light to reach the photoreceptors. The density of the cones is much greater at the macula/fovea, decreasing with increasing distance from the macula. The rods on the other hand are greater in the peripheral area.

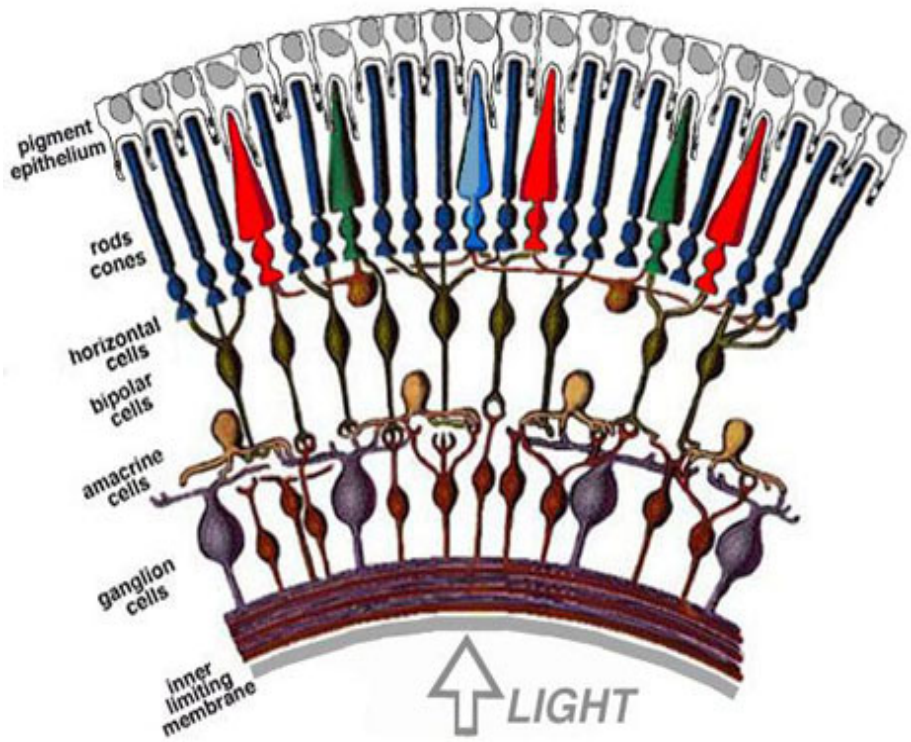

Figure 1.2: Diagram of the internal structure of the retina showing the order of the different layers, from [3].

Due to the complexity of the eye there is a high probability for an irregularity to be

present and the deterioration of the eye's visual capabilities is almost inevitable with age. Some of the most common disorders that occur in the eye are refractive error, age-related macular degeneration, cataracts, glaucoma and diabetic retinopathy [**?**].

- **Refractive error**: The most common eye disorder is refractive error in the eyes and it is easily corrected by corrective lenses as glasses or contact lenses. Short- and far-sightedness occur due to the natural thickness of the eye lens or the curvature of the cornea being out of proportion relative to the depth of the eye resulting in the focal point being behind or in front of the retina.

- **Cataracts**: A cataract is an opacity in the eye lens. They are most commonly caused by ageing, but can also occur from trauma, smoking, toxins and heredity. In the presence of a cataract a person's vision will appear clouded, the severity of the clouding being dependent on the severity of the cataract. The most common treatment for cataracts is the surgical removal of said cataract, either by removing the nucleus and cortex of the lens, leaving a lens capsule behind, or by removing the lens together with its capsule.

- **Age-related macular degeneration**: Age-related macular degeneration is a multifactorial progressive disease and is the leading cause for irreversible blindness in the developed world. It is not exclusively related to old age and can occur at earlier stages in a person's life. Degeneration can occur due to the blood vessels around the macular thickening or thinning (thickening being the much more common occurrence). There are currently limited solutions to treating this disease all of which involve magnifying or telescopic visual aids.

- **Glaucoma**: is the second leading cause of blindness after cataracts worldwide [4]. It is described as an optic neuropathy characterised by retinal ganglion cell death and corresponding nerve fibre layer loss. It is also the leading cause of

preventable blindness in America, as around 50% of people with glaucoma remain undiagnosed. Typically there is an increase in pressure within the eye, which also changes the shape of the optic nerve. Some medical treatments exist for glaucoma, but there is also the possibility of surgical treatment through the release of pressure in the eye.

- **Diabetic Retinopathy**: occurs in patients with either type I and type II diabetes. It occurs in patients with type I diabetes around 3-5 years after the onset of diabetes, whereas it is expected to take immediate effect in type II. Diabetic retinopathy can be classified into nonproliferative retinopathy, maculopathy, and proliferative retinopathy. Nonproliferative retinopathy is characterised by small-vessel damage and occlusion, appearing as micro-aneurysms and flame-like haemorrhages. Maculopathy is characterised by focal or diffuse retinal thickening or edema. Proliferative retinopathy is defined by the formation of new vessels that leak serum protains profusely. Treatments are available, but early detection is essential to prevent vision loss.

Due to there being such a variety of disorders that can occur in the eye there are a number of standard examinations that one must regularly go through to ensure that any disorder present is detected early on and can consequently be treated quickly.

The most common test is for visual acuity, the procedure of which involves recognising letters or shapes of a particular on a chart. The smaller the lettering that a person can read the better the visual acuity of the patient. Normal vision is described to be the ability to read the letters at a distance of 20 feet when they subtend an angle of 5 minutes of arc. If the patient is struggling to do this corrective lenses will be used to aid the patient. The patient decides which lens power provides him with the best image of the letters.

Corrective lenses can only provide visual aid for refractive error. If any other disorder is present there will still be problems with reading the chart. Other techniques must therefore be used to determine the eye disorder to be able to provide the correct treatment.

A further procedure is the slit lamp examination. This instrument projects a thin, slit of light onto the patient's eye while the observer looks through a magnifying lens system. The position of the light beam can be altered, such that the observer is able to view different crossections of the eye. It is used to closely observe the anterior section of the eye including the iris and cornea. The lens can also be partially observed depending on the dilation of the pupil.

As previously mentioned glaucoma can cause the pressure inside the eye to increase. The standard technique to test eye pressure is called tonometry, which involves determining the force it takes to flatten the cornea by a certain amount. A more common technique now is non-contact tonometry. This involves blowing pulses of air at the eye. Applanation is detected by an electro-optical system. Ocular pressure is then determined by detecting the force of the air pulse at the point of applanation. Tonometry however is not a definitive assessment of glaucoma, as the onset of glaucoma is still possible without a change in eye pressure. The optic nerve must be analysed in order to confirm a glaucoma diagnosis.

The analysis of the retina is a vital part of eye examinations as many of the eye disorders can be diagnosed this way. The method of viewing the inside of the eye is called ophthalmoscopy. Typically a practitioner would use direct ophthalmoscopy to view the retina. Direct Ophthalmoscopy involves using a specially designed hand-held magnifying lens system positioned directly in front of the eye. A small light attached to the device helps illuminate the retina. A real, upright image is produced, but the field of view is small. Indirect Ophthalmoscopy can produce a much wider field of view, but

the image is virtual and inverted. An indirect ophthalmoscope can provide a magnified, stereoscopic view of the retina. While the objective lens for the system is close to the patient's eye the observer can be some distance away, making it a more comfortable process of evaluation.

In the past few decades many new methods of analysing the retina have emerged, such as confocal scanning laser ophthalmoscopy (CSLO), scanning laser polarimetry (SLP) and optical coherence tomography (OCT). Fundus cameras have also become more sophisticated to in order to produce better images of the retina. All the instruments are designed to improve the reliability with which a practitioner can diagnose the various retinal diseases.

As these techniques become more and more complex, so does the price of actually making use of them. The price of the latest models is staggeringly high and it makes them unavailable to a wider community.

Many advancements have also been made in the treatment of eye disorders. Laser eye surgery to reshape the inside of the cornea, correcting for refractive error, is now a very common procedure. The procedure involves making a small incision to create a flap in the front of the cornea, which is pulled back to provide access to the middle of the cornea. Pulses from a laser vaporises portions of that cornea section after which the flap is replaced.

The lens replacements for cataracts used to be made by very rigid materials, but can now be made from flexible materials. The benefit for flexible lenses is that only a very small incision is needed to insert the lens reducing the risk of any side effects from the procedure. The most recent developments in intraocular lens research are lenses that have multifocal capabilities enabling the eye to still have its accommodating function [5].

1.2 Adaptive Optical Devices

The term adaptive optical devices covers a large number of instruments that in some form or other can alter the way they manipulate light. However, unlike traditional optical systems this is achieved without using a series of optical components or the repositioning of optical components. Some devices can change their shape, while others are able to change their interior structure. This has become possible due to the invention and greater understanding of flexible materials such as liquid crystals and a variety of polymers.

Adaptive optics has become a very well known technique for producing high quality astronomy images due to the ability for correcting atmospheric aberrations. An adaptive optics system consists of a wavefront sensor to detect the light disturbance, a deformable mirror that changes shape to compensate for the light aberration and a control computer to interpret the sensor information [6]. Such adaptive optics system have found wider use and can now be found in other industries as well, for example in microscopy where vision through tissue can be difficult [7].

The instruments used to view the retina can produce very high quality images, but the quality can often be limited by aberrations caused by the eye itself. Any abnormalities in the ocular lens or the cornea will prevent instruments designed for retinal analysis from producing maximum quality images.

There are a number of sophisticated adaptive optical devices now readily available that have the potential to be beneficial in the examination process of the eye as well as in the production of new visual aids.

1.2.1 Liquid Crystals

Liquid crystals (LC) are now found in a whole range of different electronic devices, such as watches, calculators, mobile phones and computer and TV displays. While LCs are known for their practical use in devices for everyday life they have also become incredible useful in many scientific optical applications including adaptive optics systems, optical tweezers and beam shaping [8].

One reason for their wide application is the anistropic organisation of their molecules. The interaction between light and LC therefore has a directional dependence on the orientation of the molecules and the orientation of the magnetic field of the incident light as well as its propagation direction.

The second reason for the popularity of LCs is their liquid-like behaviour. The organisation of the molecules within the LC can be controlled by temperature, electric, magnetic and optical fields.

Incident light therefore does not only have special interactions with the LC, we can also determine how the LC will interact with the light. LCs have become a very common light manipulator in many systems. The ability to control light manipulation can also be taken to a level where the interaction changes across an LC. For example LCs have been used to create phase profiles that can be used as a tip-tilt corrector in optical systems [9].

One of the most recent applications of LCs in vision science comes in the form of an intraocular lens containing an LC layer that can be controlled wirelessly [10]. Such a devices would provide patients that have cataracts to undergo lens replacement and still maintain their ability to change focus.

This intraocular lens is an example of how an LC can be used to create a variable

focus lens. As LCs are such versatile materials there is a whole number of ways that an LC can be used to create focus changing lenses. They can therefore be tailored to the specific requirements of the system that they will be used for.

1.3 Summary of Thesis

This research has been inspired by the desire to improve and maintain our visual perception of the world. The aim of this thesis is to analyse three different ways birefringent materials combined with liquid crystal plates can provide simple and cheap solutions to improving visual acuity tests , retinal imaging for glaucoma diagnosis and visual aids for patients with severe loss of vision.

Chapter 2 discusses a variety of focus variable lenses. An in-depth description of liquid crystals is provided with particular mention to thermotropic liquid crystals and the order of the molecules within them. The majority of focus variable lenses are covered in this chapter ranging from the very first liquid crystal lenses to thermal liquid lenses. A brief overview is provided for each lens apart from the focus switching lens for which a more detailed operational analysis is provided.

Chapter 3 introduces the three different fields within vision science that are of particular relevance to the research projects in this thesis. The fields discussed are defocus perception, retinal imaging and severe visual impairment. In the visual acuity section research is presented analysing a person's ability to perceive small shifts in defocus [11, 12, 13]. The retinal imaging section describes the importance of retinal analysis for the diagnosis of glaucoma and the different instruments that are used. of particular interest is the reliability of each method. The severe visual impairment section dis-

cusses research conducted by Watson *et al.* into image jitter that could help improve the ability of a patient with severe vision loss to read and recognise facial expressions [14].

Chapter 4 introduces the possibility of using defocus shifting to improve the speed and accuracy of visual acuity testing. A technique to use a focus switching lens to switch between equal and opposite blur is presented and how small differences in defocus create flicker. Simulated defocus shifting is created as well as experimental shifting, which is used to determine a person's ability to perceive small amounts of flicker. Additionally a small number of test patients are used to find a point of perfect focus without the focus switching lens and to find a point of equi-blur with the focus switching lens.

Chapter 5 presents initial simulations that are analysed to determine the potential for introducing focus switching lenses into the imaging arm of a fundus camera. Possible advantages of this technique over other existing methods is discussed. Birefringent lenses as well as plates are tested at different positions in the system. Spot diagrams for the each set of conditions are shown from which the best option can be determined.

Chapter 6 is an extension of the research conducted by Watson *et al.* The methods with which image jitter is created is discussed and the variables that were considered during the testing process. Results from each method are then presented. The performances of different image jitter methods is compared and analysed for different patients.

Chapter 2

Adaptive Optical Devices

Adaptive optical devices are becoming commonplace in many optical systems in a whole range of industries. The major areas of interest have been wavefront correction, adaptive optics, in astronomy and microscopy [15], and variable focus lenses, which are starting to be used for smartphone cameras [16]. It is only in the last decade that variable lenses have become commercially available. Companies such as Varioptic and Optotune have formed within the last ten years, specialising in creating such lenses for use in optical systems [16, 17]. Several companies such as Superfocus and PixelOptics have even created variable focus glasses to compete with varifocal and bifocal lenses [18, 19] .

The focal length of a typical optical system is usually changed by the repositioning of one or more of its lens components along the optical axis. The implementation of such a system can therefore be complicated if space is limited. For this reason alone an attractive solution would be to create a single lens with variable focus. Several ways of constructing a variable-focus lens have been realised, but most of them can be assigned to one of two categories: liquid lens and liquid crystal (LC) lens. The liquid lens is based on changing the shape of the liquid, where as the LC lens is based on controlling the refractive index of the LC [20].

This chapter is a review of past research and development in variable focus lenses and devices. An in-depth description of LCs is provided for a better understanding of how their structure can be controlled. The liquid crystal lens types are then presented with a brief description of how each type operates. A range of liquid lenses are also presented with a description of their structure and operation.

2.1 Liquid Crystals

LCs are organic materials that are liquid, but show some structural properties that would usually be found in crystals. The types of LCs are distinguished by different phases (called mesophases), which are defined by the positional and orientational order of the molecules. It is important to also note that the molecular order can be short-range or long-range [21, 22]. The two most common categories of LCs are thermotropic (temperature dependent) and lyotropic (two or more components surrounded by a solvent). In photonics research the majority of LCs used are of the thermotropic kind.

Thermotropic LCs are pure compounds or homogeneous mixtures possessing one or more anisotropic liquid phases at temperatures between the melting point, below which the material exists as a crystalline solid, and "clearing point", above which the material exists as an isotropic liquid. Thermal phase transitions are shown in figure 2.1.

Thermotropic phases can be broken down into three major phase types: nematic , cholesteric and smectic. Cholesteric and smectic types have many possible mesophases. Due to the huge variety of LC types they have been used in a great number of applications, one of the most common examples being the LCD display.

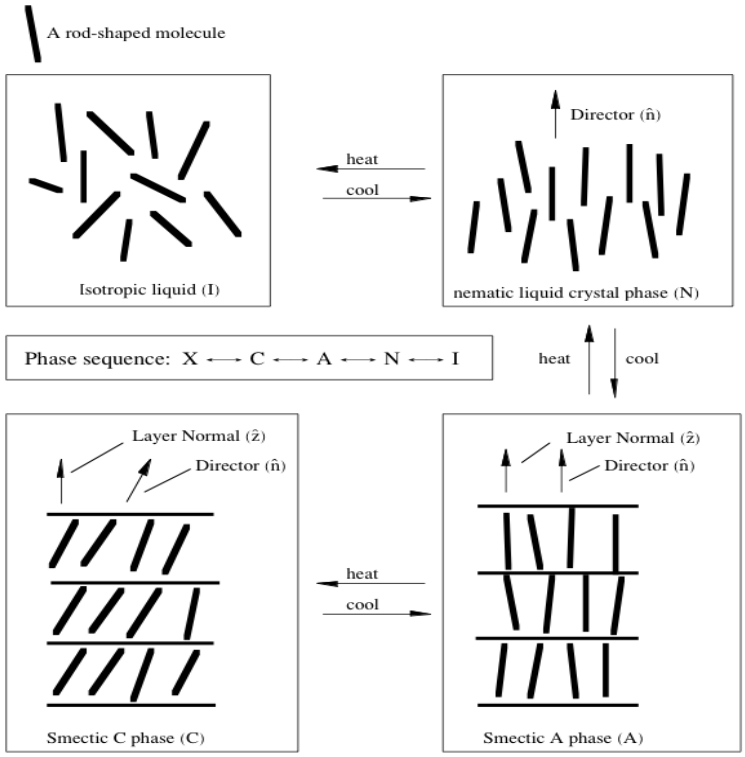

Figure 2.1: Temperature dependent phase transitions in a thermotropic LC that can occur between the isotropic and crystal state from [23]. The cooler the LC is the more ordered the molecules become.

The molecular shape for mesomorphism to occur must be geometrically anisotropic; most commonly in thermotropic phases the molecules are rod-shaped, but can also be disc-shaped. The most important feature of LCs is orientational order. In the nematic phase the LC molecules have an average direction called the LC director. LCs therefore posses anisotropic physical properties, meaning they react differently to electric fields, magnetic fields and shear depending on the direction. If the molecule can be freely rotated around the long axis, i.e. no preferred direction for the short axes, then the LC will usually be uniaxial and will therefore be birefringent [24]. Nematic LCs have been the most common choice due to high birefringence. An externally applied voltage can control the orientation of the molecules. If the incident light is polarised linearly, then

the orientation of the molecules will affect the refractive index the light is subjected to. Typically the light will be polarised along the LC's extraordinary axis.

There are a huge variety of cells that can be created, but the common choice for the use in LC lenses is the homogeneously aligned nematic LC cell with positive dielectric anisotropy. The LC is sandwiched between two glass substrates. These substrates are lined with a transparent conductive film and an alignment layer. Without an external field the alignment layer determines the orientation of the LC molecules. Rubbing the alignment layer produces grooves along the rubbing direction that control the orientation of the LC molecules. When an external electrical field is applied the molecules reorientate themselves parallel to the field, for positive dielectric, or perpendicular to the field, for negative dielectric. The field-induced reorientation is called the Freedericksz transition [20].

2.1.1 Ferroelectric Liquid Crystals

A twisted nematic LC has in the past been the most common choice for polarisation switches in LCD displays and adaptive optics [25, 26]. However, the FLC is also popular due to its faster response time [27, 28]. FLCs are now being used as optical switches [29, 30], tunable filters [31] and phase shifters [32].

The FLC modulator can be viewed as a wave-plate whose extraordinary axis corresponds to the orientation of the LC director. The LC director switches between two orientations with a relative angle θ when the sign of the addressed voltage changes. For the standard configuration, the FLC modulator acts as a half wave-plate (i.e., it introduces a phase shift $\phi = 180°$), and the orientation of the LC director switches with a relative angle $\theta = 45°$ [33].

The LC in the FLC cell is a thermotropic phase called smectic C* or chiral smectic

C. Due to the symmetry of the phase it was deduced, in 1971, that there must be polar order and hence it has to be ferroelectric [34]. The smectic C* phase is the most ordered of all LC phases wherein no nearest neighbours are invariant in time (i.e. true "monomeric" liquids). The C* phase has molecules randomly positioned in equally spaced layers. Thus, the C* phase consists of a stack of true two dimensional liquids; within the layers the centres of the rods move as an isotropic two dimensional liquid, but motion across layers is much less free [23]. The C* phase alignment in an FLC cell can be seen in figure 2.2.

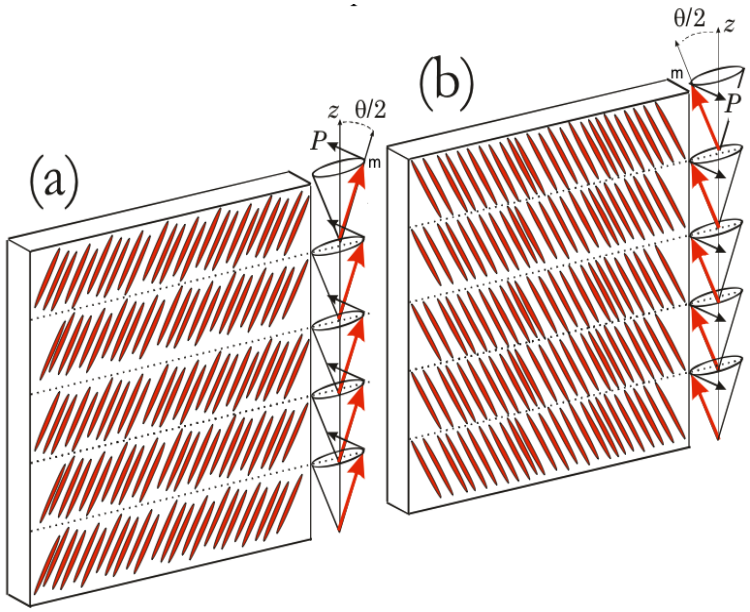

Figure 2.2: SSFLC illustration depicting the two possible molecular orientations and the resulting direction of the polarisation; from [33].

In general, the molecular chirality results in the formation of a helical structure. The molecular director describes a rotation on the surface of the smectic cone defined by the normal to the LC layers and with a tilt angle $\theta/2$ [31], which cancels the average polarisation. The helix is removed in the surface stabilised ferroelectric liquid crystal (SSFLC) by having a cell thickness of the same order as the helical pitch, forcing the LC

molecules to lie parallel to the surface plane. A net spontaneous electrical polarization, P, appears in the direction perpendicular to the surface plane, given by the vectorial product of the cell normal (z) and LC director (m), $z \times m$ [25]. Two orientations are possible, corresponding to the possible orientations of the molecules. They can be switched with the application of an electric field in the direction perpendicular to the surface, created by transparent electrodes coated to the surfaces. The polarisation direction of the cell is reversed when the electrical field is reversed. The total resulting angular rotation of the director is therefore θ.

For LCs in general, the effective refractive index experienced by a normally incident light polarised parallel to the orientation of the aligned molecules is

$$n(\gamma) = \frac{n_o n_e}{(n_e^2 sin^2\gamma + n_o^2 cos^2\gamma)^{1/2}}, \tag{2.1}$$

where n_o, n_e are the ordinary, extra-ordinary refractive indices and γ is the angle between the wave vector of the light ray and the optic axis.

. The induced phase retardation of the light beam is then

$$\phi = \frac{2\pi}{\lambda} \int_0^d n(\gamma) dt, \tag{2.2}$$

where d is the thickness of the LC layer [35].

Figure 2.3 shows the standard operational mode of the FLC. The angle that the molecules rotate by is 45°. If the FLC is in state 1 as in figure 2.2a) and the polarised light is parallel then the light passes through unchanged. If the electrical field is reversed, then the molecules rotate to state 2 in figure 2.3b). The FLC acts as a half-wave plate and rotates the polarisation by 90° [33].

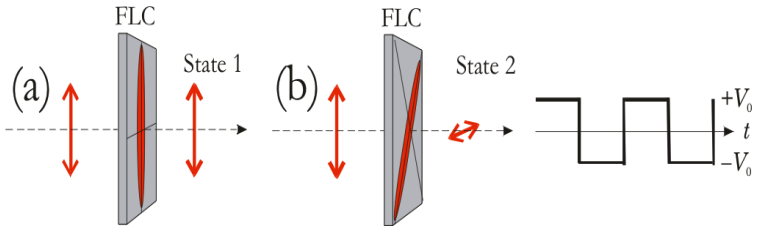

Figure 2.3: Example of the SSFLC in operation. In a) the molecules are parallel to the polarisation and therefore do not change the polarisation orientation. In b) the molecules are at a 45° angle to the polarisation due to the electric field being reversed. The polarisation is rotated to horizontal; from [33].

2.2 Adaptive Liquid Crystal Lenses

2.2.1 Curved Cell Gap Lens

The first recorded account of a tuneable lens made of LCs dates back to 1977, where a curved cell gap was used [36]. A curved cell gap is created by simply using glass surfaces that are concave or convex, as shown in figure 2.4. When there is no external voltage the focal length of the cell is polarisation dependent. Polarisation parallel to the LC director is called the extra-ordinary ray and polarisation perpendicular to it is the ordinary ray. The focal length, f, of the cell is therefore dependent on the radius of curvature of the cell, R, the refractive index of the cell, n_{LC}, and that of the glass substrates, n_g,

$$f = R/(n_{LC} - n_g). \tag{2.3}$$

If the external field is turned on, the refractive index of the cell has range limited by extraordinary and ordinary indices, hence $n_e \leq n_{LC} \leq n_o$. For polarisation along the extraordinary axis, $n_{LC} = n_e$ for $V = 0$ and $n_{LC} = n_o$ for $V \to \infty$ [37].

The creation of this cell is very simple and it is easy to produce, however it does have

some problems. A curved cell varies in thickness radially resulting in a nonuniform electric field. In consequence the refractive index also varies radially. The difference in thickness also means that the response and recovery times vary.

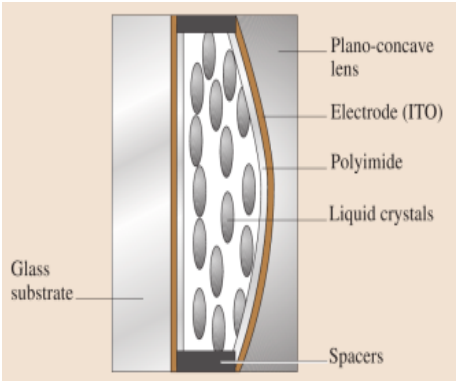

Figure 2.4: Cell structure illustration of a curved cell gap lens from [37].

2.2.2 Line-pattern electrode Lens

The majority of modern LC lenses use a planar cell gap to create a gradient refractive index profile within the LC cell [20]. One method used is to create patterned electrodes, examples of which are line-, hole- and Fresnel patterns. As shown in figure 2.5 we can see that such a cell consists of an LC placed between a ground electrode plate and a glass plate with an electrode pattern.

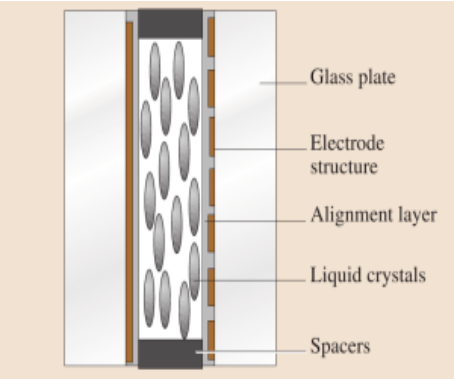

Figure 2.5: Side view illustration of a planar cell gap with line-pattern electrode structure from [37].

In the case of a line pattern the electrode voltages are individually controlled such that the refractive index forms a parabolic shape across the cell creating a phase transformation equivalent to a cylindrical lens. Two cells with orthogonal arrays of electrodes would produce a phase transformation of a spherical lens [38]. The refractive index must be at a maximum when $r = 0$, $n_C = n_e$. At the edge of the cell, the refractive index is an intermediate value, n_E, where the value range is $n_o \leq n_E \leq n_e$. The focal length of such a lens is determined by

$$f = \frac{r_0^2}{2d(n_C - n_E)}, \tag{2.4}$$

where r_0 is the aperture size, d the cell thickness. The focal range of the lens is therefore dependent on the birefringence of the LC. The aperture size of the lens is of importance as well. For large aperture sizes the focal power will be significantly reduced. High birefringence or cell thickness could compensate for this, but increasing cell thickness increases response time and LCs with very high birefringence have high viscosity also resulting in slow response time. Of course for very thick cells alignment of the molecules is non-uniform as well [39]. LC lenses based on this technique are therefore much more suited to being used as microlenses [20].

2.2.3 Hole patterned

A hole-patterned electrode has also successfully been used to create an LC lens [40]. Using an electrode with a hole in produces an axially symmetric, continuous inhomogeneous electric field. Figure 2.6 illustrates a side-view of the hole-pattern electrode structure. The angle between the cell normal and the electric field increases from the centre to the edge.

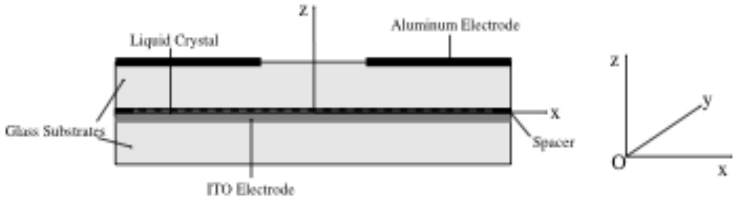

Figure 2.6: Side-view of a hole-electrode LC lens, showing the individual layers and electrodes; from [40].

A gradient refractive index is produced across the hole with the maximum value at the centre and the minimum value at the edges. An increase in voltage reduces the gradient of the refractive index increasing the focal length and as the voltage further increases the LC cell becomes a diverging lens [40].

Hole electrode LC lenses have been manufactured that have a wide range of optical power. The aperture size of these lenses is limited though and they require a high voltage to operate correctly.

2.2.4 Fresnel/Diffraction liquid crystal lens

Rather than using simple line electrodes to control the LC it is possible to create a much more complex circular pattern to create an LC diffraction lens. In this case discrete ring electrodes have been used to produce a Fresnel zone pattern.

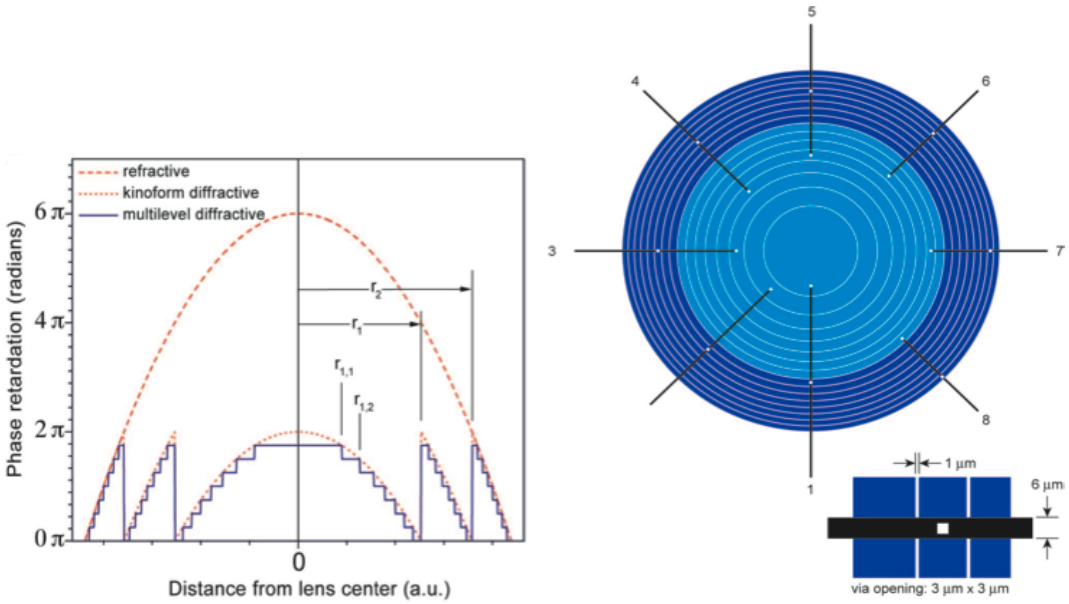

(a) 4th-level approximation of a diffractive lens

(b) Layout of a one-layer electrode pattern

Figure 2.7: Designs for an LC diffractive lens from [41].

An example of a diffractive lens using a one-layer patterned electrode is detailed here with figure 2.7 showing electrode pattern designs [41]. The lens is based on changing the refractive index of a $5\mu m$ thick nematic LC layer using a circular array of transparent electrodes. The outer radius of each zone is given by

$$r_m = \sqrt{2m\lambda f}, m = 1, 2, ..., M, \tag{2.5}$$

where m is a counting index that refers to successive Fresnel zone starting in the centre, λ is the wavelength, and f is the focal length. Each zone needs to be digitised, so the zone is broken down into further subzones with a series of discrete phase levels

$$r_{m,n} = \sqrt{2[(m-1) + n/L]\lambda f}, n = 1, 2, ..., L, \tag{2.6}$$

where L is the number of phase levels per zone and n is the counting index of the

individual phase levels. The diffractive efficiency increases by increasing the number of subzones. The diffractive efficiencies for 2, 4 and 8 subzones are 40.5%, 81.1% and 95%. In this example a phase map is obtained from the wavefront generated by the first-diffracted order by using a phase-unwrapping algorithm. From this phase map the focal length of a diffractive lens is calculated by using,

$$f = \frac{r_0^2}{2\mathrm{OPD}}, \tag{2.7}$$

where OPD is the peak-to-valley optical path difference from the centre to the edge and r_0 is the test area of the lens [41].

These kind of diffraction lenses have shown great potential. They have been produced with high diffraction efficiency, high optical quality and fast response time [20]. Their design is somewhat more complex than the other lenses due to the sophistication of the electrode pattern. However, they have been produced with large apertures and have been used by PixelOptics to produce focus variable corrective glasses that could revolutionise the industry [19].

2.2.5 Modal liquid crystal lens (MLCL)

The defining feature of an MLCL is the high resistance electrode and the low resistance control contact. The type of lens is determined by the contact configuration. To obtain a spherical lens an annular contact would be used and in the case of a cylindrical lens two linear parallel contacts would be used (see figure 2.8).

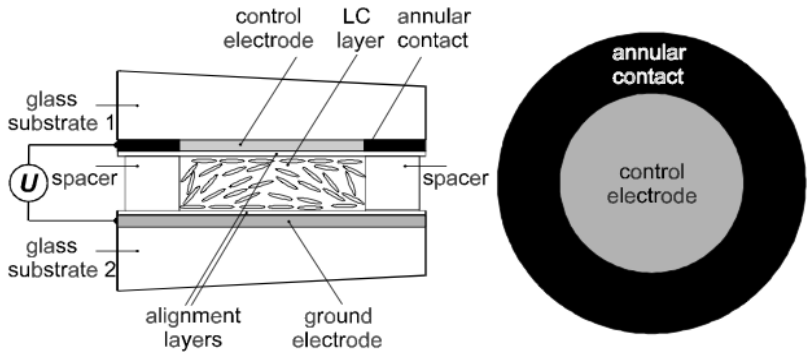

Figure 2.8: Layout of a modal LC lens. One can see the individual molecules have different alignment across the slice indicating a radial change in refractive index; from [42].

The control voltage is applied to a low resistance annular electrode around the active area of the lens. The voltage across the lens decreases radially towards the centre of the lens, because of the potential divider that is formed by the high resistance control electrode and the capacitance of the LC layer. Conversely, the optical path length of the LC layer increases from the periphery to the aperture centre.

The lens uses the electronic response of the LC to an AC field. The change in voltage at the centre of the control electrode lags behind the change of the voltage applied to the contact electrode occurring due to the resisitive-capacitative nature of the cell. The delay increases as the voltage frequency increases reducing the rms voltage at the centre of the aperture. At the same time the refractive index increases from the edge to the centre forming a phase profile of a lens. The phase profile of the lens is determined by the amplitude and frequency of the applied voltage. While this may offer additional freedom in optimising the lens, the amplitude and frequency have to be selected very carefully. The reason for this is to minimise phase aberrations caused by undesirable distribution of the electric field across the aperture and the nonlinear electro-optical response of the LC against the applied field.

MLCLs can be created simply and have shown to smoothly change the focal length by controlling the amplitude and frequency of the applied AC voltage. Such lenses have been able to change focal power between 0-3D. The MLCL focal length can be evaluated by equation 5.1. While the possibility of using both the amplitude and frequency of the applied voltage could offer more freedom to optimise the lens, there is the drawback that only specific combinations are possible that produce minimal phase aberrations.

2.2.6 Ferroelectric Liquid Crystal Lens

The FLC lens used in the projects discussed in this thesis was created by Nishimoto [43]. The lens consists of three components: a linear polariser, an FLC and a birefringent lens as shown in figure 2.9. This lens is different from all the other aforementioned lenses due to it being a focus switching lens and not a focus variable lens. It does not possess a range of focal lengths, but has exactly two that are dependent on the birefringent lens used. In this case the LC is used simply as a polarisation switch and all the molecules have the same orientation across the cell, as described in section 2.1.1. The focal lengths are therefore given simply by the standard lens equation,

$$f = R/(n-1), \tag{2.8}$$

where n is the ordinary or extraordinary refractive index of the birefringent lens.

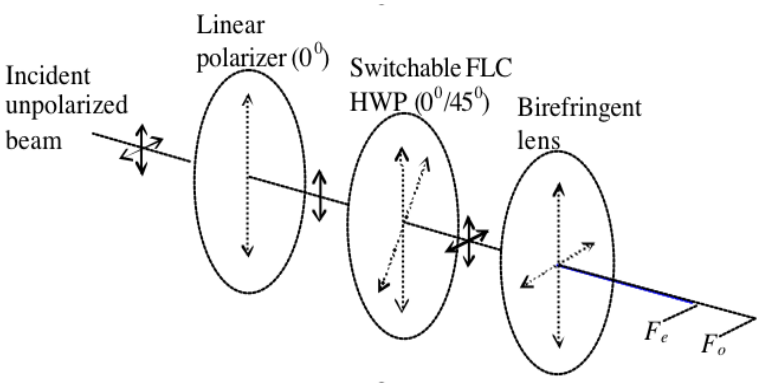

Figure 2.9: Illustration of an FLC lens from [44].

Figure 2.9 illustrates how the FLC controls the polarisation of the propagating light and therefore controls focal length of the system.

The advantages an FLC lens has over some of the other variable lenses is that the image quality obtainable would be better due to the focusing being done by a fixed lens. It would also be possible to work with high optical power and complex lens surface geometries. The design and production of this lens is less complex than some of the variable lenses mentioned before, which could make them a cost effective solution for optical systems.

2.3 Adaptive Liquid Lenses

In addition to LC lenses there are four types of liquid lenses, based on the operation mechanism: fluid membrane interaction, electrowetting effect, dielectrophoretic effect and thermal effect. The different types are described below.

2.3.1 Liquid filled membrane lens

The fluid membrane lens design and operation is described in figure 2.10. A lens based on fluid-membrane interaction consists of a liquid that is contained by two elastic membranes or one membrane and a glass plate. In such a lens the focal length is dependent on the pressure of the liquid. As the liquid pressure changes so does the shape of the membrane/s. There would typically be a small reservoir attached to the lens from which the liquid can be pumped in and out. A simple example of a reservoir would be a syringe pump. The cost of manufacturing these lenses can vary significantly depending on the complexity of the design [45, 18].

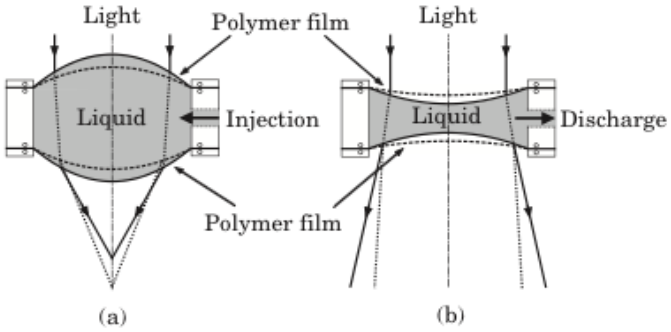

Figure 2.10: Illustration of a liquid fillled lens with membrane from [46].

2.3.2 Variable focus electrowetting lens

An example of electrowetting is shown in figure 2.11. The cell contains two liquids, one is insulating and non-polar (marked as '1') and the other is a conducting water solution (marked as '2'). The liquids have to be non-miscible [47]. The insulating liquid sits naturally on to a window specifically chosen to be hydrophobic. A counter-electrode to the conducting solution is placed on the external side of the window. The fringing field at the corners of the electrolyte droplet tend to pull the droplet down onto the electrode, lowering the macroscopic contact angle and increasing the droplet contact

area. Application of a voltage between the counter-electrode and the conducting liquid favours the wettability of the surface by the same liquid. The outer zone is treated to be hydrophilic to ensure the droplet maintains shape A even when no voltage is being applied. The typical aperture size for an electrowetting lens is around 3 mm, so it is very small. This technique has been used by VariOptic [16] to produce high quality microlenses that are now being used in smartphone cameras.

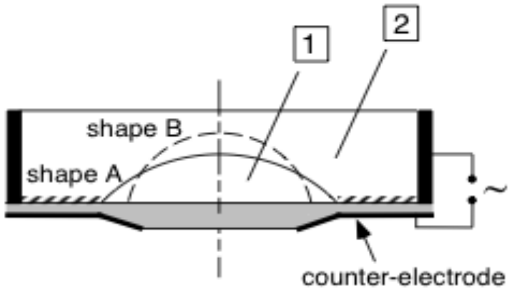

Figure 2.11: Liquid lens using the electrowetting effect containing two liquids, (1) being the insulating liquid and (2) being the conducting liquid from [47].

2.3.3 Dielectrophoretic Liquid Lens

The operation of lenses based on the dielectrophoretic effect have similarities with lenses based on electrowetting as they both use one or two immiscible liquids. A dielectrophoretic force is exerted on the liquid by a nonuniform electric field. In a nonuniform electric field the liquid preferentially collects in the regions of maximum field intensity. This implies that the dielectrophoretic effect can be used to control small amounts of water using specially designed electrodes. This does have the drawback that the aperture size of these lenses will be very small. In this case the liquid does not have to be conductive; when two liquids are used the dielectric constant must be different. The lenses created vary mainly in how the inhomogeneous electric field is generated. Figure 2.12 illustrates such a lens from [48]. Two liquids were used with differing dielectric values. The focal length range for these lenses is very small, usually only a

few millimeters and to do this requires a considerable voltage range of 0-200V in some cases. The fall time of the droplet is also usually longer than the rise time.

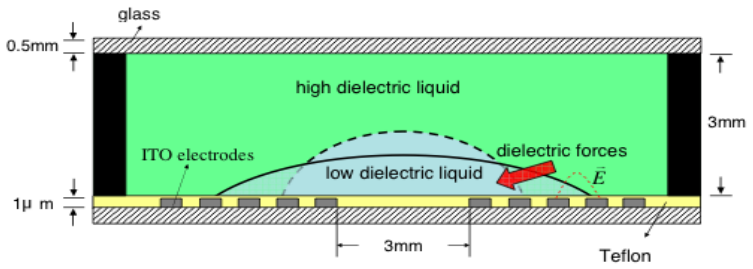

Figure 2.12: Liquid lens using the dielectrophoretic effect containing two liquids with different dielectric values; from [49].

2.3.4 Thermal Liquid Lens

Thermal effect lenses are made of thermal-responsive hydrogel to regulate the curvature of a liquid-liquid interface shown in figure 2.13. Similar lenses have been created using pH- and light-responsive hydrogels. A hydrogel ring is used to control the curvature of a liquid-liquid interface. The hydrogel is placed within a microfluidic channel system that is contained by a glass substrate on the bottom and an aperture plate on top. The bottom half is filled with water, while the top half is filled with oil. A meniscus forms at the aperture through the interface of the water and oil that is used as a microlens [50, 51].

As the hydrogel is stimulated the ring will contract or expand, changing the water volume and hence the pressure at the aperture. The contact line of the meniscus interface is pinned at the hydrophilic-hydrophobic boundary, so the change in pressure causes a change in radius of curvature, which determines the focal length of the microlens

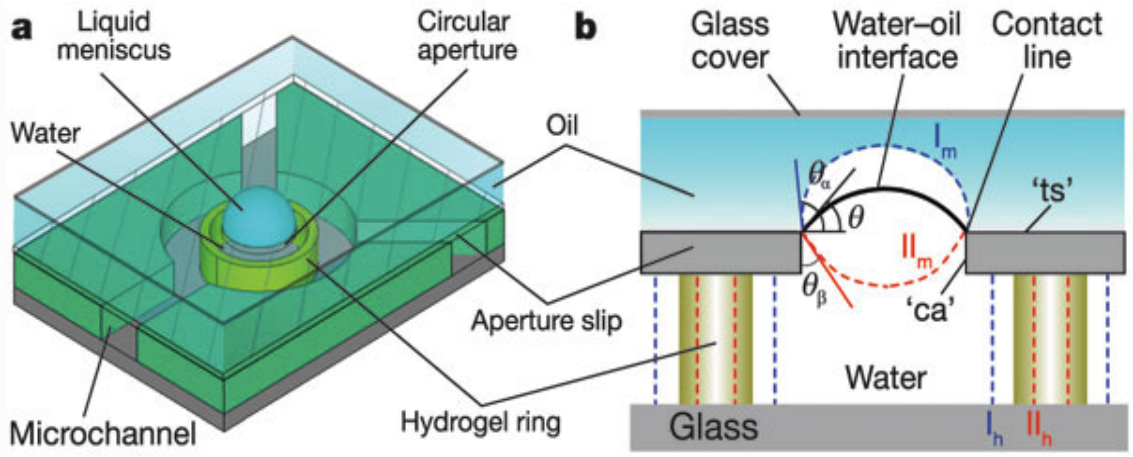

Figure 2.13: Thermal lens illustrations showing the components in detail. b) shows the possible positions of the water-oil interface. When the hydrogel expands to the size indicated by I_h the contact angle increases due to the increase in water pressure, creating a convex lens. When the hydrogel shrinks to II_h the contact angle decreases with the water pressure, producing a concave lens; from [52].

Chapter 3

Vision Science

This chapter provides a review of a number of fields in vision science. In order to use adaptive optical devices in vision science a better understanding of the fields in which they will be tested needs to be gained. In the first section we discuss the method of visual acuity testing and a person's ability to perceive change in focus. The second section reviews the different modern instruments that are used to analyse the optic nerve and retina. A detailed description of glaucoma and its progression is also provided. The third section reviews involuntary eye movements and the potential for imitating such movement to improve the perception of images with low spatial frequency.

3.1 Measuring Visual Acuity

Glasses and contact lenses are the most common form of visual acuity correction around the world. A study in the Netherlands shows that at the age of 30 four out of ten people wear glasses and that from the age of 55 almost everyone wears glasses or contact lenses [53]. At the optician's an eye examination consists of a standard series of tests, one of which is a chart reading test (Snellen Chart) [54].

It is clear that the correction of the refractive error in the human eye will provide a

significant improvement to an individual's quality of life and research has shown that uncorrected refractive error can be a cause of blindness and a major cause of impaired vision. The World Health Organisation (WHO) found that there were around 300 million people visually impaired or blind due to uncorrected refractive error [55].

The measurement of visual acuity serves many purposes. While it is commonly associated with the determination of lens correction for refractive error, it is also used to monitor visual degeneration and to assess the ability to undertake visually intensive occupations and tasks such as driving and flying [56].

A typical Snellen chart and common chart variations are shown in figure 3.1. "Normal vision" is described to be the ability to read the letters at a distance of 20 feet when they subtend an angle of 5 minutes of arc. This corresponds to the 20/20 vision mark on the Snellen chart. This level of vision is marked as being the limit with which one can cope well enough in school or industry and therefore does not require correction [57].

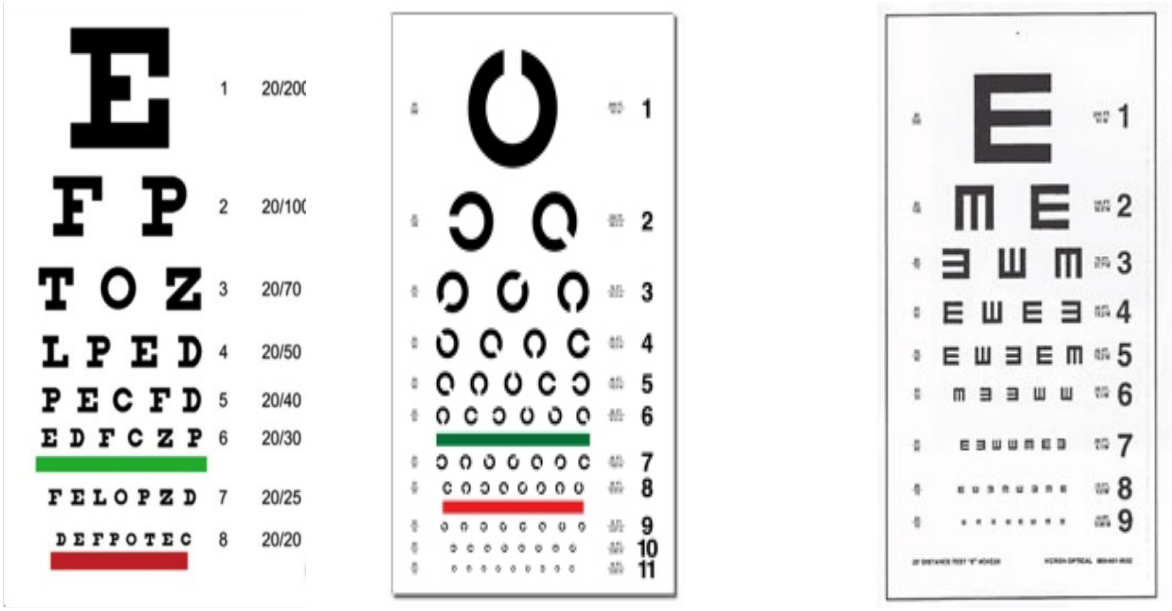

(a) Snellen Chart (b) Landolt Rings (c) Tumbling E's

Figure 3.1: Visual acuity chart types from [57].

Upon analysing patients reading the Snellen chart the conclusion was made that the letters were not equally recognisable. For this reason in 1988 Landolt proposed just using one symbol; a ring with a break in it. As shown in figure 3.1b the break in the ring is positioned differently for adjacent rings. A patient is required to determine the direction that the break in the circle is pointing. The use of this chart for visual acuity research was deemed the purest standard by the International Council of Ophthalmology [58].

The tumbling 'E' chart was created in 1976 initially to test the visual acuity of illiterate people and those unfamiliar with the Roman alphabet. Studies discovered that grating recognition and orientation is in fact superior to letter recognition in foveal and peripheral vision [59]

Overall the chart reading test at the optician's has proven itself to be a highly successful method to determine the refractive error of the human eye and hence the required prescription that a patient might need. However, the procedure and method of this test has not changed significantly for decades and the results are still heavily reliant on the patient to detect defocus when viewing the letters on the chart.

3.1.1 Defocus Perception

There has been a lot of research into the perception of defocus [60, 61]. Some research focused on quantifying the perception of edge blur in particular [62, 63], and some focused on detecting change in defocus in general [64, 65, 66]. Other factors on blur perception such as contrast [67] and spatial frequency [68] have also been analysed. A series of papers on blur discrimination were reviewed by Watson and Ahumada [69] with a comparison of the results.

Ciuffreda [61] analysed defocus at levels where it becomes 'bothersome'. The minimum amount of 'bothersome blur' is the point at which the blur demands initiation

of an eye and head movement to see clearly again. The procedure in the test used a moveable target that would gradually move between in focus and out of focus. The results in figure 3.2 show the diopter values indicated by the test patients of noticeable, bothersome and irreversible blur. They show that each target type has a significantly different result. The 20/50 'E' has smaller defocus values than the 20/200 'E' showing it is important to use objects that have a higher dominant spatial frequency to detect smaller changes in defocus. Similar findings were made in [66].

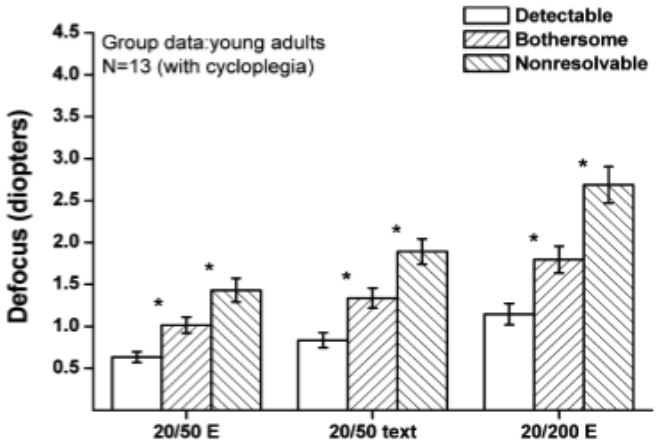

Figure 3.2: Blur thresholds for young adults as a function of target type and blur criterion used from [61]. Plotted is the mean (±1 S.E.M.)

Wang and Ciuffreda worked on a series of papers investigating other factors influencing blur discrimination [11, 12, 13]. The results for each paper were obtained using the same optical system shown in figure 3.3.

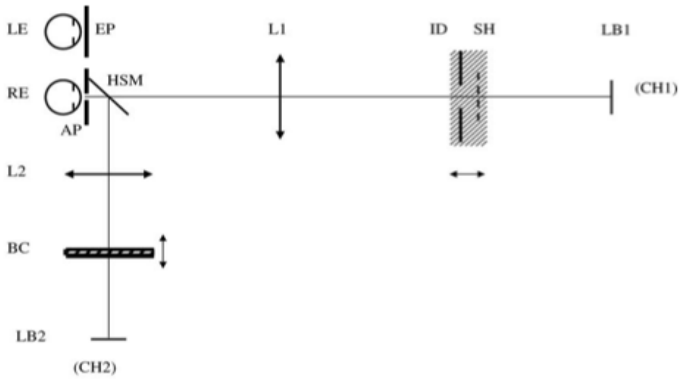

Figure 3.3: Schematic representation of the apparatus from [66]. Symbols: CH1, test target channel; CH2, fixation target channel; RE, right eye; LE, left eye; EP, eye patch; AP, artificial pupil; HSM, half-silvered mirror; L1, Badal camera lens system; L2, Badal ophthalmic lens system; ID, iris diaphragm; SH, slide holder; BC, black cross; LB1, light box 1; LB2, light box 2

The depth-of-focus of the human eye was analysed [11], focusing on the fovea and near retinal periphery. The depth-of-focus was determined by positioning the target at the far point of the eye and then moving it slowly away or towards the patient at a speed of 0.1D. The patient would then stop the moving target upon detection of blurring. The peripheral depth-of-focus was obtained by having the patient observe the focus of the edge of a circular aperture while attending to a central cross. The angular size of the aperture range from $0.5° - 8°$. The range of the periphery was chosen due to the area likely being of importance to blur discrimination. The results showed that the depth-of-focus increased linearly from 0.89D at the fovea to 3.51D at a retinal eccentricity of $8°$.

Four mechanisms are suggested that possibly have an effect on the near peripheral depth-of-focus, hence defocus discrimination:

- **Neurophysiological**: The densities of the retinal cone cells and retinal ganglion cells decline with eccentricity. However, the effect of retinal eccentricity on the cortical neuronal response remains to be investigated.

- **Sharpness Overconstancy**: An edge that is observed to be blurry when looking at it directly (foveally), appeared sharp when the observer looked away from it (non-foveally). It is speculated that the human brain assumes an edge should be sharp. When a blurred edge is perceived in the periphery the image is a combination of the information from the eye and the brain. The implication would be that more blur would be required for it to be noticeable in the retinal periphery.

- **Visual Optics**: The optical quality of the human eye is worse in the periphery as compared with central vision. Both monochromatic and chromatic aberrations have been shown to increase with retinal eccentricity. Within the foveal and near retinal periphery these factors are likely to have only a small effect on image degradation.

- **Visual Attention**: Studies have suggested that visual attention became compromised with increased eccentricity. This could have an effect on the blur sensitivity of the retinal periphery.

A separate study was made to specifically investigate blur discrimination [13]. Using the same optical set up the target was again positioned at the far point of the patient's eye. The target would then be slowly moved towards or away from the patient's eye. The point at which the patient detects initial blurring is noted down. From that point the target moved in the same direction again until a further change in blur is noticed. This procedure was repeated until the target was too defocused to be visible. The results can be seen in figure 3.4.

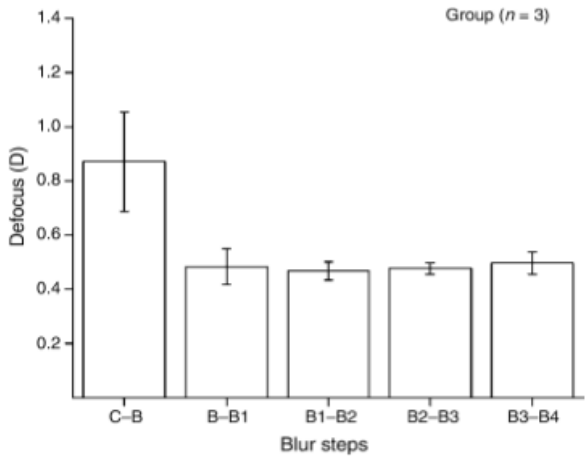

Figure 3.4: Group mean defocus (±1 S.E.M.) as a function of blur step from [13].

It is very clear that the blur detection threshold (C-B) is much higher than the blur discrimination values. What is interesting to note is that the blur discrimination has an almost constant value with the variability across the test subjects also significantly smaller than for the blur detection threshold. The blur detection threshold result is in agreement with findings by other researchers, but the consistency of the blur discrimination value appears to be somewhat unique [70, 65]. A more common 'dipper function' appears with a minimum occurring for just out-of-focus targets [70, 69].

Three reasons are proposed to explain the difference in blur detection and blur discrimination.

- **Near-focus plateau of a defocused optical system**: At near focus the reduction of the ocular modular transfer function (MTF) is very small. When the target is placed more out of focus the reduction of the ocular MTF increases.

- **Interaction between contrast discrimination and ocular MTF response to defocus**: It was assumed that the sensitivity to contrast change increased when retinal defocus reduced the retinal MTF amplitude from the blur detection level to the initial blur discrimination level; explaining a greater blur detection

threshold. Low spatial frequencies have been found to be more robust to defocus. The ocular MTF decrease would therefore become smaller and smaller. The increase in contrast discrimination and the resistance of low spatial frequencies to defocus would therefore keep the blur discrimination at a constant level.

- **Blur Buffering Mechanism**: A 'neural sharpening mechanism' was theorised by Jacobs *et al.* [71] that indicated the brain acted to maintain the focus of a target in near-focus positions. This mechanism would be similar to the sharpness overconstancy effect in near-foveal vision.

There is general agreement that blur discrimination is easier for targets that are slightly out of focus. There are several reasons that have been speculated that cause this, but there is currently no unified theory. Watson and Ahumada have used a visible contrast energy (ViCE) model to describe the blur discrimination of edge blur from a series of past papers [69]. However, the model as of yet has not been confirmed to successfully describe blur discrimination for more complicated targets.

3.1.2 Contrast Sensitivity

As previously mentioned it is well known that defocus has a detrimental effect on contrast sensitivity. It is however important to note that contrast sensitivity is also dependent on the spatial frequency and temporal modulation of the observed target [68].

The contrast sensitivity dependence on spatial frequency can be seen in figure 3.5. One can clearly see that the low and high spatial frequencies are difficult to spot at low contrast while it is still possible to see the grating for the medium spatial frequencies.This was first demonstrated by Cambell and Robson [72].

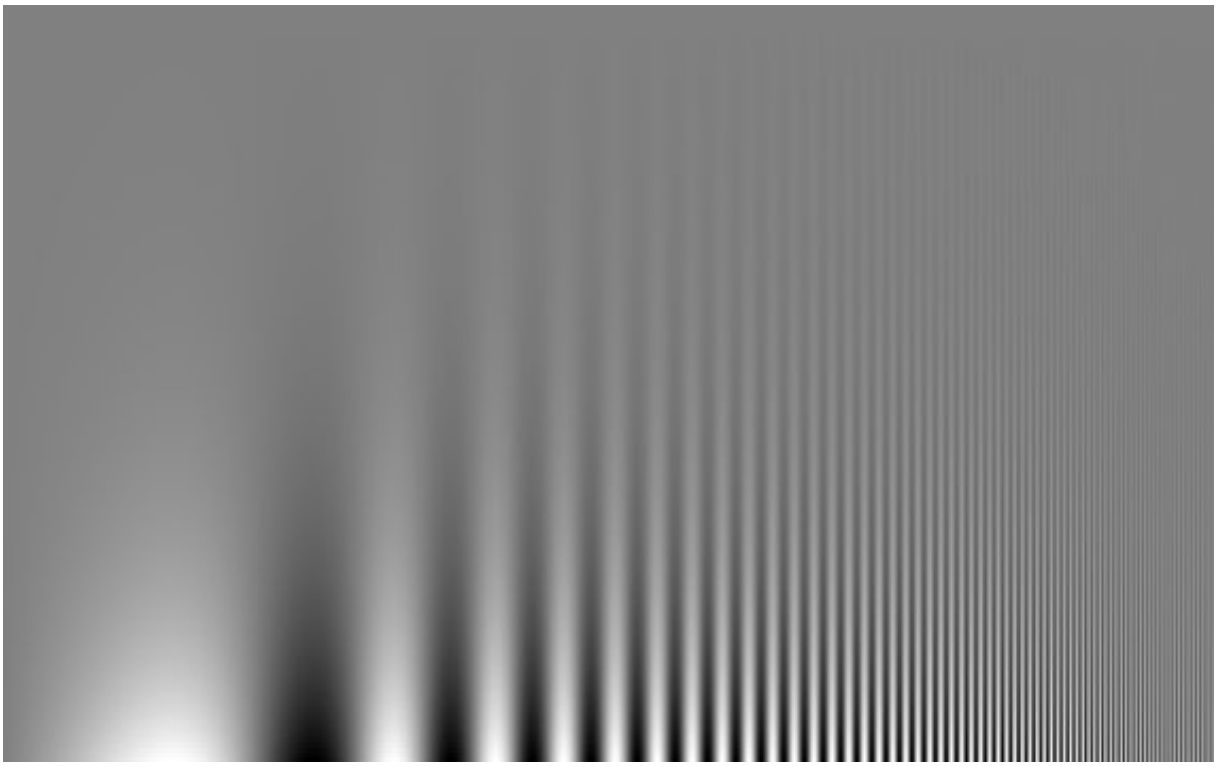

Figure 3.5: Cambell-Robson Contrast Sensitivity Chart from [73].

Previous research has shown that high spatial frequencies are much more sensitive to changes in defocus than low frequencies [70]. This would imply that there would be an optimal spatial frequency where contrast sensitivity and blur discrimination can be maximised.

3.2 Retinal Imaging

A person's visual performance is dependent on the health of each component in the eye and as such the retina of the eye must be checked regularly. Retinal imaging is of great importance, as it is useful for examining a whole range of retinal problems and diseases. Examples of these problems are macular degeneration, diabetic retinopathy, drusen, neovascularization, retinal detachment and glaucoma. Common technologies

used for imaging the optic nerve head (ONH) are fundus photography, confocal scanning laser ophthalmoscopy (CSLO), scanning laser polarimetry (SLP) and optical coherence tomography (OCT). The more accurately an optometrist can view the retina the easier it is to diagnose the problem and also detect these problems at an early stage of development [74].

3.2.1 Optic Nerve Head

The majority of glaucoma patients suffer from primary open-angle glaucoma (POAG). In POAG degradation of the ONH typically precedes any detectable change in visual field meaning detailed analysis is of great importance. Characteristics of a glaucomatous ONH are for example enlargement of the cup, disc haemorrhage, thinning of the rim and loss of nerve fibre layer. By the time the change in visual field is noticed it is too late to prevent long term damage. With accurate imaging of the optic nerve it would be possible to identify early signs of glaucoma and take steps to prevent its progression. The ONH is a slight oval shape and is on average 1.76mm$\times$1.92mm, with a depth less than 1mm. Due to its size it is difficult to analyse. The retina is not designed to reflect light, so a lot of light is needed to illuminate the inside of the eye [75]. Due to the difficulty of viewing the ONH there are often discrepancies in the observations.

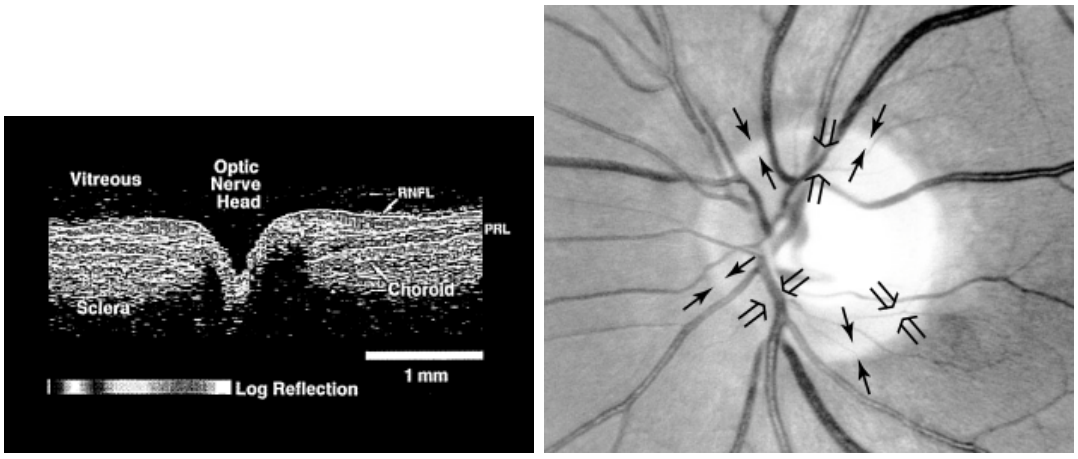

(a) Optical coherence tomograph of the optic nerve head taken perpendicular to the papillomacular axis, from [76].

(b) Normal optic nerve head - scleral rim (arrows), neuroretinal rim thickness (open arrows), from [75].

Figure 3.6: Optic Nerve Head Images.

An enhanced photograph of the normal ONH and a tomographical image is shown in figure 3.6. The key features of the ONH are the cup, the neuroretinal rim and the scleral ring. It is crucial to be able to detect any change in these features, particularly the ratio of cup size to ring size (C/D ratio). The C/D ratio is often used to detect glaucoma. However, picking out specific parts of the ONH can be difficult. On top of the difficulty to pick out the features, the ONH area can vary up to 7-fold in size amongst individuals. For this reason it is possible for an examiner to mis-interpret the size of the neuroretinal rim, hence the C/D ratio. The neuroretinal rim area (NRA), related to the C/D ratio, is one of the most important parameters for the observation and detection of glaucoma. Research has shown that the NRA correlates highly with ONH damage [77]. There is also evidence the the cup size is related to the disc diameter [78]. It is therefore possible for mis-interpretation to occur due to large discs.

3.2.2 Imaging Technologies

The development of new technologies has partially been fuelled by the lack of inter-observer and intraobserver repeatability when determining the C/D ratio. It has in the past been reliant on observer experience, whereas more recently a more objective measurement can be made, thereby increasing repeatability.

Fundus cameras use the basic principle of indirect ophthalmoscopy, which uses a large objective lens close to the eye to improve the field of view of the image. The observer is some distance away from the patient's eye and in between the objective lens and the observer a virtual image is produced. As the retina is not a very reflective surface the fundus camera has two arms; the illumination arm and the imaging arm.

In the past such cameras have been criticised to have limitations such as limited diagnostic accuracy by itself for screening, expert grading requirement and difficulty attaining true stereophotographs in about half of subjects [79]. However, the advancements contained in the newer models enable the fundus camera to obtain similarly good diagnosis repeatability as the other technologies [80].

The CSLO device generates up to 64 transaxial scans through the ONH to create a 3-dimensional reconstruction of the tissues. Each layer is scanned, producing a 2-dimensional image. Depending on the cup depth, up to 64 successive equidistant images are obtained in order to form a 3-dimensional construct of the ONH region. Surfaces of the optic cup, optic rim, and peripapillary retina are determined by a change in reflectance intensity along the z-axis at each point. This allows for the creation of a topographic map from which parameters such as cup-to-disc (C/D) ratio, rim area, and other optic-disc parameters can be calculated [74].

The OCT obtains axial cross sections of tissues based on optical backscattering, similar to ultrasound technology. The optical backscattering of low-coherence laser light (850 nm) as it passes through layers of differing optical density is recorded by an interferometer and amplified to construct a 2-dimensional image of the scanned area. It is also possible to use the OCT to create 3-dimensional reconstructions of the ONH.

The SLP measures the RNFL thickness by assessing the change in polarization (retardation) of the reflected laser beam (780 nm). The retinal nerve fibre layer (RNFL) consists of ganglion cell axons, which cause proportional change in the polarization of the laser due to their birefringence. A high-resolution image of 256×256 pixels is created of the optic nerve and peripapillary retina [74].

A comparison of CSLO, OCT and SLP showed none of the methods was significantly better than the other for optic disc analysis and all three systems performed very highly [81].

It is important to note that these modern devices do come at a price, making them a costly solution to the problem [82]. Other cost-effective solutions should therefore be investigated that could potentially be accessible to a wider range of practitioners. Simlarly Douglas points out that the latest technologies are only available to the most affluent of practitioners and emphasises the use of more cost effective techniques [75].

3.2.3 Evaluation Reliability

Several methods have been developed to analyse the retina and the optic disc. This has partially been fuelled by the variability in the assessment of the optic disc that is even present amongst expert observers [83, 84]. The evaluation of the cup-to-disc ratio must

be reliable as it is essential to the diagnosis and monitoring of POAG. The appearance of the optic disc has a wide variability, which makes it extremely difficult to provide a diagnosis of glaucoma from one examination. Particularly for detecting glaucoma at early stages of development it is typically required to detect some form of change [79]. For this reason it is paramount that there is accurate and precise documentation of the optic disc.

A study by Spry *et al.* analysed the reliability of three different tests for monitoring and detecting glaucoma: intraocular pressure, visual field score and cup-to-disc ratio [85]. The results showed that the C/D ratio, determined from stereo disc photographs, was of least value in differentiating true variable change from measurement 'noise'. From these results it was determined that to be 95% certain that a true change has occurred a pair of C/D measurements must differ by 0.35. The accepted value of change for the C/D ratio classed as a 'clinically significant' change is ≥ 0.20. This indicates that changes of 0.2 will be missed or perceived by chance even though there is no change. As there is potential for significant variability the usefulness of disc monitoring showed clear limits, especially for cases with different observers as the inter-observer variation. It therefore indicates that it is very important that the same clinician undergoes the re-evaluation of the optic disc.

In the past there have been a few contradictory results on the improvements from stereoscopic disc photographs relative to standard clinical measure. Spry found there to be no significant improvement on the agreement of individual measurements, while other studies have shown that such photographs clearly do improve intra- and inter observer repeatability [86, 87]. Generally the conclusion is that monoscopic evaluation relative to stereoscopic evaluation of the C/D ratio has increased variability due to the boundaries having to be inferred by the observer rather than being perceived. In a report comparing clinical measurement to semiautomated measurement the conclusion

was made that a clinician would be subject to more bias than a system that has strict criteria for determining the edges of the cup and disc. The report concludes that importantly the inter observer variability of semiautomated measurements is smaller, which is essential to follow-up studies [87].

3.3 Visual Impairment

In many cases eye disease can have progressed to severe levels where prevention or correction with glasses is not possible. A study by WHO has shown that across the world there are more than 84 million people whose vision loss is uncorrectable [55]. Possible symptoms of vision loss are clouded vision, constricted fields, or large scotomas.

Currently there are very limited solutions to helping low vision patients whose visual defects cannot be corrected by standard corrective lenses. Commonly 'low-vision aids' will be simple handheld magnifiers or telescopes depending on the visual task.

In the case of clouded vision the effect is a general blurring of vision, making fine detail impossible to perceive.

3.3.1 Involuntary Eye Movement

When our eyes fixate on an object they are never truly still. These eye movements are very small and so are not perceived by us during fixation. They are necessary to prevent neuroretinal adaptation and they occur subconsciously. The consequence of neuroretinal adaptation is the loss of vision as the response of the neurones are normalised in the face of unchanging or uniform visual stimulation [88].

There are three main types of involuntary eye movement: tremor, drifts and mi-

crosaccades.

Tremor, also called physiological nystagmus, is an aperiodic, wave-like motion of the eyes with a frequency of around 90Hz. It is the smallest of the eye movements and its specific function is still unclear.

Drifts are simultaneous movements with tremor, but are slow such that a fixated object could move across many photoreceptors. Drift occurs in between the microsaccadic eye movements.

Microsaccades are fast jerky movements of small amplitude that can quickly move an image across a large amount of photoreceptors. They can have similar amplitude to small voluntary saccades. The size of the microsaccades has been shown to relate to the distance an image has drifted, acting as a fixational correction. There is strong evidence that microsaccades prevent neuroretinal adaptation.

It has been possible to track the natural motions of the eye and counteract them by moving the target accordingly. The result was that the target would fade out. In studies by Ditchburn *et al.* it was noted that the perception of a stabilised image would go through a cycle of good visibility followed by a "fade out" and then the image would re-emerge at a rate of one image every 5 seconds [89]. At the point where the image is completely faded out the individual will perceive a uniform field. The target could be regenerated very quickly by inducing fast jerky movements replicating the action of microsaccades. There has also been some evidence that microsaccades significantly enhance sensitivity to edges, re-sharpen the image and improve spatial resolution [90].

The minute eye microsaccades are sufficient to prevent fading of visual objects processed by small-sized receptive fields near the fovea, tuned to fine details, whereas the larger receptive fields in the periphery, sensitive to low-spatial-frequency images, would require large microsaccades to prevent fading. In the visually impaired, small involuntary eye movements are unlikely to be effective because the blurred low-spatial-

frequency retinal images they perceive are processed by neurons with large receptive fields.

Watson *et al.* hypothesised that microsaccades are less useful to those with central visual impairment. Such people could therefore be helped to see better through induced retinal-image jitter. Previous research has shown that image jitter typically causes image degradation rather than enhancement, which means this new theory would contradict past results. Studies have shown that reading speed [91] and visual acuity [92] are both reduced during induced image jitter. Tests provided evidence of patients having better performance in word recognition and recognising facial expressions, when the image jitters rather than when it is stationary.The jitter was of higher frequency and larger amplitude relative to standard involuntary microsaccades.

One of these experiments used people with simulated low vision and tested a wide range of jitter frequencies. Figure 3.7 shows the results, demonstrating that word recognition only improves for specific jitter parameters. For inter-jitter intervals of more than 100ms there were signs of improvement to the ability of word recognition, whereas a shorter inter-jitter interval proved to impair word recognition.

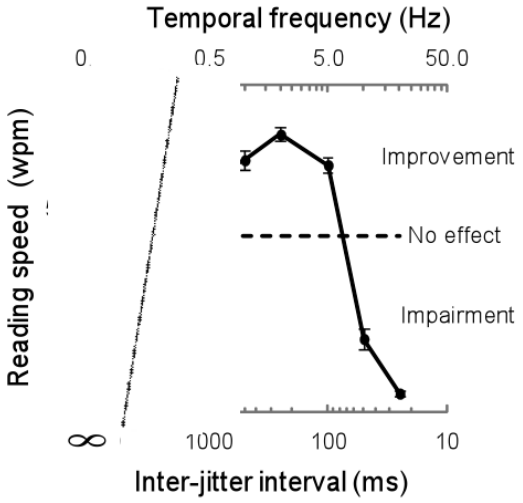

Figure 3.7: Word recognition speed as a function of inter-jitter interval duration for subjects (n=9) with simulated low vision, using Bangerter filters to reduce acuity to 1.2 logMAR. Word recognition speed improves for inter-jitter intervals of 500, 250 and 100 ms and is impaired for inter-jitter intervals of 50 ms and 25 ms. The upper horizontal axis shows temporal frequency calculated as $1/(2T)$, where T denotes the inter-jitter interval duration in seconds. Error bars illustrate SEM, from [14].

The filters used create a general reduction in visual acuity without the presence of a scotoma. One can therefore also infer from these results that the improvement in word recognition is not simply due to image shift away from a central field loss that could be present due to a scotoma on the patient's eye retina.

The seemingly paradoxical findings of enhanced word recognition speed with image jitter found here and the reduced reading speed with image jitter found in previous research can be explained by differences in the temporal characteristics of the image jitter [91, 92]. Our Control Experiment 1 showed that in simulated low vision conditions jittering text with inter-jitter intervals of 500, 250 and 100 ms (1-5 Hz temporal frequencies) enhanced the speed of word recognition, while shorter inter-jitter intervals of 50 and 25 ms (10-20 Hz) impaired performance in comparison with that for stationary text (Fig. 3).

A second experiment was designed to isolate the effect of temporal modulation on

visual sensitivity to low spatial-frequency stimuli. Patients with age-related macular degeneration were tested. Figure 3.8 shows the results for determining contrast threshold for discriminating grating orientation. The test subject was required to choose between two grating orientations (45° and -45°). The contrast threshold was determined from the number of correct and incorrect answers that the subject gave. One can see a clear improvement for contrast modulations of 5-10Hz relative to stationary stimuli.

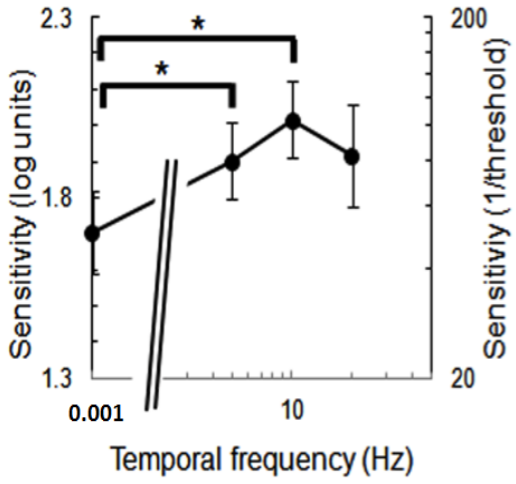

Figure 3.8: Contrast sensitivity (inverse of contrast threshold) for discriminating grating orientation as a function of temporal frequency for subjects (n=7) with age-related macular degeneration. Asterisks (*) denote significantly higher differences in contrast sensitivity at $P < 0.05$ Error bars illustrate SEM, from [14].

While these results show promising signs for using jitter to improve the visual capabilities of patients with low vision it would be of great use to produce a low vision aid that could be worn everyday. This would increase the number of options available to patients with low vision. it would be highly desirable to create an optical system that could produce image jitter of similar amplitude to that used in the experiments. Birefringent material linked with an FLC could prove a useful tool in making this a reality.

Chapter 4

Visual Acuity from Flicker

The typical method for testing blur discrimination in the past was to use a slow moving target, as mentioned in chapter 2 [61, 13]. There has also been some research into the perception of small temporal changes in focus using an oscillating target [70], but the frequencies that were analysed were limited to a range below 10 Hz.

This chapter discusses the possibility of using a birefringent lens, made from barium borate (BBO), and a ferroelectric liquid crystal (FLC) to switch between equal and opposite defocus levels to determine the optimum focus correction by making use of the human eye's sensitivity to flicker. With the use of the FLC it is possible to change focus without changing position of the target in under 1 μs, creating a close to instantaneous shift in focus. In addition it is possible to test a wide range of temporal frequencies to optimise the blur discrimination. With this technique it could be possible to more accurately determine a patient's prescription without the indecisiveness that can occur with small changes in prescription strength.

4.1 Flicker Sensitivity

In our field of view certain changes to what we see are able to capture our attention. Examples of fundamental changes are colour, luminosity and position. While we are susceptible to many different cues, the faster and more sudden a change is the more it captures our attention. For the sake of the research detailed in this thesis we will concentrate on visual field cues occurring due to change in luminosity.

Previous results have shown that dynamic luminance changes have a much greater impact on our attentional allocation than a static luminance difference of the same absolute magnitude [93]. A simple demonstration would be the case where a light is in your peripheral vision. If the light is off and then turned on the sudden change in luminosity will come to your attention. The same would happen if the light started to flicker when turned on. After the initial onset of this sudden change the flickering light would capture your attention more than the case where the light that was permanently on.

Research into the attention capture of static and flickering cues have shown that both cues lose their effectiveness over time [94]. However, while a static cue decays very quickly to a low effectiveness, the flickering cue decays much slower and retains a certain level of effectiveness for a long time. Interestingly the research showed that for the initial onset of the cue a static cue showed dominance over flicker in all the examined cases. This encouraged the conclusion that a static cue had very high initial efficiency, but decayed very quickly. After 1890 ms the flickering cue took over as the dominant cue in 90% of the cases. The effectiveness of the static cue decayed very quickly to zero, whereas the flickering cue's effectiveness declined slowly reaching an asymptote level well above zero.

There are two important factors that determine the effectiveness of flicker cues, the amplitude of the luminosity change and the temporal frequency. A greater change in luminosity will naturally attract more attention than a small change. The temporal frequency has to firstly be less than the flicker fusion frequency, which is about 30 Hz [95]. Research discussed in the same article determined a good range to be 3-10 Hz, with best results at a frequency of 4 Hz.

There is also some evidence that there are neurons selective for temporal frequency [96]. At a psychophysical level, two kinds of temporal frequency channels are evident: one broad and low-pass ("sustained") and one band-pass and high-frequency selective ("transient"). The peak of the "transient" channel is around *8-12 Hz*. This would contradict the findings previously mentioned. This could indicate that the optimal flicker frequency is dependent on the task at hand.

4.1.1 Utilising Flicker

Blur perceived by the human eye, if an object is defocused equal amounts either side of the retina, has the same shape provided the optical system is aberration-free [97]. Figure 4.1 contains images created with -1.0D, 0.0D and +1.0D, showing that the defocused images are identical. A focus switchable lens (FSL) as described in chapter 2 can be used to switch between equal and opposite amounts of defocus by placing an object between the two points of focus. The position of equal defocus would be dependent on the visual acuity of the patient looking through the FSL. A screen positioned for a patient with perfect visual acuity produces a flickering image for a patient with myopia or hyperopia, which can be corrected with the appropriate lens.

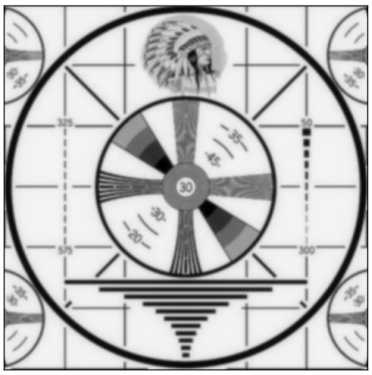

(a) 0.0D defocus

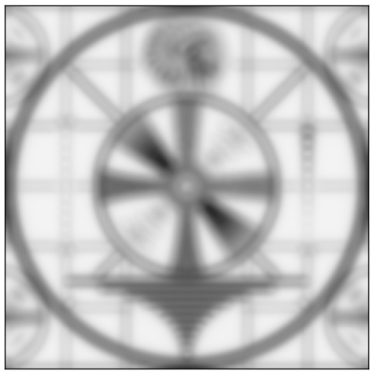

(b) +1.0D defocus

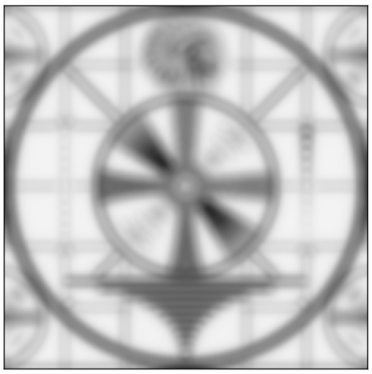

(c) -1.0D defocus

Figure 4.1: Simulated defocus effects on an object. Each image is 300×300 pixels large with a total angular size of $0.027 rad$. a) is an image of a test pattern. b) is subject to +1 wave of defocus and c) is subject to -1 wave of defocus. b) and c) appear identical.

4.2 Flicker Simulations

To simulate defocus, an in-focus image can be convolved with a pupil function containing defocus. The array made for the pupil function has to be the same size as the original image. The aperture diameter in the array was set to be half the width of the array to ensure an oversampling factor of 2.

Wavefront aberrations are commonly described using Zernike polynomials [98], and the Zernike polynomial for defocus is

$$Z_2^0(\rho, \theta) = 2\rho^2 - 1, \tag{4.1}$$

where ρ represents the radius for a unit disc, ranging from 0 to 1. The pupil function, including defocus, for the aperture array is given by

$$P(\rho) = exp[-i2\pi A(2\rho^2 - 1)]. \tag{4.2}$$

where A is the magnitude of the defocus in waves. The function is then multiplied by the circular aperture, which is used to obtain a point spread function (PSF) given by

$$PSF = |FFT(P(\rho))|^2, \tag{4.3}$$

where FFT is the Fast Fourier Transform. The PSF of the pupil function is then used to convolve with the in-focus image to create an image including defocus. Figure 4.2 shows images of the in-focus pattern, the defocused pupil image, and their convolution, an out-of-focus image.

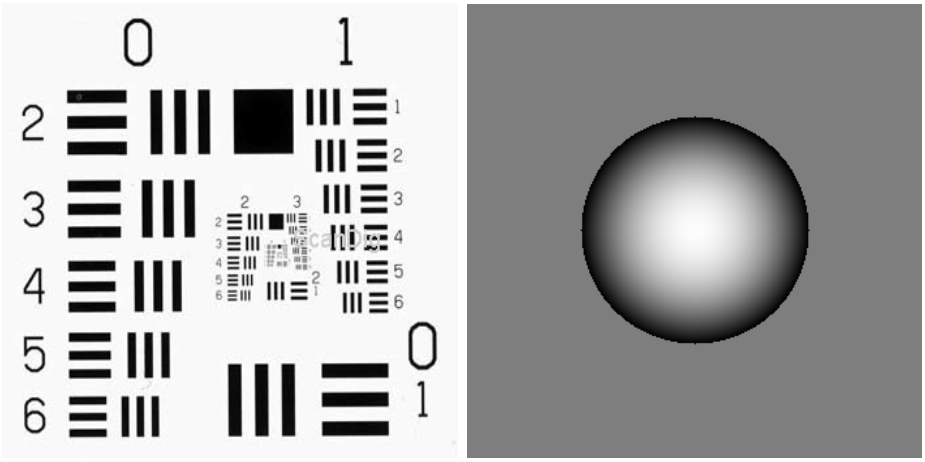

(a) In-focus test pattern

(b) Pupil image with pixel intensity between -1 and +1

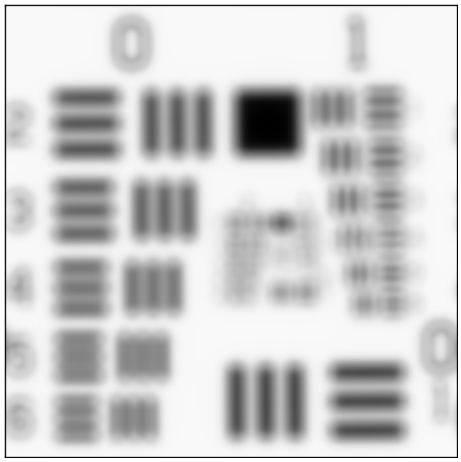

(c) Resulting out-of-focus image

Figure 4.2: The in-focus image in (a) is convolved with the PSF of the pupil function shown in (b) to produce an out of focus image as shown in (c).

As a reference the first image produced is created using a pupil function without defocus. From this image the minimum and maximum pixel intensity ranges, for the images with defocus, are obtained to ensure that any difference in contrast is visible.

The pixel scale of the PSF in radians is defined by

$$v = \frac{\lambda}{\alpha W}, \tag{4.4}$$

where λ the wavelength, α the oversampling scale and W the eye's pupil size [99]. The pixel scale has to be the same for the resulting image. Therefore the field of view for an image, scale $m \times m$, is

$$V_I = mv. \tag{4.5}$$

From the field of view of the image it is possible to determine at what distance the image should be viewed using simple trigonometry,

$$S = \frac{s}{2} tan(V_I/2), \tag{4.6}$$

where S is the separation between the observer and the screen and s is the size of the array on the screen. As an example using a wavelength of $550nm$, an oversampling scale of 2 and a pupil size of $3mm$, from 4.6 we obtain a pixel scale of $9.17 \times 10^{-5} rad$. For an image which is 320×320 pixels the field of view will therefore be $0.029rad$. All images and video clips shown as part of this report were created at a size of 320×320 pixels. From the angular size it is possible to determine the viewing distance for the images and videos. To view the full size image one would have to stand more than $3m$ away from the screen.

The images were viewed on a 15.4-inch (diagonal) antiglare widescreen TFT LED backlit display on a Macbook Pro (early 2008 model). A 'flicker-video' could be created from alternately showing two defocused images created from the same in-focus test pattern. The defocus for each of the two images could be set, as well as the rate at which the images would alternate. These videos were used to test sensitivity to flicker. A test patient would view the videos on top of a black background.

Flicker Simulation Experiment 1

The flicker simulation videos were purely tested by the author. The author is a well corrected myope, with eyeglass perscriptions of L=-4.00 and R=-5.00. To remove any problems of having to operate the computer while trying to view the screen so far away the images were shrunk to a width of $3cm$. At this image width one would have to be $1m$ away from the screen to have the correct pixel scale. Before viewing any images or videos it is important that the screen is angled directly towards the observer, otherwise aberrations or changes could be perceived that are not actually present. The observer was required to sit perfectly still $1m$ away and watch the video. Each video was 10 seconds long. Within that time a decision had to be made whether it was possible to observe flicker or not.

An iterative process was used for changing the defocus of the images that made up each video. For all videos in this experiment the rate at which the images alternated was 10Hz. The first video observed had two images of defocus 0.0D and 0.1D, making a defocus shift of 0.1D. After observing the video if no flicker was observed an additional 0.1D was added to both images, keeping the defocus shift at 0.1D, and the video was viewed again for 10 seconds. This process continued up to a maximum defocus of 1.0D. This was the first set of videos. After the first set of videos the difference in defocus between the two images was decreased by 0.05D and the process was started again. The second set of videos would therefore have a defocus shift of 0.05D starting with the two images having 0.0D and 0.05D.

Detecting a shift of 0.1D became easier the more out of focus the initial image was. From these tests the minimum starting defocus required to observe $0.1D$ flicker was determined to be $0.5 \pm 0.1D$. At this range it is possible to just detect some form of flicker in the target on screen. If the target was any closer to perfect focus it appeared to not change at all. For a defocus shift of 0.05D it was difficult to notice flicker even at an initial defocus of 1.0D.

(a) 0.5D (b) -0.7D

Figure 4.3: Two defocused images of the original test pattern shown in figure 4.2a.

Figures 4.3a and 4.3b show two images of a test pattern that have been convolved with pupil functions containing defocus. There is a magnitude difference of 0.2D between the amount of defocus in each pupil function; one image has a defocus of 0.5D and the other -0.7D. The images have been scaled down to 3cm to ensure they can be viewed at the same distance as they were initially perceived during testing. Simply looking at the images, from a distance of 1 m, it is not easy to spot any difference between them. However, if the images are shown alternately at a low frequency rate it is easy to spot a change.

To emphasise the difficulty of detecting defocus it is worth comparing the difference between the above two images in figure 4.3 and the difference between the two images in figure 4.4. While it was already difficult to point out a difference in figures 4.3a and 4.3b it is impossible to do so close to perfect focus. For the images in figure 4.4 it isn't even possible to perceive any flicker.

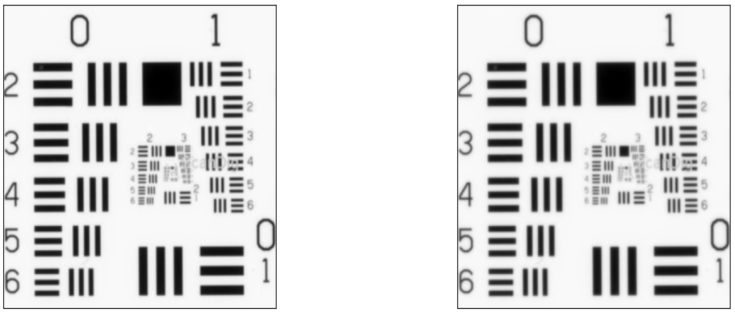

(a) 0.0D (b) -0.2D

Figure 4.4: Two images of a defocused test pattern, original shown in figure 4.2a.

Flicker Simulation Experiment 2

Robson analysed the effect of spatial and temporal frequency on contrast sensitivity of the eye [68]. From figure 4.5 it is clear that there is an optimum spatial and temporal frequency to obtain a maximum contrast sensitivity. This implies that if a patient's eyes are to be tested with the use of flicker, then it is imperative that the correct rate of flicker is used and that the images being viewed have the most useful spatial frequency.

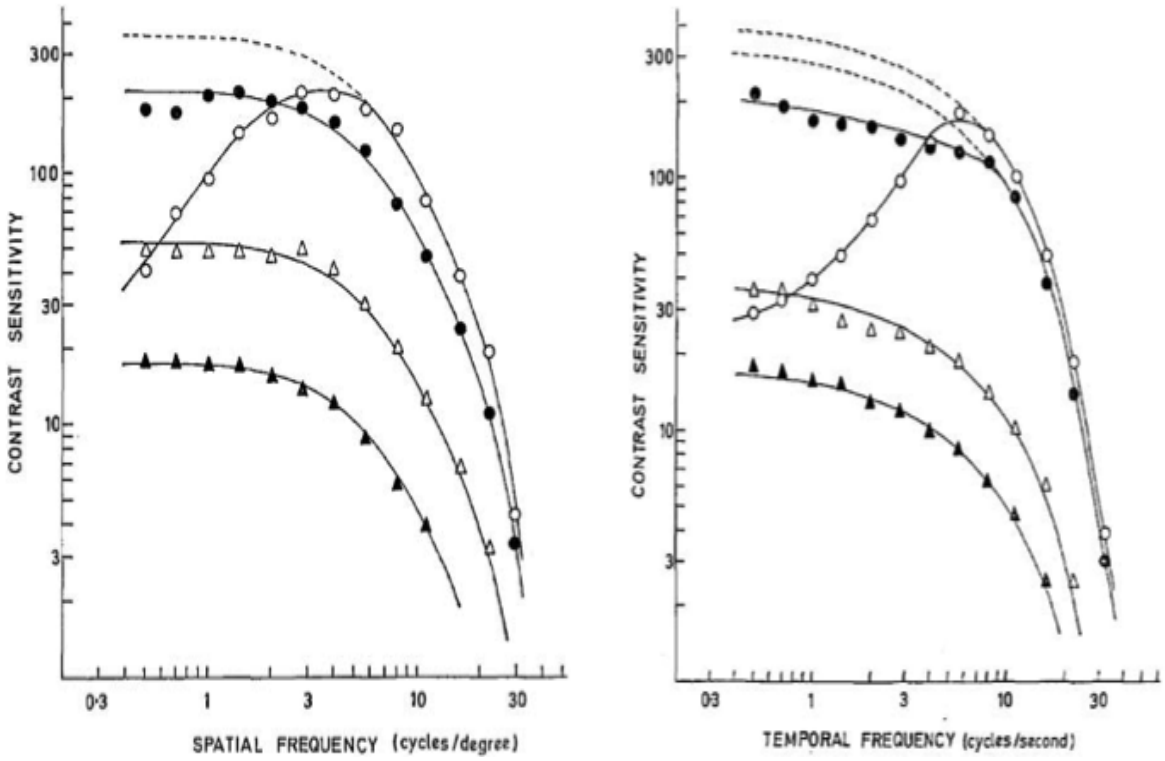

Figure 4.5: a) Spatial contrast-sensitivity for different temporal frequencies: ∘ 1 cycle per second, • 6, △ 16, ▲ 22; b) Temporal contrast-sensitivity for different spatial frequencies: ∘ 0.5 cycle per degree (c/deg), • 4, △ 16, ▲ 22, from [68].

In a convolution, the fourier transform of each function is multiplied together. Therefore if a sine wave grid is used the only possible effect is that there will be a change in contrast. A square grid would therefore change more significantly when subjected to defocus than the sine wave grid. Walsh and Charman speculated that the difference in blur response between sinusoidal and square wave grating types might be because of the presence of higher-order odd harmonic spatial frequency components for the square wave gratings [70]. From this we conclude that any image that would be used for this testing flicker sensitivity would have to contain sharp-edged shapes. It is even clearer when looking at the contrast values of the individual frames. The contrast

modulation is defined by

$$C_M = \frac{L_{max} - L_{min}}{L_{max} + L_{min}}, \tag{4.7}$$

where $0 \leq C_M \leq 1$, L_{max} and L_{min} are maximum and minimum pixel values in the image frame.

A series of sine and square wave grating images were created with varying spatial frequency, ranging between $7 - 20c/deg$. From each image a further two defocused images were created with a difference in defocus of 0.1D. The contrast modulation for each of the defocused image was calculated. The difference in contrast modulation for each defocused image pair was obtained. The contrast difference values for sine and square wave gratings were compared. For any spatial frequency tested the contrast difference between two frames of a defocused square wave grating was greater than for a sine wave grid.

Figure 4.6 shows the contrast difference results for the defocused image pairs of the square wave gratings. It is very clear how the contrast difference is dependent on the spatial frequency and baseline defocus. Low spatial frequencies have a significantly smaller contrast difference. However, the optimum spatial frequency is dependent on the baseline defocus. At a baseline defocus of $0.5D$ using a grating of spatial frequency $18.70c/deg$ the greatest contrast difference is observed for an increase in defocus of $0.1D$. Figure 4.6 shows clearly how below and above a starting defocus of $0.5D$ the contrast difference is lower.

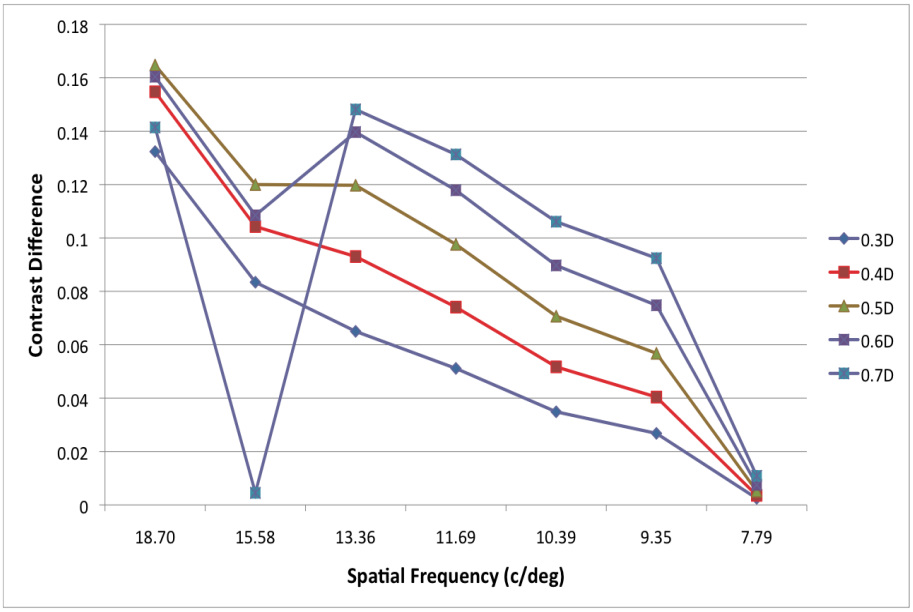

Figure 4.6: Contrast difference dependence, for a defocus shift of +0.1D, on spatial frequency for different baseline defocus values.

When considering a defocus of $0.4D$ or lower the lack of contrast difference could be explained by the diameter of the blur. Considering the size of the blur from a point, as the amount of defocus increases so would the diameter of the blur. If there are two points next to each other the two blur circles created will increase with increasing defocus until they eventually meet. We can relate this to two adjacent black lines in one of the grid targets. If a shift of $0.1D$ is great enough to cause the blur from each line to meet then there will be a jump in contrast due to the loss of the gap between the two blurred lines. If the blur size is much greater than the gap between lines, then there will be an overlap of blur from several lines. This causes less of a change in contrast. One can see that there is a significantly lower contrast difference value in figure 4.6 for a particular baseline defocus and shift. It is assumed that in such a case the blur circles have already overlapped and no extra overlapping occurs.

The contrast sensitivity at low frequency flicker is highly dependent on the spatial

frequency according to Robson, but in the case of flicker produced by defocus there is also an important relation between the grid spatial frequency and the change in image contrast due to the defocus shift. It was very clear that detecting small shifts in defocus require a high spatial frequency. It was therefore important to analyse the effects of temporal frequencies purely for the spatial frequency with which the fixed shift of $0.1D$ produced the greatest contrast difference.

A square wave grating of $18.70c/deg$ was used to create images with defocus of $0.5D$ and $0.6D$, creating a defocus shift of $0.1D$. A series of 'flicker-videos' were created using these two images, but with varying temporal frequency. The frequency range was 6Hz to $20Hz$. The conditions under which the author viewed the videos were the same as described in section 4.2.

From analysing the videos it appeared that at a frequency of $6Hz$ it was harder to observe the presence of flicker or change in the video. Frequencies below $10Hz$ were therefore deemed less suitable for flicker detection. As a comparison the test pattern used in 4.2 was used instead of a uniform grating to see if the effects of temporal frequency were similar.

In each video there seemed to be the illusion that the grid was moving or jittering, which could interfere with detecting low frequency flicker. This grid movement is also present in videos created without flicker. This leads to the assumption that involuntary eye movements are creating what appears to be grid movement. This illusion of grid movement was only present for uniform grids, where it was difficult to concentrate on a specific target. No such movement was perceived when viewing the test pattern in 4.2, which is assumed to be due to the fact that it is possible to concentrate on a specific target in the video. The optimum frequency was determined to be between 10 and $16Hz$, due to a higher or lower frequency having a smaller impact on the detection of

flicker.

Robson has already shown that at high frequencies there is a strong decline in a person's contrast sensitivity. It was therefore very clear that high frequency flicker would be difficult to perceive. Flicker at high frequency rates are hard to spot due to the relatively small change blending into one uniform image.

When analysing flicker using the test pattern shown in figure 4.2a it was clear how crucial spatial frequency is to detecting small defocus shifts. Detecting flicker at $6Hz$ was easier with the test pattern due to the variety of spatial frequencies compared with a uniform grid. Observing the test pattern at a range of frequencies confirmed that the optimum frequency range was $10 - 16Hz$.

4.3 Optical System Flicker

Consider a BBO lens as having a fixed focal length and let the change in polarisation state be represented by the addition of an extra lens. If the initial focal length is f_o, representing the ordinary axis of the BBO lens, then the second focal length is given by

$$1/f_e = 1/f_o + 1/f_v, \tag{4.8}$$

where f_e represents the focal length of the extra-ordinary axis of the BBO lens and f_v is the imaginary lens we would have to add to switch between the two focal lengths.

The focal length, f_v, required to change the initial focal length to the secondary focal length, without changing the polarisation, is therefore given by

$$f_v = (1/f_e - 1/f_o)^{-1}. \tag{4.9}$$

For a given lens we assume the difference in retardence between the marginal and chief ray is equal to the shift in focus (Δ) caused by the imaginary lens f_v [42].

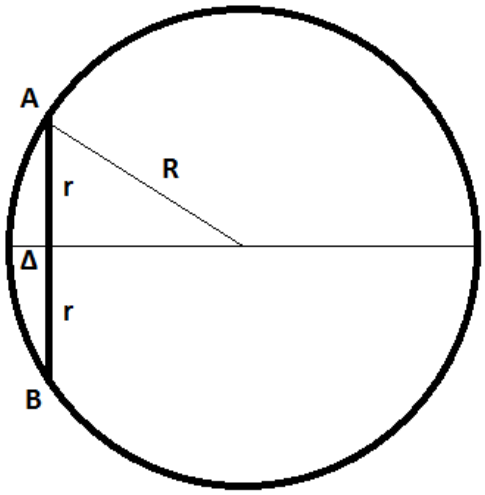

Figure 4.7: Side-on view of a spherical lens bounded by A and B placed on a circle of equal curvature. R is the radius of curvature of the lens and circle. r is the radius of the lens and Δ is the thickness of the lens.

Figure 4.7 shows a side-on view of a lens. Δ is the thickness of the lens. If we assume the lens is spherical we can use the dissecting chord rule to show that

$$\Delta(2R - \Delta) = r^2, \tag{4.10}$$

where R is the radius of curvature of the lens and r is the radius of the lens. For the cases where $\Delta << R$ we can assume the equation can approximate to

$$2R\Delta = r^2. \tag{4.11}$$

For a spherical mirror a common approximation is $2f = R$. For an equivalent lens we have approximated that the focal length would be half the focal length of the mirror.

We can therefore substitute in the focal length f_v using the approximation $f_v = R$. The focal length of this lens can then be related to the shift in defocus as follows:

$$f_v = \frac{r^2}{2\Delta}, \tag{4.12}$$

where Δ is the magnitude of the defocus shift. We now have the potential to set the shift of defocus to the magnitude we desire.

Using equations 4.9 and 4.12 we can determine the defocus shift due to a certain birefringent lens. The whole calculation can be done backwards when a certain amount of defocus is required. We can see from (3) that if we wanted a small shift in defocus, then f_v has to be large. This means that the difference between the two focal lengths of the system would have to be small.

The lens maker's equation is

$$1/f = (n-1)(1/r_{c1} - 1/r_{c2}), \tag{4.13}$$

where n is the refractive index of the material, r_{c1} the radius of curvature of one side of the lens and r_{c2} the radius of curvature for the other side. If we are using a plano-convex lens, then the equation simplifies to

$$f = r_c/(n-1). \tag{4.14}$$

Also $p = 1/f$, where p is the power of the lens. The difference of the lens power between the two refractive indices can be written as

$$\Delta p = p_e - p_o = (n_e - n_o)/r_c, \tag{4.15}$$

where the subscripts e and o refer to the extra-ordinary and ordinary powers and indices. From equation 4.12 we can see that

$$\Delta p = 1/f_v. \tag{4.16}$$

The radius of curvature can therefore be related to the defocus shift by

$$r_c = (n_e - n_o)\frac{r^2}{2\Delta}. \tag{4.17}$$

Hence we can determine the radius of curvature for the BBO lens. We now have the ability to create a lens that can shift defocus accurately and by the desired amount. Assume we want to be able to shift the defocus by 2 wavelengths. With this defocus shift we would want to shift between +1 wave and -1 wave. This means the radius of curvature will have to be $0.636m$ which means the focal lengths will be $0.94m$ for the extra-ordinary and $1.16m$ for the ordinary axis.

To ensure that when the FLC is activated the image is switching between +1 and -1 defocus, a point needs to be found between the two object points, R_s. This point is not necessarily in the middle of the two object points. The screen would be set up so that a person with perfect vision perceives no change in the image. If a person has short- or long-sightedness the effect on the images would be to break the state of equilibrium between the two images. When switching polarisation states a flicker will be perceived. To find R_s we need to use another equation for defocus, D,

$$D = \frac{n}{2}(1/R_i - 1/R_O)r^2, \tag{4.18}$$

where R_i is the image point and R_O is the observation point [100]. r is the radius

of the lens. It is important to note that D is not the same as Δ. D is the amount of defocus at a given point relative to the image point and Δ is the shift in defocus between two focal lengths. For our set up we have a constant observation point, but the image point changes. The only parameter that is therefore not constant in 4.18 is R_i. For the point at which D is equal and opposite we must have

$$(1/R_e - 1/R_s) = -(1/R_o - 1/R_s), \tag{4.19}$$

where R_e and R_o are the image points from the lens for both BBO focal lengths. The observation point at which the defocus will be of an equal magnitude for both focal lengths will be

$$R_s = \frac{2}{1/R_e + 1/R_o} \tag{4.20}$$

This point is not necessarily in the middle of the image points, due to the depth of field being different for each focal length. Provided the observer has perfect vision we can now switch between two polarisation states and create the same blurred image for two different focal lengths.

4.3.1 Flicker on Camera

Flicker was first demonstrated experimentally using a camera in conjunction with an optical system containing an FSL (see Fig.4.8.) The birefringent lens was placed directly in front of the camera lens to prevent any change in image magnification due to the FSL. The optical relay in front of the FSL consists of three lenses. Lens A is fixed to the optical bench while the position of the lens pair B and C is controlled by a servo actuator. The image magnification could be controlled via the separation between lens B and C. The point of equi-blur can then be determined by using the actuator to

reposition B and C. An iris was positioned between A and B to mask the edges of the grid, as there were additional aberrations around edges that would distract from finding the point of equi-blur. The birefringent lens had a small wedge that resulted in a small shift being observed between the two FSL states. One option to compensate for this shift was to de-centre the birefringent lens along the line of the image shift. This option was ruled out though, as the misalignment of the lens increased optical aberrations across the entire image. A more favourable option was to create a grid on a computer screen that could be shifted accordingly. The switching frequency of the grid on-screen was output to the FLC driver synchronising the switching on-screen with that of the image due to the FLC.

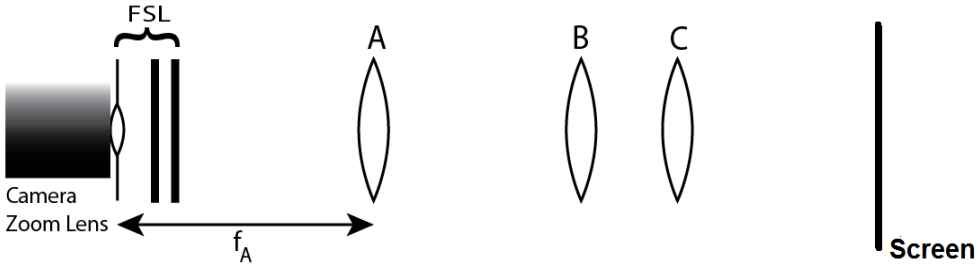

Figure 4.8: Experimental optical system for testing flicker. Lenses A,B and C are used as a zoom system to control magnification. A is fixed. The separation of B from C determines the magnification of the system, while the separation of B and C from A determines the focus.

Figure 4.9 shows the centre of the images produced with the FSL prototype when the target, a grid on a computer screen, is at focus in one state and slightly out of focus in the other. Multiple aberrations present that have not yet been corrected cause an uneven amount of focus across the full image, which would make finding the point of equal defocus much harder.

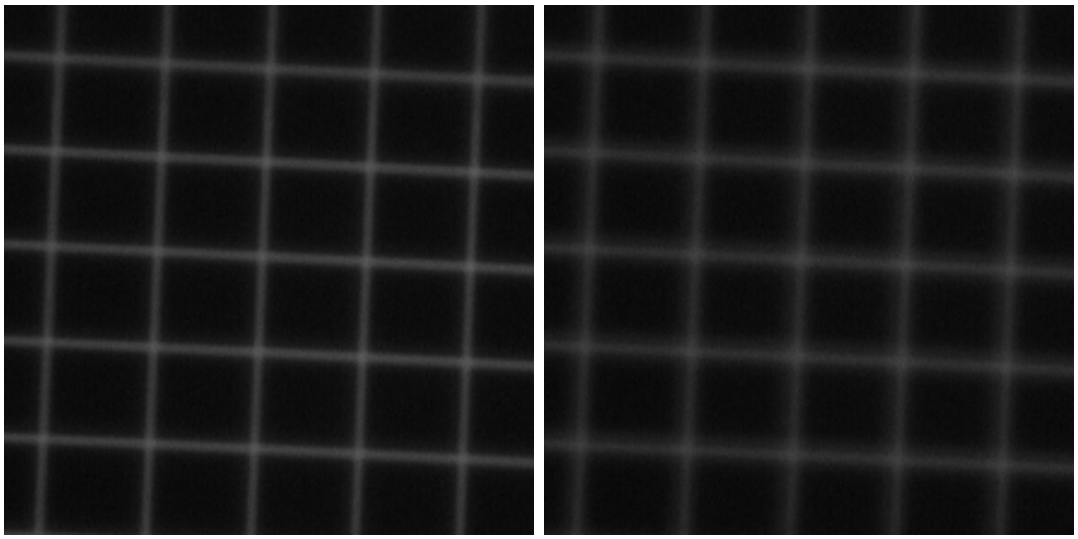

(a) In-focus central grid (b) out-of-focus central grid

Figure 4.9: Example images obtained by the camera of the target grid when the lens system is set up to shift between an in-focus and out-of-focus image.

Using this set up a series of experiments were conducted analysing peoples' performance in finding equi-blur. By turning off the flicker it was possible to then test the ability to find perfect focus. A comparison could then be made to determine the level of improvement in positional accuracy due to flicker.

Optical Flicker Experiment 1

The camera at the end of the optical system was able to provide a live feed of the computer generated grid on the screen. This live feed was displayed on the same computer used in section 4.2. This experiment was conducted purely by the author as an initial proof of concept. The observer was required to be seated one metre away from the screen making sure that the screen was angled directly at him. The lens pair, B and C, was positioned away from the point of equi-blur such that there was a very clear amount of flicker in the image. The author was then required to utilise the actuator, while viewing the camera video feed, to position the lenses back to the point of equal

blur. The position of the lens pair was then recorded. Three different frequencies were observed, 6Hz, 12Hz and 20Hz. At each frequency 10 measurements were made.

The same procedure was used when the flicker was turned off. The author was faced with an out of focus image and was required to reposition the lens pair to find perfect focus. Again the finishing position of the lens pair was recorded for each attempt.

Table 4.1 shows the standard deviation results for finding the stationary flicker point. It is clear from these results that it was easier to find a point of equal defocus, with the help of flicker, than finding perfect focus without flicker. The standard deviation values for flicker at all frequencies were significantly better than the values obtained by a non flickering target.

	Flicker (Hz)			
Grid Spacing	0	6	12	20
25	0.51	0.22	0.13	0.15
50	0.67	0.16	0.11	0.35
75	0.60	0.16	0.12	0.19

Table 4.1: Test results for defocus discrimination. The standard deviation values show the precision with which it was possible to position the lens pair B and C. At $0Hz$ it was necessary to find perfect focus. The use of flicker is clearly favourable due to the standard deviation results being much lower for all frequencies.

One can also see that there are signs that flicker at a frequency of $12Hz$ helps finding the equilibrium point better than the other frequencies. For all three grid settings flicker at $12Hz$ obtained the best results. The difference is only small, so significantly more data would be needed to confirm that this is a fair conclusion. However, it does provide more weight to the conclusions that were made from the experiments involving simulated defocus in section 4.2.

There was no clear correlation visible from having tested different spatial frequencies for the target grid. The difference between each result for a given frequency was very small, but the most precise results were documented for a frequency of 12Hz. This

could further indicate it being the most suitable frequency for flicker detection out of the tested frequencies tested.

Optical Flicker Experiment 2

Flicker sensitivity was tested for two voluntary test subjects. Both subjects were in their early twenties, 23 and 22, one of which had perfect vision and did not require any visual aids. The other suffered from a low level of myopia and wore contact lenses during the testing procedure.

Each subject was tested for two different spatial frequencies of the grid. The temporal frequency of flicker was not tested and remained at 12Hz. The procedure was the same as in experiment 1. While observing the live feed of the video camera the test subject was required to reposition the lens pair to find the point of equi-blur. After testing for finding equi-blur the test subject was required to find perfect focus without flicker. The results from the experiment are recorded in table 4.2. On average the equilibrium point with flicker was easier to find than trying to find best focus without flicker and that larger jitter amplitude reduces the precision. The standard deviation was improved by up to 40% .

	Standard Deviation of Lens Position (mm)			
Grid Square Size (pixels)	Flicker		No Flicker	
	Subject 1	Subject 2	Subject 1	Subject 2
16	0.34	0.39	0.24	0.23
40	0.50	0.55	0.56	0.40

Table 4.2: Test results for defocus discrimination. The standard deviation values show the precision with which the subjects were able to position the lens pair B and C.

One can see that there is a clear indication that trying to find the absence of flicker is an easier task than finding best focus for a target that is not flickering. It is also possible to see that it is crucial to use the right spatial frequency for the target for a given amount of flicker. The lower spatial frequency of the target increased the stan-

dard deviation values. As can be seen from table 4.2, subject 1 results showed a greater variation for the flickering target. Interestingly in both the flickering and non-flickering states there was an increase in deviation for both subjects with grid square size. It is possible that the standard deviation increases generally due to there being less information in a target of lower spatial frequency.

Furthermore, previous research found that flickering cues that change size while doing so capture more attention than cues that do not change size. It is hypothesised that the extra novelty of the object changing size constitutes the appearance of a new object [94]. A shift in defocus creates a change in blur size, which would indicate that such change would be very good at capturing attention.

4.3.2 Directly Visualised Flicker

Another similar optical system was set up without the camera. In place of the camera a head-rest was positioned to enable the test subjects to directly visualise the flickering grid. The optical system was redesigned to ensure the test subjects would perceive a similar spatial frequency for the grid as they had when observing it on the computer screen. It was very important for the eyes to be in a relaxed state in order to prevent the flicker from changing due to the eye re-focusing.

When using the head rest it was not possible to have the birefringent lens positioned immediately in front of the eye. A second relay system had to therefore be placed between the birefringent lens and the eye to conjugate the plane of the birefringent lens onto the eye. Additionally the relay system was required to magnify the shift in defocus as it was initially not visible.

Flicker sensitivity was again tested by the author for more than one frequency, before using test patients for more general results. After placing the head in the head rest the

procedure was the same as for experiment 1. At a frequency of 6Hz the standard deviation was higher than for a frequency of 12 Hz, showing there is a consistency in all three methods of flicker testing (simulated flicker, on-screen flicker and direct visual flicker). The temporal frequency of the flicker was therefore kept at 12Hz for any further testing.

Optical Flicker Experiment 3

A total of three test subjects were used for this experiment. The third additional test subject was again in his early twenties, 24, and was hyperopic. The test subjects head was aligned with the optical system by using a closed iris. The test patient was required to set the head rest such that the centre of the iris was at the centre of their vision when looking straight ahead. It was crucial that the observer did not reposition themselves during each measurement.

The lens pair was positioned away from the point of equi-blur. The iris would then be closed and the test subject would be required to position their head. Once the test subject was ready the iris would be opened and the test subject would reposition the lens pair to find the point of equi-blur. The observer would then remove his head and relax for a brief second before repeating the procedure. This procedure was conducted 10 times. The position of the eye plays a crucial part in what the observer perceives, so it was decided to try a second set of measurements. During the second set of measurements the observer was not allowed to remove their head from the head rest in an attempt to ensure the eye stayed in the identical place for each measurement. Again 10 measurements were taken. The final set of measurement were taken without flicker and the test subject was required to find perfect focus. The test subject was able to relax between measurements.

	Flicker			No Flicker		
	Subject 1	Subject 2	Subject 3	Subject 1	Subject 2	Subject 3
Test1	1.30	1.33	2.28	2.75	5.07	1.91
Test2	1.77	3.40		2.01	1.57	

Table 4.3: Test results for defocus discrimination. The standard deviation values show the precision with which the subjects were able to position the lens pair B and C. Without flicker they were required to find best focus and with flicker they had to find the point of equilibrium where the flicker disappears.

Figure 4.3 shows the set of results obtained from three test subjects. At first glance one can see that on average the deviation for a flickering target was lower than for a non-flickering target. Under the same testing conditions the three subjects have produced varied results. For subject 1 and 2 it was clearly easier to find an optimum position for the lens when the target was flickering. However after testing a third subject there appears to be a case where a non-flickering target provided better results. The preliminary results are therefore promising, but they are not entirely conclusive.

Initially it had been hoped that in method 2, where all measurements were taken without the subject moving their head, the results would improve as there would be no chance of the eye changing position. The prolonged state of having to view a target through the optical system proved to be too tiresome for the test patients. In subjects 1 and 2 there was a distinct pattern to the lack of rest between each measurement. When observing flicker the standard deviation would get worse while the standard deviation for non-flicker improved. It appears that a person observing flicker for a period of time lasting longer than a couple of seconds quickly finds that they are in a certain amount of discomfort and this can lead to fatigue. It is also possible that the brain could try to compensate for the flicker and any unnatural image aberration. In the case of a person observing a target that does not flicker this discomfort is not present and therefore viewing the target for a longer period of time would help pinpoint the position of best focus. It appears that even though a flickering cue can capture attention for a longer

period of time a prolonged exposure to the flicker can have negative results.

The amount of time it took the subjects to choose a position for the lens was significantly shorter with a flickering target during experimental method 1. This was to be expected as a gradual change of focus is harder to concentrate on than a clear point where there is a significant reduction in activity in relation to flicker. The speed at which repeat measurements were made was also increased for a flickering target, whereas there was less of an increase for a non-flickering target. While the time to take a measurement was not specifically timed these observations were very clear during the testing process and was also noticed by the test subjects. This finding would also be supported by the fact that a flickering object can hold attention for longer than a non-flickering cue [94]. It would suggest that attention while the non-flickering target changes focus is lost and a person would rely on memory to determine whether there was a change or not. Each test patient would therefore have to scan across the focus point several times before reaching a decision.

It is important to point out that, relative to the results obtained using a camera, there is a significant increase in the standard deviation for all measurements. Non-flickering images from the camera were compared to the grid observed through the optical system directly. It was concluded that the small differences in the noticeable aberrations between the images could not justify such a great change. For this reason the conclusion was drawn that the depth-of-focus was not kept constant. One can therefore not directly compare results obtained through visual flicker with those obtained using the camera, but they show potential for flicker to improve defocus detection.

We can conclude from the findings, that it is possible to use flicker to improve the detection of shifts in defocus and that it could therefore be a useful tool to help in testing visual acuity. However, from this research and with support from previous research it is

clear that it would be necessary to shift between equal and opposite amounts of defocus far greater than the capabilities of the birefringent lens currently being used. The reason for this being that an initial amount of defocus greatly improves the ability to perceive small shifts. From this research a starting defocus in the region of $0.4D - 0.6D$ would at least be required to detect small shifts of $0.1D$. A birefringent lens would need two focal lengths that have a differing refractive power of approximately $1.0D$ to achieve this. Using equation 4.17 we can determine the radius of curvature for such a lens. A lens made from the birefringent material BBO would require a radius of curvature of $0.12m$.

Such a lens could be used in conjunction with a diverging lens to produce a two lens system that switches between $0.5D$ and $-0.5D$. This may seem like a large magnitude of defocus for the eye to observe. However, the results obtained by Ciuffreda when determining levels of bothersome blur show that 0.5D of defocus are below the levels of blur at which the eyes would be strongly inclined to refocus [61]. It would be possible to use such a pair of lenses without having to use any relay systems. A system of only two lenses will be subject to much less aberration, making it easier to detect flicker. An additional focusing lens could be used to conduct similar tests. Another possibility would be to use the lens system to test patients while viewing an eye chart and analyse the effectiveness of such a set up.

4.4 Summary

- Perceiving shifts of defocus is made easier by switching quickly back and forth between two levels of defocus, creating flicker.
- Small defocus shifts require high spatial frequencies present in the target to improve the visibility of the shift. The optimum frequency to detect flicker ranges

between 10 and 16 Hz

- The precision with which a test subject can place a lens is easier when trying to find equal blur magnitude during flicker compared to finding perfect focus of a target without flicker.

- By designing a lens that can switch between equal and opposite refractive power it could be possible for patients to observe flicker due to small refractive error of their own eye.

Chapter 5

Fast Focus Switching Fundus Camera

The focus switching lens (FSL) that plays a vital role in the creation of flicker in chapter 4 can just as easily be used to create a camera that can change focus at high speeds. Rather than using the FSL to look at a specific point of interest with differing defocus the same system can be used to switch between multiple in-focus targets.

As mentioned in section 3.2 several retinal imaging instruments have been created from the desire to create increased interobserver and intraobserver repeatability in the diagnosis of the optic nerve. This has great impact on the detection of early signs of glaucoma. These instruments are very costly and are therefore not readily available to everyone.

Optic nerve heads are not as smooth as the rest of the retina. The optic nerve head has more depth to it and as such it can be more difficult to focus correctly. This chapter discusses the use of birefringent material in a retinal camera, such that the focus of the camera can be switched to different depths of the ONH at high speed, making it easier to obtain an image of the ONH from which a consistent glaucoma diagnosis can be

made at early stages of the disease. Birefringent lenses and plates have been tested in simulations using Zemax to determine feasibility.

5.1 Fast Focus Switching Camera

A simple camera consists of a focusing lens and a CCD. If an FSL is used as the focusing lens the camera will have two focal lengths to switch between. The way an FSL works is described in section 2.2.6. FSLs can even be set up in series to increase the number of focal lengths. Such a lens would only need one linear polariser. In the case where two FSLs are being used in an optical system the lens pair can either be in the same state, o-o and e-e, or they can be in opposite states, o-e and e-o (o = ordinary axis, e = extra-ordinary axis). In a lens with positive birefringence the o-o state will have the weakest focal power and e-e the greatest power.

When adding another lens to a system, the new effective focal length will be

$$f = \frac{f_1 f_2}{f_1 + f_2 - d}, \tag{5.1}$$

where f_1 and f_2 are the focal lengths of the FSLs and d their separation [101]. When using multiple FSLs we have 2^N focal lengths available, where N is the number of FSLs used. If however two identical FSLs are being used then from equation 5.1 we can see that there would only be three effective focal lengths. In the general case the number of focal lengths would then be $(N+1)$. However the equation for the front focal length (FFL) of a system is

$$f = -\frac{f_1(f_2 - d)}{f_1 + f_2 - d}. \tag{5.2}$$

This implies that even in the case where two identical lenses are used it is possible

to have 4 different focal-plane positions, provided that $d \neq 0$, even though there are only three possible effective focal lengths. A camera could therefore switch between multiple focal lengths without repositioning any lenses.

It is interesting to note that it is possible to create a focus switching system that has an equal shift in power from one state to the next [102]. The incremental change in dioptric power ΔD remains constant when

$$\Delta D = 2(n_e - n_o)\left[\sum_{i=1}^{N} \frac{1}{r_i}/(2^N - 1)\right], \tag{5.3}$$

where r_i is the refractive index for the ith birefringent lens. The values of $R_1, R_2, R_3., ..R_N$ must be related to each other as

$$\frac{1}{R_1} = \frac{2}{R_2} = \frac{4}{R_3} = \frac{8}{R_4} .... = \frac{2^{N-1}}{R_N}. \tag{5.4}$$

Provided each FLC in the system can be controlled independently from the others it is possible to set the order in which the focal length changes as well as the rate of switching. FLCs have the capability to switch at very high rates, which implies that the rate at which the images can be taken will be limited to the maximum frame rate of the camera.

5.1.1 Light Propagation through a Calcite Block

An alternative option to the birefringent lens was considered. A standard lens combined with a calcite block could also act as a birefringent lens. The optical path length of a ray passing through a medium is given by nt, where n is the refractive index and t is the thickness of the block. The point of focus for an optical system can therefore be altered by simply changing the refractive index at a any point in the system. The new focal length, f_N, of the system will therefore be given by

$$f_N = f - t + nt, \tag{5.5}$$

where f is the focal length of the lens.

If the block added to the system is birefringent then there would be two possible focal planes. When stacking a series of plates it is important to note that the number of possible focal planes is $N+1$. Therefore to obtain 4 focal shifts, which can be produced by two birefringent lenses, one would need more than 2 birefringent plates.

An important factor to consider with a birefringent block is that the rays are not normal to the block surface. It can therefore not be assumed that the refractive index for the extra-ordinary ray will be the same for all rays. Simiarly, this effect would be observed when using birefringent lenses. The light rays that are not parallel or normal to the optic axis experience a refractive index between n_o and n_e. The effective refractive index, n_{eff}, is given by

$$n_{eff} = \frac{n_e n_o}{\{n_e^2[1 - (\hat{k}_r \bullet \hat{z}_3)]^2 + n_o^2(\hat{k}_r \bullet \hat{z}_3)\}^{1/2}}, \tag{5.6}$$

where $\hat{k_r}$ and $\hat{z}_3$ are the wave vector of the light ray and the vector representing the optic axis [103].

For the case of an unpolarised light ray incident on a single uniaxial crystal block, the separation between the ordinary and the extra-ordinary ray, d, is given by

$$d = D \tan\alpha = D\frac{(n_e^2 - n_o^2)\tan\theta}{n_e^2 + n_o^2 \tan^2\theta}, \tag{5.7}$$

where D is the thickness of the block, α the dispersion angle between the ordinary and the extra-ordinary ray, and θ the angle of the optic axis relative to the incidence angle of the light ray.

Unless the incident light is perpendicular or parallel to the optic axis the extra-

ordinary ray is subject to crystal astigmatism. Astigmatism leads to two focus positions. Longitudinal astigmatism, ϵ_l, is given by,

$$\epsilon_l = \frac{Dn_o \tan\theta \tan\alpha}{n_e\sqrt{n_o^2 \sin^2\theta + n_e^2 \cos^2\theta}}. \tag{5.8}$$

For an imaging system, 'smearing' of an image is given by transverse astigmatism, $\epsilon_t = \frac{\epsilon_l}{F}$, where F is the f-number of the light beam [104].

This indicates that if a lens is used in conjunction with a birefringent block there will be astigmatism in the extra-ordinary ray, the magnitude of which will be dependent on the power of the lens as well as the birefringence and thickness of the block.

5.2 The Fundus Camera

Past research has determined that there are two dominant designs for the fundus camera [105]. These designs, shown in figure 5.1a and 5.1b, contain the typical imaging and illuminating arms required to successfully image the retina, but they differ in the incorporation of the illumination arm. The first has an internal illumination arm and uses a mirror with a central hole, placed conjugate to the pupil of the eye to combine the two systems. The second design has an external illumination arm and a beamsplitter linking it with the imaging system.

The illumination arm projects a light source onto the pupil of the eye to illuminate a large portion of the retina. The general design has to take into consideration that the cornea is a highly reflective surface and also the back reflections from the optical system are more powerful than the reflection power of the retina [105]. The reflections off the cornea are removed by placing a central obscuration, elements 9a and 10b, in the system that is conjugate to the pupil of the eye. This results in an annular illu-

mination pattern at the pupil of the eye. For the internal illumination system a black dot, element 8b, is placed conjugate to the back surface of the objective, element 2b, removing any back reflections from that lens.

The imaging arm consists of two main components, an objective lens and a zoom system. There are two important considerations to be made in the design of the imaging arm. It must firstly be able to accommodate for the refractive error of the patient and must therefore function for near-sightedness and far-sightedness covering at least 95% of refractive error found in patients, -8D to 5D. Secondly, the pupil entrance of the system must be located at the pupil of the eye. The entrance pupil diameter is controlled by the baffle in figure 5.1b and by the mirror in figure 5.1a. Both are placed conjugate to the pupil of the eye.

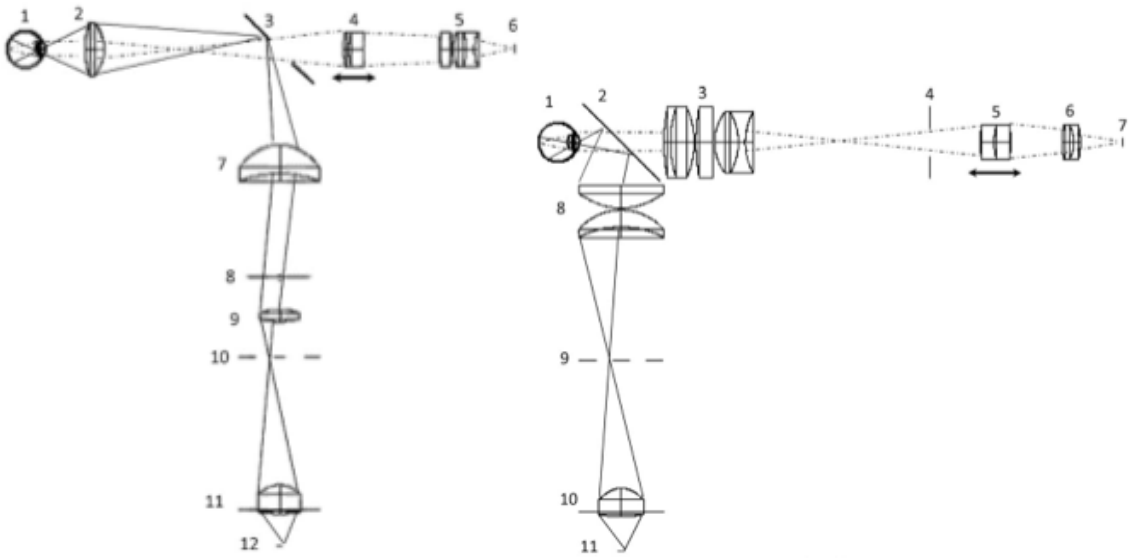

Figure 5.1: Fundus camera system design modelling schematics in patent literature: a) internal illumination design: 1- eye, 2- object lens, 3- mirror with circular aperture, 4,5- zoom lens components, 6- ccd, 7,9,11- lenses used to image the light source onto the mirror, 8- black dot placed conjugate to the back surface of the objetive, 12- light source; and b) external illumination design: 1- eye, 2- beam splitter, 3- object lens, 4- baffle designed to reduce back reflections from the cornea, mirror with circular aperture, 5,6- zoom lens components, 7- ccd, 8,10- lenses used to image the light source onto the mirror, 9- black dot placed conjugate to the back surface of the objetive, 11- light source from [105].

The fundus camera must also meet further criteria. It must have a minimum field of view of 30°, an f-number of f/5.4 and an image plane size of a 1/2-inch CCD camera 4.8mm × 6.4mm [105]. Such complicated and technical equipment can be very expensive. From a report in 2007 the prices for the HRT III, Stratus OCT and GDx VCC were $40 990, $61 950, and $47 950, respectively. The report also points out the additional cost of having to hire a skilled technician to obtain the imaging scans. [106]. What is then even more surprising, when considering the cost of these instruments, is that the HRT III and the GDx have been reported to not be effective as stand-alone screening devices for glaucoma detection [107].

5.3 Focus Switching Retinal Camera

In the past several methods have been utilised to refocus the fundus camera. Traditionally imaging system designs would involve a movable element to change focus, such as the eyepiece, objective lens or CCD. In some cases the entire system would shift. The movement of each element has an attached disadvantage to it, such as shifting of conjugate image planes and non-stationary images. Image illumination could also be affected [108].

To avoid the issues of an imaging system with multiple moving parts, a series of birefringent lenses could be used, in a similar fashion to how they would be used for a focus switching camera. With the use of FSLs the optic nerve can be imaged for a range of different focal lengths, targeting different depths of the nerve. This could help to determine the C/D ratio, avoid any image shift due to movement of the patient or lenses and therefore improve the repeatability of optic nerve diagnosis. As the images can all be taken at high speed, this method would reduce the time a patient's eye has to be analysed, making the process less invasive. If the system can take pictures quickly with varying focus, then a technical expert may not be needed to obtain a good image. Additionally this technique could have a lower cost than many other well developed technologies.

The illumination of the retina is an important factor for a fundus camera and as such a well illuminated retina is much easier to analyse. It is important to note that the amount of light reaching the CCD would be reduced by at least half, if an FSL were to be used in conjunction with a fundus camera, due to the necessity of a linear polariser for the focus switching to work.

The amount of light used to illuminate the retina is limited to a power that will not

damage the eye and be of significant discomfort to the patient. As the FSL would only be in the imaging arm of the fundus camera there would be little possibility to increase the illumination power. When analysing the two common types of retinal camera the internal illumination system was described to have a much higher illumination efficiency. Therefore the camera design in figure 5.1a would be much more favourable to use with FSLs.

5.3.1 Zemax Simulations

A simple imaging arm has been designed in Zemax using a model of the human eye and a series of paraxial surfaces, loosely based on a design by DeHoog [109]. The eye model used is based on the design by Liou and Brennan [110]. The essential optical components from the general design in figure 5.1a have been used, which are the objective lens and a zoom system to magnify and focus the light onto the CCD, as shown in figure 5.2. The lenses were positioned such that the image-space was telecentric to try and mnimise distortion. The lenses in the system were represented by paraxial surfaces and the performance was analysed by judging the spot diagrams produced at the image surface of the central point of the retina.

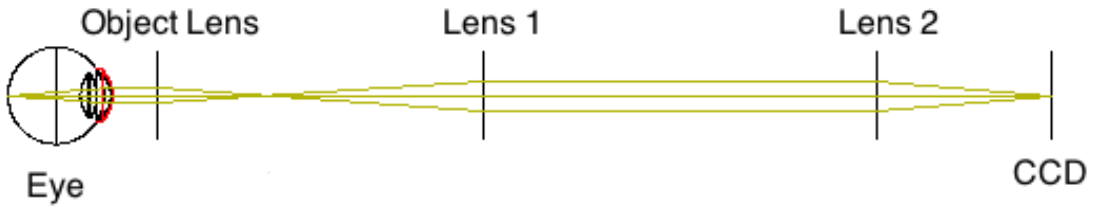

Figure 5.2: Imaging arm design used to test fast focus switching, without FSLs between Lens 1 & 2.

Retinal Camera with FSL

Birefringent lenses were tested by adding them to the components of the imaging arm

of the retinal camera such that the position of the original components did not need to be changed. As mentioned in section 5.1.1 aberrations and refraction angle of the extra-ordinary ray are dependent on the angle of the ray relative to the optic axis. The ideal conditions for birefringent lenses would be a location within the optical system where the rays are parallel to each other and perpendicular to the material's optic axis. Hence, the best position for a birefringent lens would be between lenses 1 and 2. If positioned at the mid focal point between the two lenses the aperture can be minimised and it would be conjugate with the pupil of the eye.

Two birefringent materials were tested for their suitability to create a focus switching retinal camera. The two birefringent materials were quartz, $\Delta n = +0.009$, and calcite, $\Delta n = -0.172$. These materials were used due to them having very different amounts of birefringence and are common materials used in optical systems.

The optic nerve has a depth of less than $1mm$, so it is important that we are able to incorporate FSLs that enable the optical system to switch focal plane by fractions of a millimetre. Additionally we would want a system that can shift focus the same amount each time, creating evenly spaced focal planes.

To test the ability of multiple birefringent lenses a pair of birefringent lenses were added to the retinal camera imaging arm. The optical system can therefore analyse four different layers within the optic nerve. From the estimate that an optic nerve has a depth of less than a millimetre it was inferred that $1mm$ should be the maximum separation between two focal planes. For an optical system that has four possible focal plane positions the maximum separation of adjacent planes would therefore be $0.33mm$.

The birefringent lenses can be designed with specific dimensions such that the focal planes are evenly spaced with a separtion of $0.33mm$. To obtain an equal shift in focal

power we can use equation 5.4. The radius of curvature for the two birefringent lenses would therefore have to be in the ratio of 2:1. As an approximation we have assumed that the focal planes will therefore be evenly spaced as well.

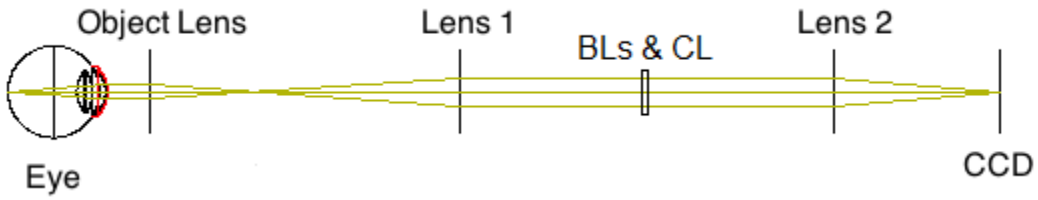

Figure 5.3: Demonstration of the location and size of the birefringent lenses (BLs) and compensating lens (CL).

Figure 5.3 shows where the new components were positioned in the imaging arm. The addition of these lenses would change the image plane of retinal camera, which would require the repositioning of one of the original components to accomodate for this. To avoid this a compensating lens was added with the birefringent lens pair.

An additional three optical components are therefore now part of the imaging arm of the retinal camera. Figure 5.4 demonstrates the arrangement of the three components as they were in the simulation. It should be noted that radii of curvature of the lenses is not to scale and was altered to demonstrate clearly how the surfaces were orientated. Each of the optical components was given a thickness of $2mm$. The power of the compensating lens needed to either be set to compensate for the birefringent lenses when they were in state o-o or e-e, the longest or shortest focal length of the birefringent lens pair. In this instance the power of the compensating lens was set to counteract the refracting power of state o-o. The rays exiting the compensating lens would therefore still be travelling parallel to the optical axis of the system.

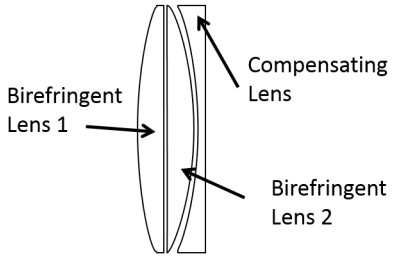

Figure 5.4: Illustration of the arrangement of birefringent lenses and compensating lens.

First, calcite lenses were tested. The shift in refractive power is dependent on the birefringence and the radius of curvature of the birefringent lens. If a material is used with low birefringence, then a lens made from that material will need to have a smaller radius of curvature, than a material of higher birefringence, to obtain the same change in power. As calcite has a large birefringence the lenses needed a very large radius of curvature. It was not known what the ideal curvature was, so a trial and error process for a range of lens curvatures was required. The birefringent lenses were placed in the imaging arm without the compensating lens. The separation between the focal plane of the o-o state and the e-e state was calculated. The starting radius of curvature was deliberately short, giving the lens pair a high focal power, which meant the separation would initially be too large. The radius of curvature was then incrementallly increased until the separation of the focal planes for the o-o and e-e states was only $1mm$. Now that the radius of curvature for the birefringent lenses was set, it was possible to determine the lens power needed for the compensating lens. The compensating lens was added and the auto-focus feature in Zemax was used to quickly set the radius of curvature such that the image spot radius was optimised when the birefringent lenses were in the state o-o.

The same procedure was undertaken for a pair quartz lenses. Figure 5.5 shows the optimised spot diagrams for each material. All three wavelengths present in the spot diagrams were taken into account, evenly weighted. Only the results for the extra-

ordinary axis are shown, as the ordinary axis refracts light like any other lens, so it is of less interest.

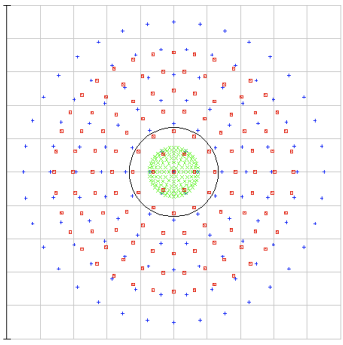

(a) No FSLs, Airy Disk = 2.433 μm RMS Radius = 5.433 μm.

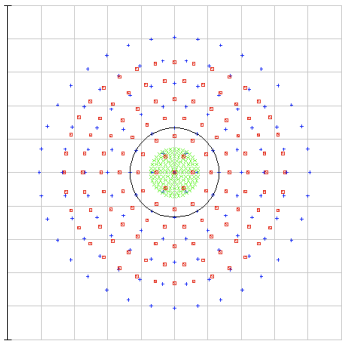

(b) Quartz FSLs, Airy Disk = 2.692μm RMS Radius = 4.752 μm.

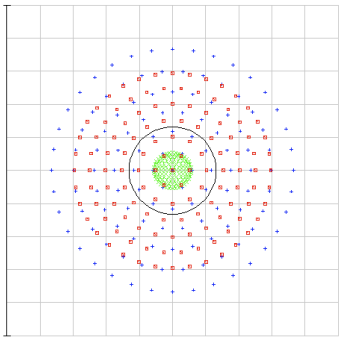

(c) Calcite FSLs, Airy Disk = 2.636 μm RMS Radius = 4.155 μm.

Figure 5.5: Spot diagram results for the use of FSLs in a simulated imaging arm of a retinal camera. The Airy disk of the system is represented by the central black ring. Wavelengths shown in the diagrams are 500nm(blue dots), 587.6nm(green dots) and 656.3nm(red dots).

The spot diagrams in figure 5.5b & 5.5c, obtained when FSLs were added to the system, are very similar when compared to the spot diagram obtained for the imaging system without FSLs, figure 5.5a, and do not show any signs of astigmatism. There are very small differences which should be pointed out. The ratio between the RMS

radius value and the Airy disk value for each diagram was determined and the values for the ordinary and extra-ordinary axis of the quartz lens were the lowest. It can also be seen from the diagrams, that the radii for each wavelength is smaller with the quartz lens. These differences are only slight, so from these results one would infer that calcite and quartz lenses are both viable options. While the spot diagrams paint a positive picture for both the materials, the actual required dimensions for the lenses of each material vary considerably due to the large difference in birefringence. The radius of curvature for the calcite lenses were 3000 mm and 6000 mm, whereas they were 170mm and 340mm for the quartz lenses. As the required radii of curvature for the calcite lenses are so high it could indicate that manufacturing lenses of calcite for the system would be harder and therefore make it a more costly process than for quartz lenses.

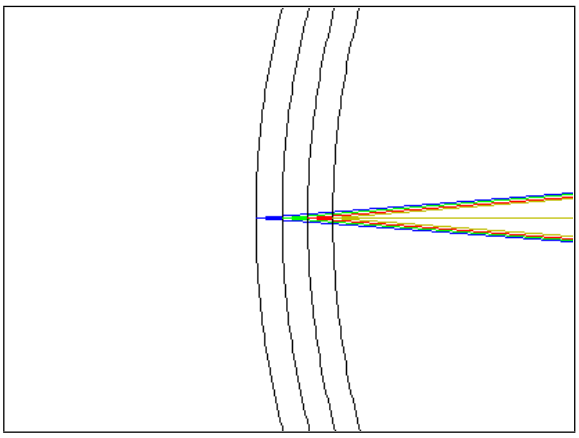

(a) Retina layers in the eye. Layer separations ~0.33mm.

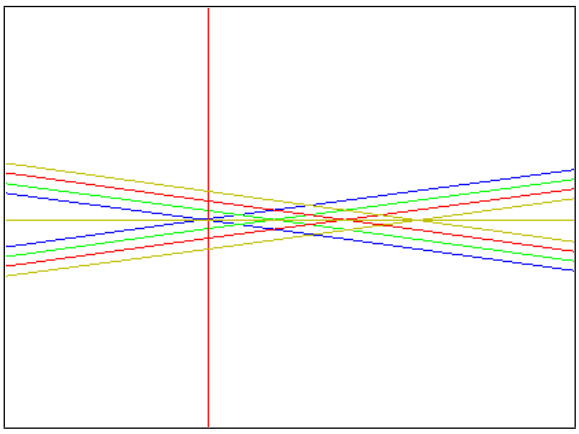

(b) CCD plane. Focal points spread across 0.5mm.

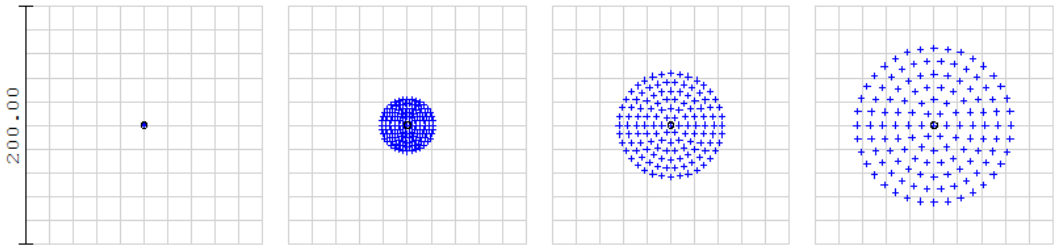

(c) Configuration Spot Diagrams: o-o,o-e,e-o and e-e. Each diagram represents an area of 200μm $\times$ 200μm.

Figure 5.6: Simulation of the imaging arm without an FSL system. The light rays from the different imaging layers do not all converge at the location of the CCD; $\lambda = 587.5nm$. The spot size is larger for more shallow depth layers. The airy disc can not be seen due to the scale of the spots.

Using the quartz lenses and calcite lenses all four possible focal powers were tested. Figure 5.7 shows simulations of how the quartz lenses could produce in focus images for different depths in the eye. The calcite lenses produced identical results, so it was unnecessary to provide them as well. Figure 5.6 shows that, using a standard imaging arm, it would not be possible to produce the same quality images of different depth levels without repositioning a lens component. Figure 5.7b shows that each FSL configuration can focus light onto the CCD from a different depth level without any lens having to change position. The spot diagrams in figure 5.7c for each depth level are identical due

to the FSL system, which is much better quality than the spot diagrams in figure 5.6b.

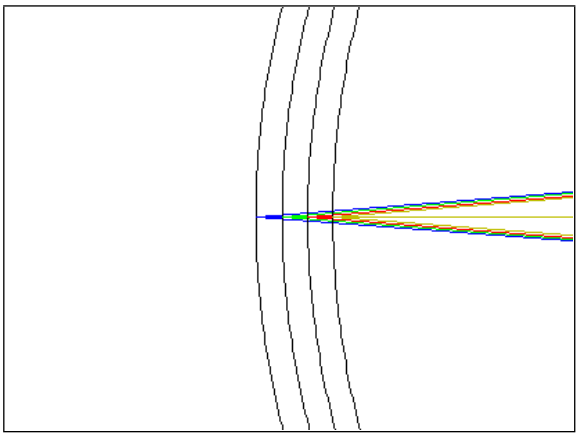

(a) Retina layers in the eye. Layer separations ~0.33mm.

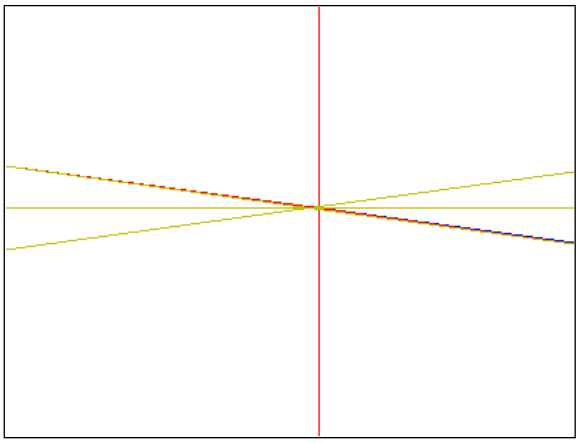

(b) CCD plane. All light rays focused on the CCD.

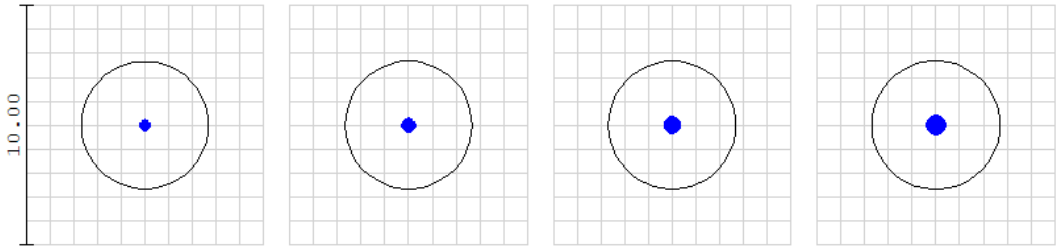

(c) Configuration Spot Diagrams: o-o,o-e,e-o and e-e. Diagram size in μm.

Figure 5.7: Simulation of the imaging arm with an FSL system. The light from the different retinal layers are all focused onto the CCD by the different FSL configurations; $\lambda = 587.5nm$. Light from each layer produces close to the same spot size, all within the Airy Disc.

Birefringent Plate Testing

As a comparison, quartz and calcite plates were tested in the imaging arm instead of birefringent lenses. A birefringent plate would only change the location of the focal plane if the incident light is converging or diverging. A birefringent plate must therefore be placed in front of lens 1 or behind lens 2 and not in between them.

As described in section 5.1.1 the thickness of the birefringent plate would determine the separation of the focal planes for each polarisation state. A trial and error process was again used to find the correct dimensions. Only a single birefringent plate was

used for this test. An example of the position of the birefringent plate is shown in figure 5.8. An initial plate thickness of $10mm$ was used. When analysing the spot diagrams for each polarisation state it was clear that there was a severe amount of astigmatism present when using a birefringent plate. The thickness of the birefringent plate was incrementally decreased by $0.1mm$ and the spot diagrams were viewed at each stage. Due to the large astigmatism present in the resulting spot diagrams of the extra-ordinary axis there was no optimum plate thickness, for which a focal shift of $1mm$ would occur.

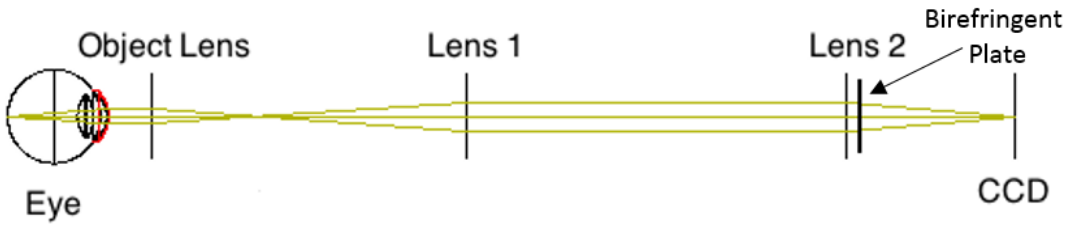

Figure 5.8: Demonstration of the location of the birefringent plate in the imaging arm of the retinal camera.

Very thin plates of calcite were also tested, of thickness less than $1mm$, to reduce the amount of astigmatism due to the birefringent plates. Less astigmatism was present, but the focal shift was too small for it to be of use. The spot diagrams in figure 5.9 show the different levels of astigmatism in the extra-ordinary axis. One can see that the amount of astigmatism in the image is greater if the birefringent plate is placed in front of lens 1. This is in agreement with the equation for image 'smearing' discussed in section sec:block, as it states the astigmatism is dependent on the f-number of the light beam. The spot diagram for the thin calcite plates, figure 5.9c, is quite similar to that of the thicker quartz plates, figure 5.9b, even though calcite has a larger birefringence. One can see that thinner plates produce less astigmatism for the extra-ordinary axis, but the possible focus shift is much too small to make the plates useful. From these

results a clear conclusion can be made that the birefringent plates would not be possible options for fast switching retinal cameras. As the birefringent plates are of no use to improving a retinal camera, only FSLs need to be investigated further.

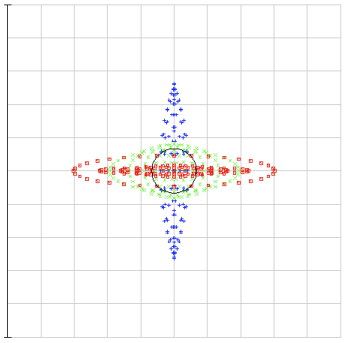

(a) 10mm thick Quartz plate in front of lens 1, Airy Disk = 2.673 μm RMS Radius = 5.583 μm.

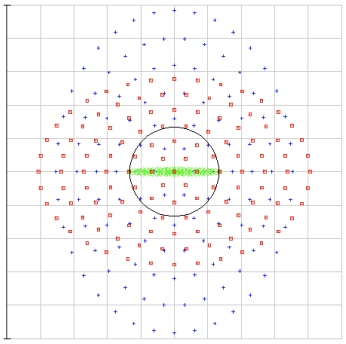

(b) 10mm thick plate behind lens 2, Airy Disk = 2.673 μm RMS Radius = 4.882 μm.

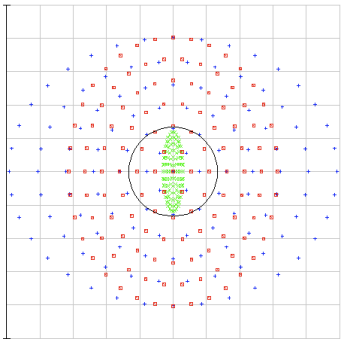

(c) 0.5mm thick calcite plate behind lens 2, Airy Disk = 2.673 μm RMS Radius = 5.113 μm.

Figure 5.9: Spot diagrams when using birefringent plates in a simulated imaging system for a retinal camera.

So far simulations have only been conducted for imaging a central part of the retina. The optic nerve is approximately 15° away from the centre of the fovea [111], so any light coming from the optic disc would be entering the birefringent lens at an angle. From the analysis of the birefringent plates one can see that light rays entering a birefringent material at an angle could cause astigmatism in the extra-ordinary axis.

Field Curvature Testing

The field curvature was tested separately for the FSL component. An object field of 20° was analysed. A paraxial lens was positioned behind the birefringent lenses identical to the position of lens 2 in figure 5.2. The field curvature diagrams for the extra-ordinary axis are shown in figure 5.10. Clear signs of astigmatism are present in both diagrams . As expected the astigmatism due to the calcite lenses is greater, but due to the radius of curvature being so large the percentage of distortion is much lower than that for the quartz lenses as the angle of incidence increases.

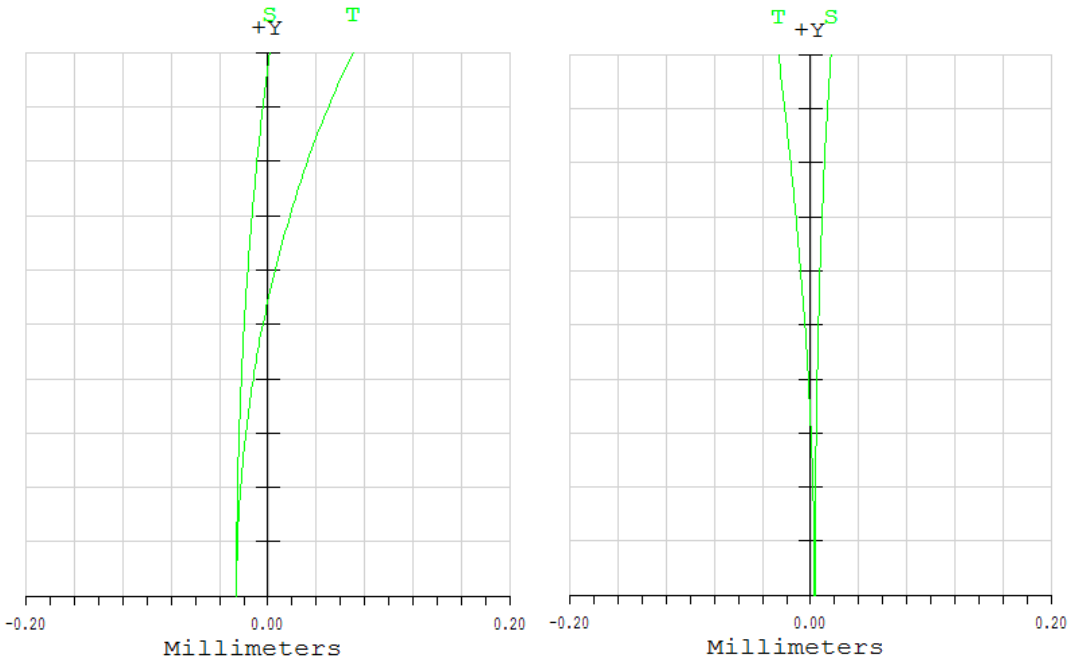

(a) Calcite Lenses

(b) Quartz Lenses

Figure 5.10: Field Curvature for the extra-ordinary axes of incident light up to an angle of 20 degrees. The vertical ais represents the distance from the optical axis and the horizontal axis the height above a transverse reference plane. There is clear separation of the tangential and sagittal rays

5.4 Analysis

The results obtained from Zemax simulations show that a birefringent lens could be used to switch focus by very small amounts in an imaging arm of a retinal camera. Both birefringent lenses showed good ability for focus switching in the Zemax design, indicating that high birefringence and low birefringence materials could be used to create FSLs for the imaging arm of a retinal camera. The quartz lenses would likely be preferable though, due to the focal lengths of the lenses being of a more sensible magnitude.

A very positive picture has been painted of the performance of these lenses, but it is important to point out some potential problems as well. The importance of luminance has previously been mentioned and it should be pointed out again, that using an FSL in an optical system of any kind will reduce the light transmission by 50%. Even if the FSLs could help to find good images of the optic nerve information could still be lost due to the significant loss in the amount of light passing through the imaging system. Methods do however exist that can compensate for this problem. A simple option could be to digitally enhance the image. An optical alternative would be to use a further LC system that creates phase modulation of unpolarised light as described in [112].

The other problem that should be noted is that the efficiency of the FLC is not 100%. This means that a double image could be produced, creating interference that would hamper the analysis of the optic nerve. Efficiency could be increased by using the optimum light wavelengths of the FLC, but the amount of light passing through the imaging arm would again be reduced.

So far the FSL components were placed in between the zoom lenses, but it could be

possible to create zoom lenses that have birefringent components. As an example one could create a doublet lens, where one component is a typical plano-convex lens and the other a plano-convex birefringent lens. In between the two parts an FLC would be sandwiched to control the light polarisation. This would reduce the number of optical elements in the system and remove the requirement to add a compensating lens for the birefringent lenses. It is not possible to replace an entire zoom lens with a birefringent lens, as the power of the zoom lenses is much higher than that of the birefringent lenses. The focal shift would therefore be too great and the FSL would be useless. It may however be useful to keep the FSLs separate from the fundamental imaging arm elements, as it could then be an added feature that would be inserted if needed.

The results from testing angled incident light on birefringent lenses shows that image quality will be affected by astigmatism. As the object of importance is the optic nerve it would be useful to change the orientation of the FSL component such that light from the optic nerve is actually normal to the surface of the birefringent lenses. This would require the entire end of the imaging arm to be repositioned in line with the birefringent lenses.

A definitive design of an imaging system for a retinal camera should be created with bierfringent lenses as one of the components. This would help determine the effect of the problems mentioned. Without actual experimental testing of a system it will be difficult to determine how useful FSLs can be in retinal imaging as the impact of light reduction and double imaging it may cause can not be determined through simulations.

5.5 Summary

- Fast focus switching retinal camera could be created by simply adding FSLs with a compensating lens. This technique could improve the repeatability of optic nerve diagnosis without having to use other very costly instruments that have so far failed to be definitive solutions.

- An even cheaper option of introducing birefringent plates can not be used due to increased aberrations from severe astigmatism.

- Using birefringent lenses could make it possible to obtain images of optic nerve at different levels without any image shift due to moving parts. The time with which these images can be taken will be very small and a technical expert to obtain the correct focus may also not be needed.

- Limited light transmittance, due to light polarisation, and double images, due to less than 100% polarisation rotation efficiency, are great disadvantages that would strongly reduce the likelihood of good quality optic nerve images being produced. Real images need to be obtained to determine the impact of these problems.

- Incident light that is not normal to the birefringent lenses will suffer from astigmatism. It is therefore important to ensure that the incident light from the optic nerve is close to normal incidence.

Chapter 6

Image Jitter as a Visual Aid

The visual aids available to patients that suffer from low vision, uncorrectable by standard prescription lenses, are typically limited to magnifying or telescopic devices, as discussed in section 3.3. It would therefore be of great interest to find other solutions for low vision. The hypothesis by Watson *et al.* states that induced retinal image-jitter could help such visually impaired patients see better and therefore new, alternative methods could be developed to help these patients [14].

In section 3.3 results by Watson *et al.* were also provided, showing the improvement of word recognition for patients with simulated visual impairment when the text sample is jittering, with jitter-intervals between 500 and 100 ms, compared with the sample being stationary [14]. This indicates that there would be some advantage for visually impaired individuals to recognise words in text if the text sample were to jitter. The jittering of the text sample is simulating the involuntary microsaccades of the eye, which are known to prevent neural adaptation. The results also showed that an improvement in word recognition is very dependent on the jitter interval used, as short intervals of 50 ms and 25 ms impaired the speed of word recognition whereas longer intervals of 500, 250 and 100 ms improved the speed.

This chapter discusses the potential for creating image jitter to help visually impaired individuals, whose vision can not be corrected by conventional prescription lenses. A series of experiments have been completed by patients with age related macular degeneration, testing their ability to recognise words and distinguish facial expressions. Additionally an optical system was used to create jitter to investigate the possibility of designing a wearable system that could create jitter. The results obtained are analysed and discussed as well as other optical designs that could help make jitter glasses a reality.

6.1 Computer Generated Jitter

Computer generated stimuli were presented on a 19-inch RGB monitor (VisionMaster Pro 450; Iiyama) with a temporal resolution of 120 Hz, a spatial resolution of 1024x768 pixels and a mean luminance of 30 cd/m2. A custom video summation device provided 256 grey levels and 12 bit precision. Software, written in Pascal for MSDOS, was used to generate stimuli and control the positioning of those stimuli. The 90% decay time of the monitor phosphor signal (using white color and an image formed by 1 line) was about 1ms [14].

The first round of experiments was conducted by displaying images on a screen and simulating jerky motion, characteristic of saccades and microsaccades. The stimulus appeared to jitter by changing the position of the stimulus on the screen at a certain temporal frequency between the centre and one of 4 positions at polar angles 45°,135°,225° or 315°. The image jitter amplitude was 0.5° or 1° and the inter-jitter duration was 166 or 100 ms.

It should be noted that a jittering image would not be a target one would regularly be observing. Upon viewing such a target the periodic nature can cause discomfort and neural adaptation. In an attempt to avoid such issues, the positioning of the target was randomised similarly to the involuntary movement in the eye.

Figure 6.1 demonstrates the stimuli used for word and facial expression recognition experiments. The text samples consisted of 11 unrelated words, which means the experiment is only testing word recognition not reading speed. The contrast (Weber) between the letters and the background was 86 %. The angular dimensions for the letter 'x' were 1.4°x1.6° viewed at a distance of 57 cm. The angular centre-to-centre spacing of horizontally adjacent letters was 2.12°, equivalent to a visual acuity of 1.4 LogMAR (6/150 Snellen acuity).

Facial stimuli were obtained from the Mac Brain set [113] and were angry or happy (Fig. 3A). The mean height/width±SD were $13.6 \pm 0.8°/8.5 \pm 0.6°$ at viewing distance of 57 cm. Mean luminance was 30cd/m^2.

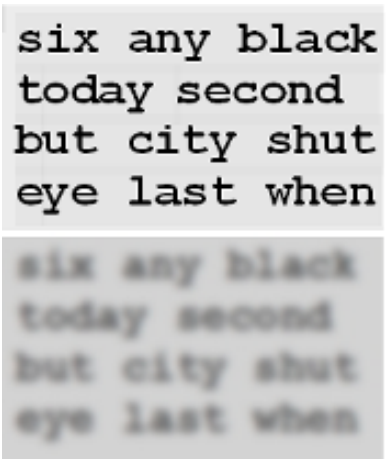

(a) A text sample as it would appear on screen with and without blur.

(b) Facial expressions samples as they would appear on screen with and without blur.

Figure 6.1: Sample stimuli used in testing.

Experiment 1. Word Recognition

Word recognition ability was measured for 14 participants (mean age±SD=79±4.4 years) with age-related macular degeneration (mean binocular visual acuity±SD=0.99±0.39 logMAR). Each person was presented with a stationary or jittering target at random and they were required to read the words out loud as fast as possible. Each text sample was presented for 30 seconds only changing earlier if the patient was able to read all the words before the time was up. A trial run was given for both conditions and was not included in the results. The word recognition ability was calculated as the number of words correctly identified per minute. Two different jitter amplitudes were tested, 0.5 and 1 deg, as well as two jitter-intervals, 100 and 166 ms.

Experiment 2. Facial Expression Recognition

Performance accuracy for discriminating facial emotions was measured for 16 volunteers (mean age±SD=79±4.6 years) with age related macular degeneration (mean binocular visual acuity±SD=1.0±0.37 logMAR). As in the previous experiment the target was randomly stationary or jittering. During the trial the patient was notified by a short warning sound followed by a stimulus that was presented on the screen for 1s. The patient was then required to determine whether the face was happy or angry. 12 rounds were used as practice trials, not included in the results, after which a further 56 trials were made. Performance accuracy in each condition was measured using a discriminability index (d'), $d' = z(H) - z(F)$, where $z(H)$ and $z(F)$ are the z-scores of the correct responses to happy faces (hits) and the errors made on angry faces (false alarms). The z-score indicates by how many standard deviations a result is above or below the mean. The bias (C), reflecting a criterion shift, was evaluated as $C = -[z(H)+z(F)]/2$.

One can see the average, normalised word recognition speeds for the four different conditions in figure 6.2. It shows there is a clear and significant improvement to the recognition speed when the stimulus was under influence of jitter, with the average improvement across all results being over 50% .

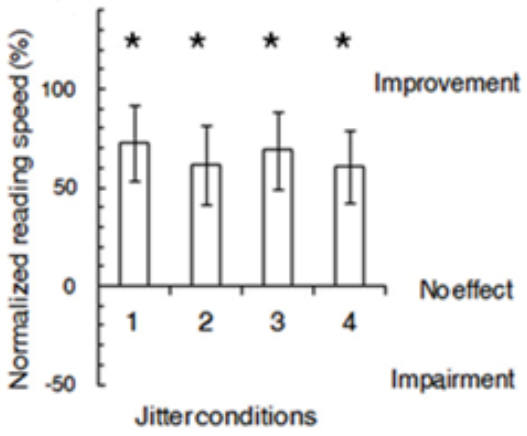

Figure 6.2: Normalized word recognition speed (NRS) averaged across participants (n=14) for temporally modulated text at various jitter amplitudes and inter-jitter intervals: 1) 0.5°/166 ms; 2) 1°/166 ms; 3) 0.5°/100 ms; 4) 1°/100 ms. Asterisks (*) denote the normalized reading speed is significantly different from zero at $P < 0.05$. Error bars represent 95% confidence intervals, from [14].

In figure 6.2 the NRS is defined as,

$$NRS = 100(RSm - RSs)/RSs, \tag{6.1}$$

where RSm and RSs denote the reading speeds for modulated and stationary text, respectively.

The speed at which each subject was able to recognise words varied greatly. The speed for a jittering image was therefore normalised by the speed for a stationary image. It appears that the effect of jitter on the speed of word recognition is dependent on the

ability to recognise words for a stationary image. The improvement due to jitter was significantly lower when the stationary word recognition ability was already high. This dependence is shown by the power function fitted to the results in figure 6.3 where it is clear to see how the effect of jitter decreases severely as the speed for recognising words in stationary text increases. Significant improvement was obtained for the patients with substantial visual loss (binocular visual acuity>1 LogMAR, mean±SD=1.31±0.25 LogMAR, n=8, Fig.2 filled circles).

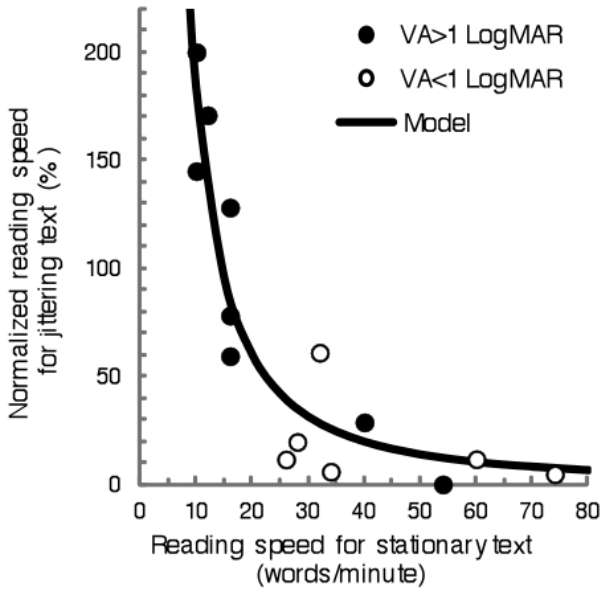

Figure 6.3: Word recognition speed normalized for each subject, averaged for different parameters of image jitter, as a function of word recognition speed for stationary text. Filled circles show data for participants with severe visual loss; empty circles illustrate data for participants with moderate visual loss. Solid line represents the best-fitting power function: $NRS = a/RSs^b$; $a = 7523$, $b = 1.61$; $R^2 = 0.86$, from [14].

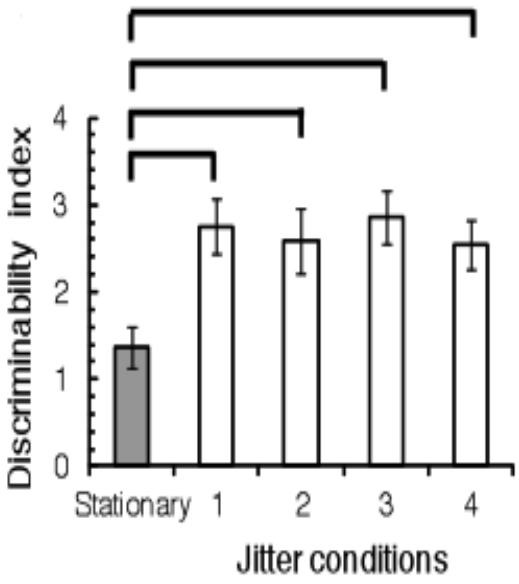

Figure 6.4: Sensitivity (d) for discriminating angry and happy facial emotions for stationary (black bar) and jittering images (empty bars) at various jitter amplitudes and inter-jitter intervals as explained in figure 6.2. Each result has a significantly different d' ($p<0.001$) compared to stationary stimulus. Error bars show 95% confidence intervals, from [14].

Figure 6.4 shows the ability to discriminate happy and angry facial expressions. Under all conditions the results showed that d' was significantly higher ($p<0.001$) for jittering images compared with stationary images, with the increase being a factor of 2 on average. Unlike with the word recognition no correlation could be found between a patient's performance and their visual acuity. For this reason the results for jittering stimuli were not normalised with the stationary stimulus results. The differences between the data for various jitter parameters were not significant. There was also no bias found towards one specific emotion.

6.2 Jitter Optics

To further support the results found by Watson *et al.* an optical system was designed that could create image jitter rather than the computer screen. The optical system consisted of a linear polariser, two ferroelectric liquid crystals (FLCs) and two Wollaston prisms, as shown in figure 6.6. A more detailed image of how the light travels when passing through a Wollaston prism is provided in figure 6.5.

Optical System

A Wollaston prism consists of two orthogonal birefringent prisms that are in most cases cemented together. Their optic axes are perpendicular to each other and perpendicular to the direction of the incident light. The ordinary and extra-ordinary rays travel through the first section undeviated, due to the optic axis being perpendicular to the direction of the incident ray, with the extra-ordinary ray travelling slightly slower than the ordinary ray, in the case of a positively birefringent material. As the optic axis of the second prism is perpendicular to the first the ordinary ray will become the extra-ordinary ray and vice-versa. At the point of incidence the ordinary ray is refracted away from the normal of the interface plane while the extra-ordinary is refracted toward it. The angle of divergence of the two rays is dependent on the wedge angle of the prisms and the birefringence of the material used.

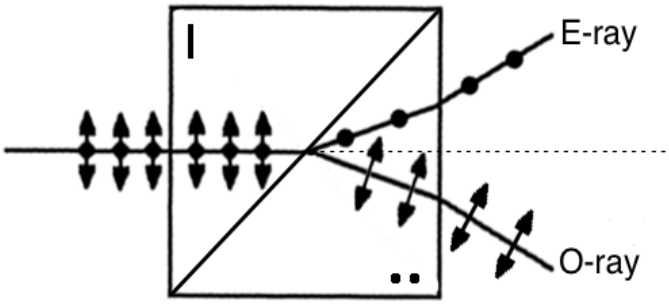

Figure 6.5: Side-on view of a Wollaston prism showing the paths that the extra-ordinary and ordinary rays take as they pass through and how they both travel at the same angle away from the direction of the incident ray.

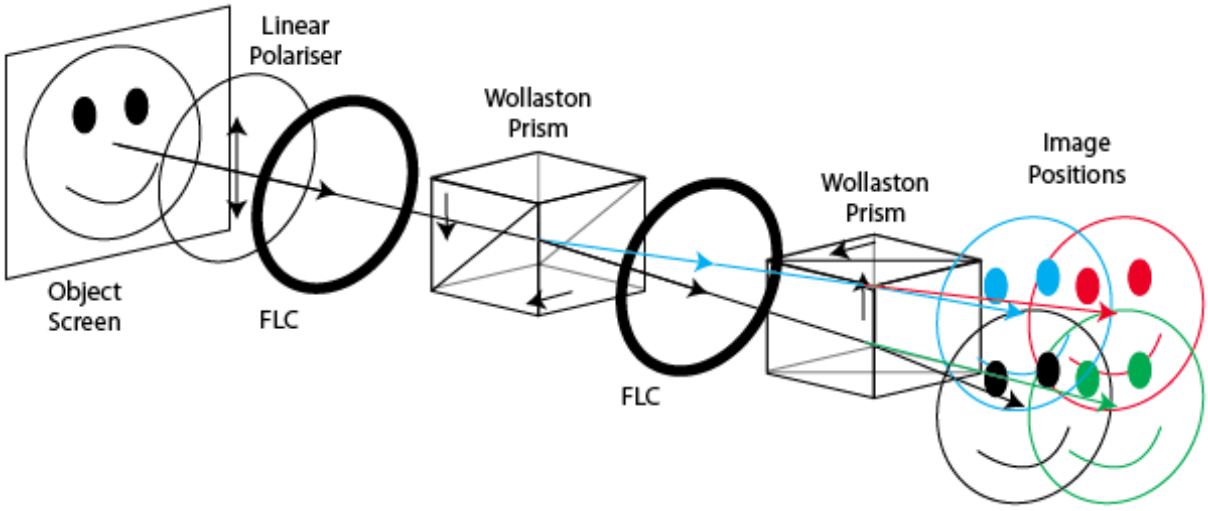

Figure 6.6: Illustration of the full setup used to create image jitter. By combining two Wollaston prisms with independently controlled FLCs it is possible to create four image positions. The path an incident ray will take is dependent on the state of the two FLCs. The different colours are designed to clarify the ray paths and image positions and do not imply any wavelength separation.

As the optical system contained two prisms it was possible to have four image positions as shown in figure 6.6. The second prism was rotated by 90° such that the plane of divergence is perpendicular to that of the first prism. As in the focus switchable lens system, described in section 3.2, the FLCs determined the polarisation of the incident light, which were controlled by separate signals from the computer producing the target stimulus. The FLCs were switched randomly to produce a jittering image.

The angular size of the square formed by the four ray paths was measured to be $1.8x1.8\pm0.1^{\circ}$. The total transparency of the system being $20\pm0.1\%$ reducing the mean luminance of the screen down to 6 cd/m^2

Experiment 3. Facial Expression Recognition using Optical System Jitter

Performance accuracy was measured for 7 participants (mean age±SD=80±3.2 years) with age related macular degeneration (mean monocular visual acuity±SD=0.73±0.27 logMAR) using the same face stimuli as in Experiment 2. The procedure was also similar to that used in Experiment 2. Participants looked with the dominant eye at the faces on screen through the optical system (figure 6.6) with the FLCs either in operation, causing the faces to jitter, or offline, leading the face to remain stationary. The jitter amplitude was either 1.8° or 2.6° depending on whether the face was re-positioned along one axis or diagonally.

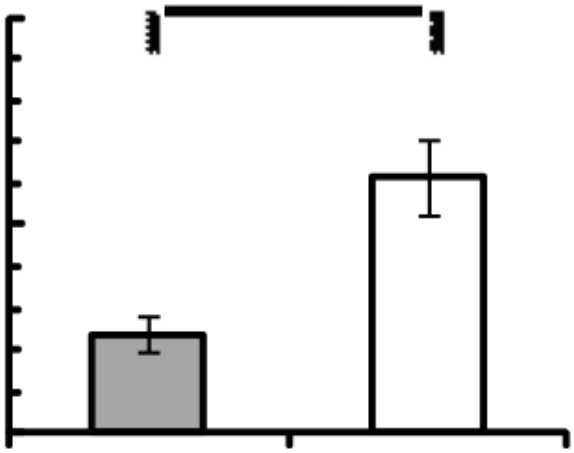

Figure 6.7: Sensitivity (d') for discriminating angry and happy facial emotions for stationary (black bar) and jittering images (empty bar) (amplitude of 1.8° or 2.6° and inter-jitter interval of 166 ms). Discriminability, d', for jittering stimuli is significantly higher than from stationary stimuli at $p<0.005$. Error bars represent SEM, from [14].

Figure 6.7 shows the results from using the optical system for jitter. The discriminability index (d') for jittering faces showed a significant improvement compared to

that for stationary stimuli, increasing by a factor of 2.8. There was no significant bias detected in discriminating the two different expressions. The improvement in discrimination shows similarity with the results obtained without the optical system even though the luminance was significantly reduced.

6.3 Analysis

Evidence obtained from the experiments carried out are in good support of the hypothesis deduced by Velitchko et al. [14]. Both facial expression discrimination and word recognition ability increased overall in all experiments when the stimulus was under the influence of jitter.

It is important to note that the results for the word recognition ability varied considerably. A correlation was found between the improvement due to jitter and the severity of the vision loss. Word recognition speed increased much more for those patients with visual acuity greater than 1 LogMAR. Correlation between stationary and jittering facial expression discrimination was not found and the variation between patients was lower.

Research into visual acuity has shown that reading speed has part dependence on the print size, which could explain the different levels of improvement due to jitter. It was found that reading speed increased with print size up until a critical point beyond which it remained constant. Extremely large print would reduce the reading speed [114]. The critical print size was not determined for the patients, but it can be assumed with confidence that the print size was smaller than the critical size for the majority of the patients with visual acuity >1 LogMAR. The critical print size can be up to twice the spatial resolution. Below the critical print size studies have shown contrast

has a large impact on the reading ability. Spatial frequency of words is defined by the spacing of the letters and was 0.47 c/deg for 57 cm viewing distance and 0.24 c/deg for 28 cm viewing distance for the word recognition experiments. A bandwidth of at least one octave, increasing from the fundamental frequency, is required to recognise the words. The spatial frequencies used during the experiments are therefore less than 1c/deg, which is low. Induced jitter could produce sustained neuronal response for the patients, who rely on the peripheral neurons of the retina, where low spatial frequency images are being processed. This would lead to an enhancement of the effective contrast of the words in the stimuli used.

A study suggested that fixation instability could improve perception of text in the peripheral of the retina for patients with central scotomas [115]. Fixational instability would be induced by the patient by saccadic movement between different targets in peripheral view. The stimulus would therefore be moving in and out of the area affected by the scotoma. It may be thought that such results would indicate that jitter could only be effective for patients with scotoma, but such self-induced movement could not result in such a large difference in word recognition speed for stationary and jittering text, as the results for the two conditions would be expected to be similar under those circumstances.

Subjects with less severe vision loss showed higher word recognition speed for stationary text than those with more severe vision loss. From the test subjects those that showed good word recognition found a much lower improvement for a jittering target. This could be due to the print size being close to their critical print size. It is theorised that patients with less than 1 LogMAR may rely less on peripheral neurons, resulting in a smaller critical print size [116]. It would also mean that the effect jitter has on word recognition is significantly less.

Relating the research on critical print size to the findings from the jitter experiments suggest that it is possible to use jitter to improve the word recognition speed for patients with severe vision loss. This could be a favourable visual aid option as it would not be required to magnify text to a person's critical print size, meaning the visible field would not be reduced.

As already mentioned in section 3.3.1 the improvement due to jitter is also linked to the temporal frequency chosen. The basis of the improvement can be found in the relationship between temporal frequency and contrast sensitivity. This relationship was already pointed out as an important factor for the use of flicker described in chapter 4 and the same research by Robson is also very relevant to the results obtained for jittering stimuli. The temporal frequency range that helped improve word recognition speed incorporated the frequency for which peak contrast sensitivity was found for a flickering grating of 0.5c/deg [68].

6.3.1 Possible Design Improvements

There have been positive results with the simple optical system that was tested, but there are many aspects of the design that have to be improved. In particular only one eye has been tested so far. It is therefore important to create a system for each eye, so a person's full vision can be tested with jitter.

Other factors that would need to be improved are the length of the optical system and the transmission percentage. Additionally for the condition when jitter is not activated it would be desirable to have the light pass through undeviated. Currently even when the target is stationary it is still being deviated away from its natural path. This could be inconvenient if a person were to be wearing glasses that do not show the true position of an object.

Naturally a wearable optical system that could create jitter would be uncomfortable if the jitter were a permanent feature. It would therefore be desirable to have the jitter as an option that could be activated by the user. When the system is not creating jitter the light rays should pass through the system without severe deviation. A Rochon prism is similar to the Wollaston prism, but the ordinary ray passes through it undeviated when incident light is normal to the prism surface, as shown in figure 6.8.

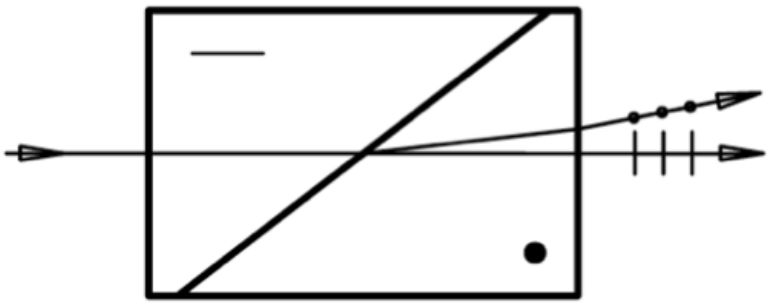

Figure 6.8: Rochon Prism illustration showing the direction of propagation of the ordinary and extra-ordinary rays. The ordinary ray passes through undeviated.

One could use these prisms in a similar way to the prisms in the already tested optical system, but each prism will only create one deviated image position. To have a system with four different, off-centre image positions one would need four prisms. This could result in the system being too long for practical use and it could also result in a lower transmission of light due to the increase in the number of elements. If it were possible to obtain similar results for jitter with less image position, then this could be a viable option. A more in-depth investigation would have to be made into the specific jitter motion that can maximise its effect positively on a patient's vision.

The current system would be very impractical to wear or use as it is very long. The best option is to change the birefringent material of the prism. We know that the angle of deviation for the light rays is dependent on the wedge angle in the prism and the birefringence of the material. We approximate that Snell's law is valid for both the

ordinary and extra-ordinary rays. The angle of refraction of the ray, once exiting the prism, can then be determined by the following equations:

$$n_o \sin\Omega = n_e \sin\theta_o \qquad n_e \sin\Omega = n_o \sin\theta_e, \tag{6.2}$$

$$n_e \sin(\Omega - \theta_o) = n \sin\theta'_o \qquad n_o \sin(\Omega - \theta_e) = n \sin\theta'_e, \tag{6.3}$$

where Ω is the wedge angle, θ_o & θ_e the angles of refraction of the light as it entres the second wedge, θ'_o & θ'_e the angles of refraction as the light leaves the prism and n is the refractive index of the medium after the prism.

The Wollaston prisms used produced an image separation of 1.8°. Quartz has a very low birefringence and therefore a large wedge angle is required to achieve such a separation. It would be possible to use calcite, for example, as it has a much higher birefringence. The wedge angle needed to create a separation of 1.8° would then only be 5.245°. A prism with an aperture of 30mm would require a minimum thickness of 2.75 mm to accommodate such a wedge angle. This would indicate that there is a possibility to create an optical system that would be less than 1 cm thick.

Jittering targets, relative to stationary targets, have shown to improve the ability for visually impaired individuals to recognise facial expressions and the speed of word recognition. Word recognition improved by around 50% and the ability to discriminate between facial expressions was increased by a factor of 2-2.8. The improvement due to jitter created by on-screen image displacement would suggest that there is possibility for software and hardware development to incorporate jittering targets. Similarly the improvement due to jitter via the optical system suggests there is potential for optical systems, based on the tested system, that could be worn by those with visual impairment to improve their performance of everyday tasks. The simplicity of the optical

system means that there is huge room for improvement with respect to the dimensions of the system, light transmission and practicality. The aim should be to create a wearable system by compacting the different components together. From the correlation between the results for on-screen jitter and optoelectronic jitter it can be inferred that the results can not be related to any prolonged viewing of a computer screen as the luminosity is much lower when the optical system is used. Image displacement creating the appearance of image jitter could therefore provide a new option to help visually impaired patients without having to magnify the target, hence preventing the reduction of the visual field.

Previous research showed that microsaccades aid the visual system in preventing neural adaptation [117]. The microsaccadic movement was determined to only affect the neurons sensitive to fine detail and not those designed for low spatial-frequency targets [88]. From the experiments described in this section it has been shown that it is possible to create image jitter that can prolong the neural response to low spatial-frequency targets in patients with severe low vision reducing neural adaptation in the peripheral neurons. It has also been shown that it is crucial to apply the correct temporal frequency in order to avoid impairing vision further. Currently there is no knowledge of the consequences induced image jitter has on the involuntary eye movement due to natural fixation. It is therefore important to determine whether the characteristics of the eye movements change, as this would alter the neural process that creates the retinal image. Retinal image dynamics could therefore be impacted.

6.4 Summary

- Patients with age related macular degeneration were found to have improved word recognition speed, average improvement of 50%, for jittering stimuli relative to a

stationary stimulus.

- Jitter could improve the word recognition speed greater when the print size is below the critical print size.

- Patients with age related macular degeneration were found to have improved facial discrimination abilities, by a factor of 2-2.8, for jittering stimuli relative to a stationary stimulus.

- Software and optoelectronic image jitter both generated improved facial discrimination abilities. Both methods of jitter could lead to new solutions to help patients with severe vision loss.

- The optical system used to create jitter could be compacted down to 1cm if calcite is used as the birefringent material in the prism.

Chapter 7

Conclusion

7.1 Flicker

With the use of a focus switching lens consisting of a linear polariser, FLC and birefringent lens it was possible to create an optical system that could change focus rapidly, creating flicker. This flicker had the ability to improve a person's ability to perceive changes in defocus.

Flicker simulations have shown that high spatial frequency targets change appearance more visibly for small defocus shifts. A shift of 0.1 diopters of defocus was only just visible in square wave gratings of approximately 18.70c/deg. The chance to actually see the focus shift was dependent on the initial amount of defocus. A shift of 0.1D was not visible when shifting between 0.1D and 0.2D, but it was visible when switching between 1.0D and 1.1D. The frequency of the flicker was important as a low frequency, below 10Hz, did not capture enough attention and a frequency of 20Hz was too high to be able to notice the change.

The standard deviation was determined for test patients positioning a lens during non-ickering and ickering targets. With a ickering target they had to nd the point where

the amount of ickering was lowest, as close to no icker as possible. With a non-ickering target they had to nd perfect focus. The standard deviation was lower for each patient when they were using a ickering target.

For future research a lens should be used that has a greater shift in focus. This either requires a material with higher birefringence or a lens with a shorter radius of curvature that would produce a bigger dierence in focal power between the two polarisation states. This would make it difficult to use in a similar optical system as was used in this research. A diverging lens would therefore be required to compensate for the increased power of the birefringent lens. The focus switchable lens system paired with the diverging lens should also be tested as a stand alone system.

7.2 Retinal Imaging

Focus switchable lens systems were presented to create a fast focus switching retinal camera. Results were obtained from simulations in Zemax showing that it is possible to successfully use FSLs within a retinal camera to focus the optic nerve head at different depths. Birefringent plates were also tested, but they were deemed inappropriate due to the creation of large astigmatism in the spot diagrams obtained from the simulations. Quartz and Calcite were both tested. The results obtained for each material were very similar, but the radius of curvature for the required lenses was very different. Due to the high birefringence of calcite a very large radius of curvature was needed to produce the correct shift in focus between the possible states of the FSL system. Quartz would therefore be more suited as the incredibly large radius of curvature for the calcite lens would be difficult to manufacture.

While it was possible to show that the principle works there are many things still

to be considered. The amount of light through such a system would be reduced by at least half, which could make it difficult to obtain images in which the optic nerve head is clearly visible. Efficiency of the FLC also needs to be considered. If it is not 100%, small residual images may be present creating multiple images in the same picture. Field curvature tests also showed that as the angle of incidence increases the more astigmatism will be present in the image. This would result in images that are blurred around the edge. It would therefore be important to centre on the optic nerve head.

An accurate optical design is required to conduct further simulations to extract more data. Once it is possible to determine the specific requirements on the FSL to function well with the imaging arm of the retinal camera then experimental testing can be done. Simulations could also be carried out on replacing the zoom system components with doublet lenses containing a birefringent element. This method would reduce the number of components in the imaging system.

7.3 Jitter

Simulating micro-saccadic movement of the eye with greater amplitude has been shown to improve the reading ability and facial expression recognition of patients with severe vision loss. Patients with severe vision loss only perceive low-spatial frequency images. The amplified jitter was able to stimulate the neurons in the eye's periphery that are designed for processing low-spatial frequency targets.

The average improvement factor for reading was 50%. The results obtained for the test patients' ability to read jittering text varied considerably. This has been determined to be correlated to the patients' critical print size, which is the size at which they are able to read non-jittering text fastest. Patients with very slow initial reading speeds

therefore improved much more when the target was jittering in comparison to those who had better initial reading speeds.

The same patients were found to have an improved ability to discriminate between happy and angry faces. The patients' ability increased by a factor of 2-2.8 relative to stationary targets. The variability in the result was not as high as with the reading test and there was no correlation found between the level of vision loss and the improvement factor.

An optical system was successfully designed that could create image jitter with the use of wollaston prisms. It was possible to change the light path of the incident rays by using an FLC in the same way it is used to control the focus in a focus switchable lens. The patients' ability to discriminate between happy and angry faces again improved relative to stationary targets.

It is hoped that such a system could one day be readily available for people with low vision as an additional visual aid option. If it is possible to create a wearable optical system to create image jitter then such a visual aid could become reality. The current system however is too long and will need to be compacted. This could be done by creating custom wollaston prisms that use birefringent materials with greater birefringence. The prisms could therefore be much thinner and produce the same jitter amplitude.

Bibliography

[1] P. Riorden-Eva and J. P. Whitcher, eds., *Vaughan & Asbury's General Ophthalmology*, ch. 1. McGraw-Hill, 2007.

[2] "National eye institute," 2012.

[3] "Non-light-sensitive retinal cells converted to photoreceptors," 2006.

[4] S. Resnikoff, D. Pascolini, D. Etya'ale, I. Kocur, R. Pararajasegaram, G. P. Pokharel, and S. P. Mariotti, "Global data on visual impairment in the year 2002," *Bulletin of World Health Organization*, vol. 82, no. 11, pp. 844–851, 2004.

[5] A. N. Simonov, G. Vdovin, and M. Loktev, "Liquid-crystal intraocular adaptive lens with wireless control," *Optics Express*, vol. 15, no. 12, pp. 7468–78, 2007.

[6] R. K. Tyson and B. W. Frazier, *Field Guide to Adaptive Optics, Second Edition*, ch. 1. SPIE, 2012.

[7] "Two-photon microscope with adaptive optics demonstration," 2012.

[8] J. Arines, "Impact of liquid crystals in active and adaptive optics," *Materials*, vol. 2, pp. 549–61, 2009.

[9] G. D. Love, J. V. Major, and A. Purvis, "Liquid-crystal prisms for tip-tilt adaptive optics," *Optics Letters*, vol. 19, no. 15, pp. 1170–2, 1994.

[10] A. N. Simonov, G. Vdovin, and M. Loktev, "Liquid-crystal intraocular adaptive lens with wireless control," *Optics Express*, vol. 15, no. 12, pp. 7468–78, 2007.

[11] B. Wang and K. Ciuffreda, "Depth-of-focus of the human eye in the near retinal periphery," *Vision Research*, vol. 44, pp. 1115–1125, 2004.

[12] B. Wang, K. Ciuffreda, and T. Irish, "Equiblur zones at the fovea and near retinal periphery," *Vision Research*, vol. 46, pp. 3690–3698, 2006.

[13] B. Wang and K. Ciuffreda, "Foveal blur discrimination of the human eye," *Ophthalmic and Physiological Optics*, vol. 25, pp. 45–51, 2005.

[14] L. M. Watson, N. C. Strang, F. Scobie, G. Love, D. Seidel, and V. Manahilov, "Image jitter enhances visual performance when spatial resolution is impaired," *IOVS*, vol. 53, no. 10, pp. 6004–10, 2012.

[15] "'adaptive optics' come into focus." BBC News, 2011.

[16] P. B. Berge, "Varioptic." www.varioptic.com.

[17] D. M. Aschwanden, "Optotune." www.optotune.com.

[18] "Superfocus." www.superfocus.com.

[19] PixelOptics, "empower!." www.pixeloptics.com.

[20] G. Li, ed., *Progress in Optics*, vol. 55, ch. 4 - Adaptive Lens, pp. 200–283. Elsevier, 2010.

[21] S. Chandrasekhar, *Liquid Crystals*. Cambridge University Press, 1992.

[22] P. Collings and M. Hird, *Introduction to Liquid Crystals*. Taylor & Francis, 1997.

[23] D. M. Walba, *Advances in the Synthesis and Reactivity of Solids*, vol. 1, ch. Ferroelectric Liquid Crystals, pp. 173–235. JAI Press Ltd, 1991.

[24] D.-K. Yang and S.-T. Wu, *Fundamentals of Liquid Crystal Devices*. Series in Display Technology, John Wiley & Sons, 2006.

[25] J. L. B. de la Tocnaye and L. Dupont, "Complex amplitude modulation by use of a liquid-crystal spatial light modulator," *Applied Optics*, vol. 36, no. 8, pp. 1730–1741, 1997.

[26] W. Osten, C. Kohler, and J. Liesener, "Evaluation and application of spatial light modulators for optical metrology," *Optica Pura y Aplicada*, vol. 38, no. 3, pp. 71–81, 2005.

[27] G. Moddel, *Spatial Light Modulator Technology*, ch. Ferroelectric liquid crystal spatial light modulators, pp. 287–359. Marcel Dekker Inc., 1995.

[28] I. Underwood, *Spatial Light Modulators*, ch. 6 - Ferroelectric liquid crystal over silicon spatial light modulators - principles, practice and prospects, pp. 76–88. OSA Trends in Optics and Photonics, 1997.

[29] E. Gros and L. Dupont, "Ferroelectric liquid crystal optical waveguide switches using the double-refraction effect," *IEEE Phot. Tech. Lett.*, vol. 13 (2), pp. 115–117, 2001.

[30] I. G. Manolis, T. D. Wilkinson, M. M. Redmond, and W. A. Crossland, "Reconfigurable multilevel phase holograms for optical switches," *IEEE Phot. Technol. Lett.*, vol. 14 (6), pp. 801–803, 2002.

[31] L. Sirleto, G. Coppola, G. Breglio, G. Abbate, G. C. Righini, and J. M. Otón, "Electro-optical switch and continuously tunable filter based on a bragg grating in a planar waveguide with a liquid crystal overlayer," *Opt. Eng.*, vol. 41 (11), pp. 2890–2898, 2002.

[32] P. Hariharan and P. E. Ciddor, "Improved switchable achromatic phase shifters," *Opt. Eng.*, vol. 38 (6), pp. 1078–1080, 1999.

[33] M. Sanchez-Lopez, P. Garcia-Martinez, P. Velasquez, and I. Moreno, "Optimization of optical switching with a ferroelectric liquid crystal modulator," *Proceedings of SPIE*, vol. 6695, no. 669505, 2007.

[34] R. B. Meyer, "Structural problems in liquid crystal physics," in *Molecular Fluids*, p. 272, Gordon and Breach, 1976.

[35] B. Wang, M. Ye, and S. Sato, "Liquid crystal negative lens," *Japanese Journal of Applied Physics*, vol. 44, no. 7A, pp. 4979–4983, 2005.

[36] C. Bricot, M. Hareng, and E. Spitz, "Optical projection device and an optical reader incorporating this device." US Patent# 4,037,929.

[37] F. Traeger, ed., *Springer Handbook of Lasers and Optics*. Springer, 1st ed., 2007.

[38] P. F. Brinkley, S. T. Kowel, and C. Chu, "Liquid crystal adaptive lens: Beam translation and field meshing," *Applied Optics*, vol. 27, no. 21, pp. 4578–4586, 1988.

[39] Y. M. Huang and L. Chen, "Correlation of liquid crystal alignments on gratings with the thickness of liquid crystal films," *Thin Solid Films*, vol. 515, pp. 2026–2030, 2006.

[40] M. Ye and S. Sato, "Optical properties of liquid crystal lens of any size," *Japanese Journal of Applied Physics*, vol. 41, no. 5B, pp. L571–L573, 2002.

[41] G. Li, D. L. Mathine, P. Valley, P. Ayrs, J. N. Haddock, M. S. Giridhar, G. Williby, J. Schwiegerling, G. R. Meredith, B. K. S. Honkanen, and N. Peyghambarian, "Switchable electro-optic diffractive lens with high efficiency for ophthalmic applications," *Proceedings of the National Academy of Sciences*, vol. 103, no. 16, pp. 6100–6104, 2006.

[42] A. Naumov, G. Love, M. Loktev, and F. Vladimirov, "Control optimization of spherical modal liquid crystal lenses," *Optics Express*, vol. 4, no. 9, pp. 344–352, 1999.

[43] Y. Nishimoto, "Variable focal length lens." US Patent# 4,783,152, November 1988.

[44] A. Kirby, P. Hands, and G. Love, "Adaptive lenses based on polarization modulation," *Proc. SPIE*, vol. 6018, no. 601814, 2005.

[45] M. G. Douali and J. D. Silver, "Self-optimised vision correction with adaptive spectacle lenses in developing countries," *Ophthalmic and Physiological Optics*, vol. 24, no. 3, pp. 234–241, 2004.

[46] R. Kuwano, T. Tokunaga, Y. Otani, and N. Umeda, "Liquid pressure varifocus lens," *Optical Review*, vol. 12, no. 5, pp. 405–408, 2005.

[47] B. Berge and J. Peseux, "Variable focal lens controlled by an external voltage: An application of electrowetting," *European Physical Journal E*, vol. 3, pp. 159–163, 2000.

[48] C. Cheng, C. Chang, and J. Yeh, "Variable focus dielectric liquid droplet lens," *Optics Express*, vol. 14, no. 4101, 2006.

[49] C. Cheng and J. A. Yeh, "Dielectrically actuated liquid lens," *Optics Express*, vol. 15, no. 12, pp. 7140–7145, 2007.

[50] L. Dong, A. Agarwal, D. Beebe, and H. Jiang, "Variable-focus liquid microlenses and microlens arrays actuated by thermoresponsive hydrogels," *Advanced Materials*, vol. 19, no. 401, pp. 1–5, 2007.

[51] X. Zeng and H. Jiang, "Tunable liquid microlens actuated by infrared light-responsive hydrogel," *Applied Physics Letters*, vol. 93, no. 151101, 2008.

[52] L. Dong, A. Agarwal, D. Beebe, and H. Jiang, "Adaptive liquid microlenses activated by stimuli-responsive hydrogels," *Nature*, vol. 442, pp. 551–554, 2006.

[53] F. Frenken, "Glasses: inevitable in the long run."

[54] Specsavers, "The specsavers guide to your eye examination."

[55] B. Holden, "Uncorrected refractive error: the major and most easily avoidable cause of vision loss," *Community Eye Health Journal*, vol. 20, no. 63, pp. 37–39, 2007.

[56] Z. Currie, A. Bhan, and I. Pepper, "Reliability of snellen charts for testing visual acuity for driving: prospective study and postal questionnaire," *BMJ*, vol. 321, pp. 990–992, 2000.

[57] J. M. Evans, "Standards for visual acuity," tech. rep., KT Consulting, 2006.

[58] J. M. Enoch, "Visual acuity measurement standard," *Italian Journal of Ophthalmology*, 1984.

[59] K. Alexander, W. Xie, and D. Derlacki, "Spatial-frequency characteristics of letter identification," *Vision Research*, vol. 11, no. 2373, 1994.

[60] P. Denieul, "Effects of stimulus vergence on mean accommodation response, microfluctuations of accommodation and optical quality of the human eye," *Vision Research*, vol. 22, pp. 561–569, 1982.

[61] K. Ciuffreda, A. Selenow, B. Wang, B. Vasudevan, G. Zikos, and S. Ali, ""bothersome blur": A functional unit of blur perseption," *Vision Research*, vol. 46, pp. 895–901, 2006.

[62] R. Watt and M. Morgan, "The recognition and representation of edge blur: evidence for spatial primitives in human vision," *Vision Research*, vol. 23, no. 12, pp. 1465–1477, 1983.

[63] J. Hamerly and C. Dvorak, "Detection and discrimination of blur in edges and lines," *J. Opt. Soc. Am. (1917-1983)*, vol. 71, no. 4, pp. 448–452, 1981.

[64] H. Radhakrishnan and S. Pardhan, "Contrast detection in noise with positive and negative defocus in myopes," *Vision Research*, vol. 46, pp. 2949–2955, 2006.

[65] D. Atchison, H. Guo, W. Charman, and S. Fisher, "Blur limits for defocus, astigmatism and trefoil," *Vision Research*, vol. 49, pp. 2393–2403, 2009.

[66] D. Atchison, S. Fisher, C. Pedersen, and P. Ridall, "Noticeable, troublesome and objectionable limits of blur," *Vision Research*, vol. 45, pp. 1967–1974, 2005.

[67] G. Westheimer, S. Brincat, and C. Wehrhahn, "Contrast dependency of foveal spatial functions: orientation, vernier, separation, blur and displacement discrimination and the tilt and poggendorff illusions," *Vision Research*, vol. 39, pp. 1631–1639, 1999.

[68] J. Robson, "Spatial and temporal contrast-sensitivity function of the visual system," *J. Opt. Soc. Am. (1917-1983)*, vol. 56, no. 8, pp. 1141,1142, 1966.

[69] A. Watson and A. Ahumada, "Blur clarified: A review and synthesis of blur discrimination," *Journal of Vision*, vol. 11, no. 5, pp. 1–23, 2011.

[70] G. Walsh and W. N. Charman, "Visual sensitivity to temporal change in focus and its relevance to the accomodation response," *Vision Research*, vol. 28, no. 11, pp. 1207–1221, 1988.

[71] R. J. Jacobs, G. Smith, and C. D. Chan, "Effect of defocus on blur thresholds and on thresholds of perceived change in blur: comparison of source and observer methods," *Optometry and Vision Science*, vol. 66, pp. 545–553, 1989.

[72] F. W. Campbell and J. G. Robson, "Application of Fourier analysis to the visibility of gratings," *Journal of Physiology*, vol. 197, pp. 551–566, 1968.

[73] I. Ohzawa, "Campbell-Robson CSF chart,"

[74] S. Lin and G. Tanaka, *Digital imaging of the optic nerve*, ch. 20. Springer, 2010.

[75] G. R. Douglas, "The optic nerve head - office interpretation," *Asian Journal of Ophthalmology*, vol. 4, no. 2, pp. 2–7, 2002.

[76] E. A. Swanson, J. A. Izatt, M. R. Hee, D. Huang, C. P. Lin, J. S. Schuman, C. A. Puliafito, and J. G. Fujimoto, "In vivo retinal imaging by optical coherence tomography," *Optics Letters*, vol. 18, no. 21, pp. 1864–1866, 1993.

[77] A. G. Balazsi, S. M. Drance, M. Schulzer, and G. R. Douglas, "Neuroretinal rim area in suspected glaucoma and early chronic open-angle glaucoma. Correlation with parameters of visual function," *Archives of Ophthalmology*, vol. 102, no. 7, pp. 1011–1014, 1984.

[78] B. Bengtsson, "The variation and covariation of cup and disc diameters," *Acta Ophthalmologica*, vol. 54, no. 6, pp. 804–818, 1976.

[79] F. A. Medeiros, *Evaluating the Optic Nerve for Glaucomatous Progression*, ch. 19. Springer, 2010.

[80] A. J. Correnti, G. Wollstein, L. L. Price, and J. S. Schuman, "Comparison of optic nerve head assessment with a digital stereoscopic camera (discam), scanning laser ophthalmoscopy, and stereophotography," *American Academy of Ophthalmology*, vol. 110, no. 8, pp. 1499–1505, 2003.

[81] F. A. Medeiros, L. M. Zangwill, C. Bowd, and R. N. Weinreb, "Comparison of the GDx VCC scanning laser polarimeter, HRT II confocal scanning laser ophthalmoscope, and Stratus OCT optical coherence tomograph for the detection of glaucoma," *Archives of Ophthalmology*, vol. 122, pp. 827–837, 2004.

[82] R. Whiteaker and V. B. Whitaker, *Photography of the Optic Nerve*, ch. 22. Springer, 2010.

[83] R. Harper, B. Reeves, and G. Smith, "Observer variability in optic disc assessment: implications for glaucoma shared care," *Ophthalmic and Physiological Optics*, vol. 20, no. 4, pp. 265–273, 2000.

[84] G. N. Shuttleworth, C. H. Khong, and J. P. Diamond, "A new digital optic disc stereo camera: intraobserver and interobserver repeatability of optic disc measurements," *British Journal of Ophthalmology*, vol. 84, pp. 403–407, 2000.

[85] P. G. Spry, I. C. Spencer, J. M. Sparrow, T. J. Peters, S. T. Brookes, S. Gray, I. Baker, J. E. Furber, and D. L. Easty, "The bristol shared care glaucoma study: reliability of community optometric and hospital eye service test measures," *British Journal of Ophthalmology*, vol. 83, pp. 707–712, 1999.

[86] R. C. W. Wolfs, R. S. Ramrattan, A. Hofman, and P. T. V. M. de Jong, "Cup-to-disc ratio: Ophthalmoscopy versus automated measurement in a general population," *Ophthalmology*, vol. 106, no. 8, pp. 1597–1601, 1999.

[87] J. E. Morgan, N. J. L. Sheen, R. V. North, Y. Choong, and E. Ansari, "Digital imaging of the optic nerve head: monoscopic and stereoscopic analysis," *British Journal of Ophthalmology*, vol. 89, pp. 879–884, 2005.

[88] M. Rucci, R. Lovin, M. Poletti, and S. Fabrizio, "Miniature eye movements enhance fine spatial detail," *Nature Neuroscience*, vol. 447, pp. 851–855, 2007.

[89] R. W. Ditchburn, D. H. Fender, and S. Mayne, "Vision with controlled movements of the retinal image," *Journal of Physiology*, vol. 145, pp. 98–107, 1958.

[90] K. Donner and S. Hemilae, "Modelling the effect of microsaccades on retinal responses to stationary contrast patterns," *Vision Research*, vol. 47, pp. 1166–1177, 2007.

[91] H. K. Falkenberg, G. S. Rubin, and P. J. Bex, "Acuity, crowding, reading and fixation stability," *Vision Research*, vol. 47, pp. 126–35, 2007.

[92] A. F. Macedo, M. D. Crossland, and G. S. Rubin, "Investigating unstable fixation in patients with macular degeneration," *IOVS*, vol. 52, no. 3, pp. 1275–80, 2011.

[93] B. Spehar and C. Owens, "When do luminance changes capture attention?," *Atten. Percept. Psychophys.*, vol. 74, no. 4, pp. 674–690, 2012.

[94] M. von Gruenau, J. Faubert, M. Iordanova, and D. Rajska, "Flicker and the efficiency of cues for capturing attention," *Vision Research*, vol. 39, pp. 3241–3252, 1999.

[95] W. P. Berg, E. D. Berglund, A. J. Strang, and M. J. Baum, "Attention-capturing properties of high frequency luminance flicker: Implications for brake light conspicuity," *Transportation Research Part F*, vol. 10, no. 1, pp. 22–32, 2007.

[96] J. Cass, E. V. der Burg, and D. Alais, "Finding flicker: critical differences in temporal frequency capture attention," *Frontiers in Psychology*, vol. 2, no. 320, pp. 1–7, 2011.

[97] R. Wilson, K. Decker, and A. Roorda, "Monochromatic aberations provide an odd-error cue to focus direction," *J. Opt. Soc. Am. A Opt. Image Sci. Vis.*, vol. 19, no. 5, pp. 833–839, 2002.

[98] A. Dehnert, M. Bach, and S. P. Heinrich, "Subjective visual acuity with simulated defocus," *Ophthalmic & Physiological Optics*, vol. 31, pp. 625–631, 2011.

[99] D. Guang-ming, *Wavefront Optics for Vision Correction*. SPIE, 2007.

[100] V. N. Mahajan, *Aberration Theory Made Simple*. SPIE, 1991.

[101] R. S. Longhurst, *Geometrical and Physical Optics*, ch. 2. Orient Blackswan, 1986.

[102] R. Eng and K. Leib, "Multiple imagery with birefringent lenses," *Applied Optics*, vol. 8, no. 10, pp. 2117–20, 1969.

[103] J. P. Lesso, A. J. Duncan, W. Sibbett, and M. J. Padgett, "Aberrations introduced by a lens made from a birefringent material," *Applied Optics*, vol. 39, no. 4, pp. 592–8, 2000.

[104] C. Keller, "Lecture 5: Liner polarizers." University of Utrecht, 2008.

[105] E. DeHoog and J. Schwiegerling, "Fundus camera systems: a comparative analysis," *Applied Optics*, vol. 48, no. 2, pp. 221–228, 2009.

[106] S. Lin, K. Singh, H. Jampel, E. Hodapp, S. Smith, B. Francis, D. Dueker, R. Fechtner, J. Samples, J. Schuman, and D. Minckler, "Optic nerve head and retinal nerve fiber layer analysis: A report by the american academy of ophthalmology," *Ophthalmology*, vol. 114, no. 10, pp. 1937–1949, 2007.

[107] P. Andreou, S. Wickremasinghe, R. Asaria, E. Tay, and W. Franks, "A comparison of HRT II and GDx imaging for glaucoma detection in a primary care eye clinic setting," *Eye*, vol. 21, pp. 1050–1055, 2007.

[108] H. Ye, Z. Gao, T. Luo, and Y. Huang, "Optical configuration of fundus camera based on inner focusing manner," *Chinese Optics Letters*, vol. 8, no. 7, pp. 689–692, 2010.

[109] E. DeHoog, H. Luo, K. Oka, E. Dereniak, and J. Schwiegerling, "Snapshot polarimeter fundus camera," *Applied Optics*, vol. 48, no. 9, pp. 1663–7, 2009.

[110] H.-L. Liou and N. A. Brennan, "Anatomically accurate, finite model eye for optical modeling," *JOSA A*, vol. 14, no. 8, pp. 1684–95, 1997.

[111] K. Rohrschneider, "Determination of the location of the fovea on the fundus," *Investigative Ophthalmology & Visual Science*, vol. 45, no. 9, pp. 3257–8, 2004.

[112] G. D. Love, "Liquid-crystal phase modulator for unpolarized light," *Applied Optics*, vol. 32, no. 13, pp. 2222–3, 1993.

[113] N. Tottenham, J. Tanaka, A. Leon, T. McCarry, M. Nurse, T. Hare, D. Marcus, A. Westerlund, B. Casey, and C. Nelson, "The nim stim set of facial expressions; judgements from untrained research participants," *Psychiatry Research*, vol. 168, no. 3, pp. 242–249, 2009.

[114] G. Legge, D. Pelli, G. Rubin, and M. Schleske, "Psychophysics of reading – i: Normal vision," *Vision Research*, vol. 25, pp. 239–52, 1985.

[115] A. Deruaz, M. Matter, A.R.Whatham, M. Goldschmidt, F. Duret, M. Issenhuth, and A. Safran, "Can fixation instability improve text perception during eccentric fixation in patients with central scotomas?," *British Journal for Ophthalmology*, vol. 88, pp. 461–3, 2004.

[116] S. Chung, J. Mansfield, and G. Legge, "Psychophysics of reading - vxviii: The effect of print size on reading speed in normal peripheral vision," *Vision Research*, vol. 38, pp. 2949–2962, 1998.

[117] S. Martinez-Conde, S. Macknik, and D. Hubel, "Microsaccadic eye movements and firing of single cells in the striate cortex of macaque monkeys," *Nature Neuroscience*, vol. 3, pp. 251–258, 2000.